The limiting DNA replication initiation factors Sld2 and Sld3 influence replication origin efficiency independent of time of origin firing in *Saccharomyces cerevisiae*

Kelsey L. Lynch

A dissertation

submitted in partial fulfillment of the

requirements for the degree of

Doctor of Philosophy

University of Washington

2018

Reading Committee:

Bonita J. Brewer, Chair

Susan Biggins

Stanley Fields

Program Authorized to Offer Degree:

Molecular and Cellular Biology

University of Washington

Abstract

The limiting DNA replication initiation factors Sld2 and Sld3 influence replication origin efficiency independent of time of origin firing in *Saccharomyces cerevisiae*

Kelsey L. Lynch

Chair of the Supervisory Committee:
Professor Bonita J. Brewer
Molecular and Cellular Biology Program
Department of Genome Sciences

During S-phase in *Saccharomyces cerevisiae*, DNA replication is initiated from roughly 300 chromosomal origins that are regulated both by DNA sequence and by interacting protein factors. The limited abundance of a set of *trans*-acting initiation proteins—Sld2, Sld3, Dpb11 and Dbf4, collectively called "SSDD"— gives rise to the disparity in origin activation observed across the genome. The biological significance of this variable firing time and efficiency—conserved features among eukaryotes—is not well understood, nor is it clear how SSDD limitation leads to differences in origin firing time and efficiency. I wanted to determine whether the association of individual SSDD factors with the assembling replication complex contributes to both time of origin activation and origin efficiency. I used auxin-induced protein degradation

to further exacerbate the SSDD limitation, focusing on the consequences for genome duplication when the abundance of either Sld2 or Sld3 is reduced.

I found that depleting cells of either initiation factor slows growth rate, increases S-phase duration, and causes viability defects, none of which are due to activation of the S phase checkpoint. Using genome-wide replication assays, I found that, compared to wild type, the same set of origins is active even when Sld2 or Sld3 are depleted from cells, implying that time of origin firing does not change in response to the availability of these two factors. Instead, I discovered that replication forks move farther when either Sld2 or Sld3 is depleted, indicating that origin firing efficiency is reduced under both conditions. I confirmed these changes to origin efficiency by 2-dimensional gel electrophoresis of multiple individual origins.

The viability defects induced by the depletion of these two limiting initiation factors suggested that the genome is destabilized by the systemic reduction of replication efficiency. Using pulsed-field gel electrophoresis to assay the integrity of whole chromosomes over the course of synchronized Sld2- or Sld3-depleted S phase, I found that all chromosomes except ChrXII are stable. Breakage occurs within the rDNA locus on ChrXII, likely due to its incomplete replication, which is not surveilled by the S phase checkpoint.

In summary, the cellular abundance of Sld2 and Sld3 contributes mostly to origin firing efficiency. In contrast to a recently proposed idea that origin firing time is a secondary consequence of origin efficiency, my work detailed in this dissertation supports the concept that efficiency and time of initiation are separable features of the eukaryotic genome.

TABLE OF CONTENTS

LIST OF FIGURES

LIST OF TABLES

ACKNOWLEDGEMENTS

I would like to thank, first and foremost, my co-mentors Dr. Bonny Brewer and Dr. M.K. Raghuraman for their support, patience, and guidance. Under their mentorship and due to the respectful, collaborative, and gracious lab environment that they foster, I've grown immensely as a scientist. While they might not realize it, the greatest skill they've helped me cultivate is the ability to trust myself and to be confident in my own scientific abilities.

My fellow Brewer/Raghuraman lab members (a.k.a. "labbies") have been essential to my success as a graduate student. The expectation of group success, of helping one another, and of lifting your colleagues up around you are attitudes that I hope to encourage and promote in all my future workplaces. In particular, I would like to acknowledge Gina Alvino and Dr. Elizabeth Kwan as being the best labbies anyone could ask for. They are my role models—both at the bench and off.

Thank you, also, to my advisory committee of Dr. Maitreya Dunham, Dr. Stan Fields, Dr. Sue Biggins, and Dr. Houra Merrikh, especially for encouraging me to graduate at the just the right time.

I would also like to acknowledge the Molecular and Cellular Biology Ph.D. program and the Department of Genome Sciences as being instrumental to my success. Both groups have fantastic administrators and faculty guidance who take the business of advocating for their graduate students very seriously. Thank you for looking out for all of us.

Without encountering some exceptionally wonderful science educators and mentors over the past years, I never would have pursued a career in science. My high school AP Biology teacher, Jean Schick, was the first to help me really understand the logic of science and conveyed the beauty of biology to me. I fell in love with bench science during an internship in Dr. Miriam Zolan's lab at Indiana University. In the Zolan lab, I worked with a fantastic postdoc, Dr. Claire Burns, who was patient and helpful and was the first person to teach me how to use a micropipette. In college, my advisor in the Biology Department, Dr. Tamara Davis, and my favorite instructor, Dr. Monica Chander, challenged me with difficult coursework and assured me that it was okay to major in biology, but not want to go to medical school. I so am thankful for the guidance and the encouragement that I received from these women along my journey to graduate school.

I am very grateful to my lovely friends, both here in Seattle and elsewhere, for helping me get through the thick and thin of graduate student life. Thank you for being up for Beerlympics, Pixar movie screenings, post-2016 election trips to Disneyland, snowshoeing, day hikes, brunches, and the fewer and fewer nights out on Capitol Hill.

Lastly, I would like to thank my family and my partner, Siva, for their love and support. I've sometimes felt like a bit of a black sheep in my family (maybe not black, but… charcoal gray?), but I appreciate and am grateful for their enthusiasm for what I've chosen to do with my life, even if it's not what they would have picked for themselves. I am grateful to Siva for putting up with my needing everything to be "just so", and for making me aware of how many cute dogs there are in the world.

DEDICATION

To my mom, Karen, for taking me to *do* stuff, even if we didn't *have* stuff.

Chapter 1. INTRODUCTION

As an introduction to the specific questions addressed in my thesis work, I will first give a broad overview of how and why eukaryotic organisms maintain variation in their use of origins of replication. I will describe the recently developed "stochastic" model of origin timing and efficiency that is somewhat controversial in the eukaryotic DNA replication field. As I summarize this model for replication timing and efficiency, I will also weigh the experimental evidence used to support its claims with the evidence that contradicts the stochastic model. In the following section, I will more comprehensively describe the SSDD limiting initiation factor model for replication time and efficiency, and how it gave rise to my thesis research. I will also provide more detailed background information about the subset of limiting initiation factors, Sld2 and Sld3, which were the particular focus of my project. To conclude, I will provide additional relevant information about the S phase checkpoint and the rDNA locus in budding yeast.

1.1 Variation in Eukaryotic DNA Replication

One of the enduring mysteries in the field of eukaryotic DNA replication is the variability in onset, or initiation, of DNA replication across a genome. Variable origin activity is observed in single-celled eukaryotes, such as *Saccharomyces cerevisiae*, the organism in which DNA replication has been best characterized, as well as in multicellular organisms with much larger, more complex genomes including humans (Koren et al., 2014; Raghuraman et al., 2001). Given how well-conserved this characteristic of eukaryotic DNA replication has proven to be, it would seem that variable initiation is biologically relevant, although the nature of its importance for genome function is not entirely clear. As our understanding of how DNA replication is orchestrated and

regulated at a molecular level, we have gained some insights into how variation of replication origin activity is achieved, although, for the most part, its biological relevance remains mysterious.

Even in the earliest years of the field, it was clear that certain parts of the eukaryotic genome are replicated earlier in S phase than others, and that the large-scale organization of chromosomes and their underlying sequence play a regulatory role in this variability (Taylor, 1960). For example, the inactive X chromosome was found to replicate much later than the other chromosomes in human cells (Gilbert et al., 1962). A short review published in 1968 summarized autoradiography studies from a range of plant and animal species in which the authors concluded that, generally, the DNA in heterochromatin replicates later in S phase compared to euchromatic DNA (Lima-de-Faria and Jaworksa, 1968). The authors went so far as to put forth a Rule of Chromosome Replication, saying that "… what determines the presence of heterochromatin also determines the late replication of a chromosome…." (Lima-de-Faria and Jaworksa, 1968). This supposition hinted that determinants of DNA replication timing are inherited and a subsequent study using pulse-labeling of newly synthesized DNA in the slime mold *Physarum polycephalum* over multiple passages through the cell cycle found that the same parts of the genome that are replicated early in the first S phase are replicated early in subsequent S phase (Braun and Wili, 1969). In short, the timing of DNA replication is preserved from cell to cell over multiple generations.

But what process was actually being regulated to generate this variability in timing? The model organism *S. cerevisiae* provided the first insights into the changes in DNA structure that underlie the DNA replication process in eukaryotes. Electron microscopy studies of *S. cerevisiae* chromosomes revealed the presence of multiple "bubble" structures along the length of a single chromosome; chromosomes purified during synchronous S phase were enriched for these

structures, suggesting that they are replication intermediates resulting from initiation of DNA replication (Newlon et al., 1974; Petes et al., 1973). Intriguingly, the bubbles found along the length of the linear DNA fragments were often different sizes [Figure 1.1]. The presence of different sized bubbles implied that initiation could occur at different times at different loci on the same DNA molecule.

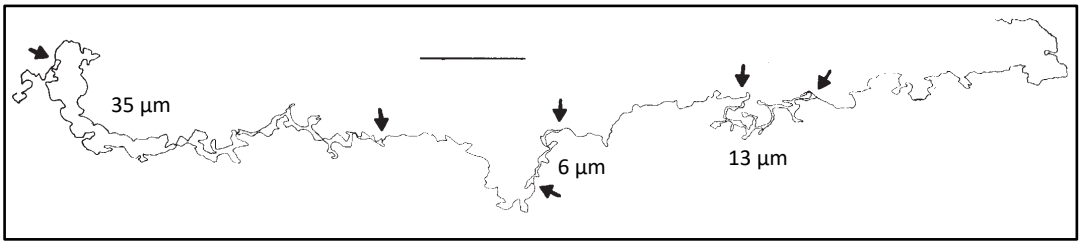

Figure 1.1. Tracing produced from an electron micrograph of a yeast chromosome.[1]

The specifics of how these replication bubbles were generated remained to be uncovered and, once again, budding yeast proved to be an indispensable tool for understanding DNA replication in eukaryotes. Please note that, from this point forward, I will be referring almost exclusively to studies performed in yeast and using yeast nomenclature. Eukaryotic DNA replication is highly conserved and while the details of origin specificity are somewhat different in metazoans, the replication complex components and their assembly are almost entirely the same across all eukaryotes (Bell and Dutta, 2002).

Eventually, Stinchcomb et al., (1980) found that there are many distinct DNA sequence fragments from yeast chromosomes capable of sustaining autonomous replication on a plasmid DNA. Those sequences, termed autonomously replicating sequences or ARSs, are potential sites of initiation of DNA replication, or origins (Brewer and Fangman, 1987). Systematic analyses of origin activation in a native chromosome context revealed that not all potential sites of initiation

[1] Image from Newlon, et al. 1974. Arrows point out the branched DNA that bounds each bubble. Bar is 5 µm. The lengths of each bubble are indicated.

are used in every cell and some are completely inactive on a chromosome (Brewer and Fangman, 1988; Newlon et al., 1991). This characteristic of variable origin use became referred to as origin "efficiency". Additionally, some of those origins become active, or fire, later in S phase relative to others, which could account for differences in time of replication across the genome (Ferguson et al., 1991). To summarize, origin activity is variable in two modes: the time relative to the onset of S phase (origin timing), and the proportion of cells that actually begin replication from that site (origin efficiency). For clarity, these two different characteristics are illustrated in [Figure 1.2].

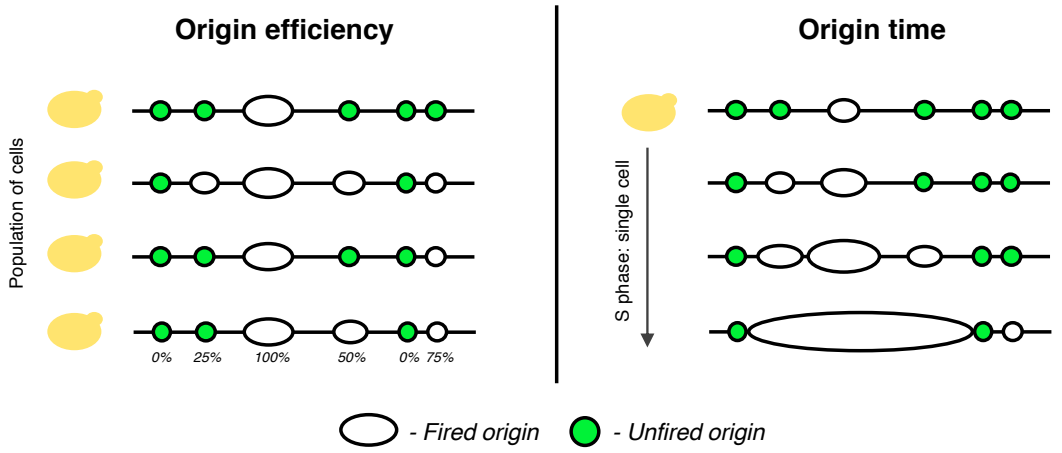

Figure 1.2. Origin firing efficiency vs. time.[2]

Two independent studies showed that each yeast origin has the same core consensus sequence motif, but variable flanking sequence requirements (Deshpande and Newlon, 1992; Marahrens and Stillman, 1992). Those differences in origin sequence structure could potentially contribute to variation in origin activity, but subsequent work revealed that the differences in origin activity can be generated from outside the origin sequence itself (Brewer and Fangman, 1994). In that study, two identical origin sequences were cloned into two different sites on the same plasmid,

[2] The efficiency of an origin is the proportion of a population of S phase cells that initiate replication at that origin. The efficiencies of the origins for the hypothetical population of cells are shown below each origin. Note that not all potential origins actually fire. Timing of origin firing is the time relative to the start of S phase at which an origin fires. The illustration shows variable origin firing time in a single cell during a single passage through S phase.

but one site was the preferred site of initiation due to a particular *cis*-acting sequence outside of the origin itself (Brewer and Fangman, 1994; Pohl, 2013). Additional analyses confirmed that the greater context of an origin's sequence, such as proximity to a telomere, influences its time of activation (Ferguson and Fangman, 1992; Friedman et al., 1996). As assays detecting origin firing across entire yeast chromosomes and, ultimately, across the entire yeast genome became possible, the full extent of variability in origin efficiency and timing was fully appreciated (Friedman et al., 1997; Raghuraman et al., 2001; Yamashita et al., 1997). Contemporaneous with these efforts to characterize the genomic landscape of DNA replication, the complex biochemical underpinnings of replication initiation were being uncovered.

The confirmation that ARS DNA fragments are sites of replication initiation (Brewer, 1987) opened the door to identifying the replication complex proteins and defining the biochemical requirements for DNA replication. DNA footprinting assays at known origins revealed that the origin recognition complex (ORC) binds origin sequences as the first step toward replication initiation (Bell and Stillman, 1992; Diffley and Cocker, 1992). From there, researchers determined that ORC, along with the replicative helicase (MCM2-7) and two loading factors, Cdc6 and Cdt1, is assembled at origins during G1—together known as the pre-replication complex (Diffley et al., 1994; Sun et al., 2013) [Figure 1.3]. A deluge of yeast genetic studies helped identify the replication complex (also referred to as the "replisome") components leading to our current understanding of replication initiation [see Bell and Labib (2016) review for a comprehensive description of replisome assembly and activation in yeast]. In short, as cells transition from G1 to S phase, a large set of replication proteins assemble at origins bound by pre-RC to form the replication complex leading to initiation of DNA replication and synthesis of new dsDNA (the elongation phase of DNA replication).

The assembly and activation of the replisome are tightly coordinated with the cell cycle, through phosphorylation of various replication proteins by the S phase-specific cyclin-dependent kinase (S-CDK: Cdc28 complexed with either Clb5 or Clb6) and the Dbf4-dependent kinase (DDK: Cdc7 complexed with Dbf4) (Bousset and Diffley, 1998; Donaldson et al., 1998; Enserink and Kolodner, 2010; Jackson et al., 1993; Labib, 2010). Clb5 and Clb6 have redundant roles in phosphorylating various replisome components as cells transition from G1 to S phase, but Clb6 is expressed only at the beginning of S phase (reviewed by Bloom and Cross, 2007). For origins to fire throughout S phase, Clb5 must be present for all of S phase (Donaldson et al., 1998; McCune et al., 2008). The variation in origin firing time is established in coordination with the cell cycle—specifically during G1 phase (Raghuraman et al., 1997). A subset of replication proteins, Cdc45 and Sld3, associate with early firing origins in G1/early S phase but are not localized to late-firing origins until later in S phase (Aparicio et al., 1999; Kamimura et al., 2001). These observations, together with the knowledge that origin context is a driver of replication time, suggested that features of the genome established in a cell cycle-dependent manner dictate the time at which, and perhaps the degree to which, certain replication proteins interact with the assembling replisome, leading to variable origin activation time or efficiency. A better understanding of what types of features affect the complex choreography of replication complex assembly and activation would then allow for comprehensive tests of why such plasticity in origin activity is conserved among eukaryotes.

Currently, a wide variety of genome features are known to impact time or efficiency of replication origin activity. On a macro level, an origin's chromatin context has the greatest impact on its activity, although the complexities are not well understood (Rhind and Gilbert, 2013). For example, histone acetylation, which results in a more open chromatin structure and increased

accessibility of the nucleosome-bound DNA, is a hallmark of early firing origins. In contrast, deacetylated, or silenced chromatin, is associated with delayed or reduced origin activity (Aparicio et al., 2004; Knott et al., 2009; Stevenson and Gottschling, 1999; Vogelauer et al., 2002). While the mechanism of how histone acetylation modulates origin firing remains to be elucidated, it may affect more than one step of replication complex assembly. For example, at some origins, ORC binding seems to depend more on chromatin state than origin DNA sequence alone and that chromatin-dependence is correlated with early time of firing (Hoggard et al., 2013). Likewise, histone acetylation has also been shown to modulate the ability of the pre-replication complex to recruit other replisome components independent of ORC binding (Mantiero et al., 2011). In addition to histone acetylation, the forkhead transcription factors Fkh1 and Fkh2 also seem to play a regulatory role for origin activity (Knott et al., 2012). Fkh motifs are found near many origins of replication and binding of those sites by Fkh1/2 is thought to coordinate recruitment of Dbf4, the regulatory subunit of DDK, to those origins, thereby advancing their firing time (Fang et al., 2017).

Broad-scale chromatin features are not the only factors that regulate origin activity. Centromere-adjacent origins fire early in S phase because the kinetochore protein Ctf19 interacts directly with Dbf4, which is thought to create a higher concentration of DDK near centromere-adjacent origins and advance their time of replication (Natsume et al., 2013; Pohl et al., 2012). Telomeres replicate late in S phase. The telomere binding protein Rif1 recruits the phosphatase Glc7, which reverses the phosphorylation of the MCM2-7 helicase by DDK and delays time of origin firing near telomeres (Hiraga et al., 2014; Mattarocci et al., 2014). The efforts to understand regulators of origin activity have been somewhat piecemeal, and it would seem that no one "master regulator" of origin firing time has emerged from the various genome features shown to modulate

origin activity. In 2011, Mantiero, et al. published a model that brings these myriad observations together and provide a more comprehensive explanation for how these various locally-acting regulators of replication initiation interact on the scale of the entire genome. This model serves as the foundation for my thesis work and will be described in more detail in section 1.4.

1.2 Why Do Cells Prefer Origin Plasticity?

Even without a complete mechanistic understanding of how origin firing time and efficiency are regulated, the known influencing features can be manipulated to address the overarching question of *why* all eukaryotic organisms vary origin usage. While it has proven difficult to pinpoint any single explanation for why variable origin activity has been conserved so widely among eukaryotes, there are a number of attractive hypotheses. Firstly, it would seem evolutionarily advantageous for cells to maintain a reserve of dormant or later-firing origins that can be activated when replication stress results in stalled replication forks. Should replication forks fail to progress through a DNA lesion, an incoming fork activated later in S phase could potentially "rescue" a stalled replication fork and prevent chromosome breakage that results from incomplete replication (Blow et al., 2011; Rhind and Gilbert, 2013). This hypothesis is supported by the observation that the pre-RC is assembled at far more origins than actually fire during S phase, but titration of available MCM2-7 helicase causes increased ARS plasmid loss due to reduced replication initiation (Lei et al., 1996). Extrapolating from the plasmid loss observation, the presumption is that if the pre-RC is not assembled at enough potential origins, there may be inadequate initiation to fully replicate the entire genome or rescue the replication forks that invariably stall even during normal S phase (Bell and Labib, 2016; Lei et al., 1996).

In multicellular eukaryotes, locus-specific time of DNA replication varies with developmental stage and differentiated cells have characteristic patterns of early- and late-replicating regions that can vary widely between different cell types (Nordman and Orr-Weaver, 2012; Rhind and Gilbert, 2013). This cell type-specific variation may reflect the unique transcriptional programs of different cell types because the early-replicating parts of the genome tend to be more transcriptionally active than late-replicating regions (MacAlpine, 2004). The advent of chromosome conformation capture, or Hi-C, has also revealed that large-scale, self-interacting regions of chromosomes tend to have the same time of replication (Ryba et al., 2010). Late-replicating parts of the human genome also tend to have a higher mutation rate, suggesting that time of DNA replication can impact the stability of the genome (Koren et al., 2012). In these cases it is difficult to establish a causal relationship between time of DNA replication, transcriptional activity, or chromatin state, but it is clear that variance in replication is linked to the variance of other types of genome metabolism.

What is more evident, however, is how dysregulation of replication timing or efficiency can impact the genome. One of the clearest cases is from the earliest stages of embryogenesis leading up to the midblastula transition (MBT), or the point at which the developing embryo transitions from maternally-driven to embryonically-driven transcription (reviewed by Farrell and O'Farrell, 2014; Langley et al., 2014). The cells of the pre-MBT embryo divide rapidly and synchronously due to very fast S phase and an almost complete lack of gap phases. For example, pre-MBT *Drosophila melanogaster* embryos replicate their genomes in as little as 3.4 minutes, whereas genome duplication can take 8-10 hours in differentiated cells (Farrell and O'Farrell, 2014). Studies of DNA replication in these rapidly dividing cells suggest that replication efficiency is very high in all parts of the genome, allowing for such rapid DNA synthesis (Hyrien

et al., 1995; McKnight and Miller, 1977; Sasaki et al., 1999). At the MBT, however, the cell cycle slows dramatically, as does S phase and rate of DNA synthesis, and the shift to zygotic transcriptional program occurs. A seminal study of the MBT in *Xenopus laevis* revealed that the reduction in DNA replication initiation during the MBT results from the titration of four replication initiation factors (Collart et al., 2013). If titration of those four factors does not occur, replication initiation is not reduced, the cells continue to divide rapidly, and the embryos fail to develop. From the *Xenopus* study it is clear that the establishment of variation in origin activity is essential during embryogenesis in multicellular organisms. Interestingly, the yeast orthologs of those same four factors have a similar role in limiting replication initiation, the details of which will be discussed in section 1.4. Overexpression of those proteins, in addition to two other limiting replication initiation proteins, causes aberrant origin activity and also leads to viability defects in *S. cerevisiae* (Mantiero et al., 2011).

Some very recent work on the human genome hints that variation in DNA replication timing between individuals may underlie predisposition to certain diseases. A study aimed at finding human polymorphisms associated with variation in time of DNA replication (called replication time QTLs, or rtQTLs) successfully identified a number of *cis*-acting alleles that influence timing of origin activation (Koren et al., 2014). It also found that differences in time of origin firing near disease-associated genes may increase the mutation rate of those genes through replication-transcription conflict. As better quality whole genome sequencing data from more genetically-varied individuals become freely available, I anticipate that the genetic determinants of variation in DNA replication time and the implications for disease will become clearer. Regardless, while no single, overarching reason for variable replication initiation has been uncovered, it is an important facet of genome organization.

1.3 Is Replication Timing a Consequence of Origin Efficiency?

In recent years groups of researchers have made an effort to model the inherent variability of DNA replication based on the probability of an origin firing in S phase as the main determinant of origin firing time and efficiency (de Moura et al., 2010; Rhind, 2006; Yang et al., 2010). The fundamental supposition is that replication initiation is purely stochastic, that each origin has a different probability of firing, and that the differences in origin firing probabilities give rise to the emergent property of characteristic origin firing time and efficiency. By this logic, any features of the genome that increase the probability of an origin firing will likewise advance its time of replication. Dr. Nicholas Rhind states as much in a 2006 theory paper when he wrote, "If all of the origins [in region A of a chromosome] are more efficient that any of the origins [in a different region of the chromosome], the origins [in region A] will usually fire first and [region A] of the chromosome will replicate early." From that initial theory paper, the Rhind group has gathered modelling-based and experimentally-based evidence for a singular mechanism that determines origin firing probabilities and, therefore, time of origin activation and origin efficiency. Below, I will examine both the evidence supporting and the evidence refuting this model.

1.3.1 *Supporting evidence*

The evidence most often cited in favor of stochastic origin firing is a 2008 publication in which Czajkowsky et al. (2008) used bromodeoxyuridine (BrdU) pulse labeling of newly synthesized DNA in S phase-synchronized yeast cells followed by stretching the labeled DNA (DNA combing) and fluorescent microscopy to show random BrdU incorporation across the length of ChrVI. After labeling and purifying ChrVI, they grouped the stretched DNA fibers together based on percent BrdU-incorporation in lieu of being able to determine the time in S phase at which the BrdU was incorporated. Fluorescent probes for ChrVI were used to locate either the left or right arm of the

chromosome (but not both on the same molecule) and used to align the fibers among the grouped samples. Comparing where BrdU was incorporated along the length of the chromosome among 105 different fibers revealed seemingly random origin selection on each molecule. However, the authors claimed that by calculating the average BrdU incorporation in 1.25 kb intervals from the ensemble of ChrVI molecules, they were able to recapitulate the pattern of replication activity along the length of the chromosome observed in population-based DNA replication profiles of ChrVI.

Single molecule-based studies of new DNA synthesis are powerful tools for studying replication fork dynamics, but the stretching of the DNA fibers in these combing assays is not uniform along the length of the molecule. If there is a lot of variability in the fiber stretching, it is almost impossible to identify precise loci on the length of the chromosome and, therefore, to align the stretched fibers with much precision, as was done in this study. Additionally, it is impossible to know that the entire length of the full chromosome has been captured as breakage is prevalent in combing assays. The BrdU antibody that indicates where the thymidine analog is integrated on the chromosome has notoriously poor specificity, which may contribute to the seemingly random integration of BrdU on ChrVI. Most troubling, however, is that no negative or positive controls were shown. For example, as a positive control, labeling the chromosome for an entire S phase would have been helpful in determining how much "stochasticity of origin use" was simply due to poor detection of BrdU incorporation. Needless to say, the conclusions from this study should be taken with a hefty grain of salt.

Undeterred by this very shaky evidence for random origin firing, the Rhind group endeavored to use mathematical modelling to explain how stochasticity of replication initiation could give rise to patterns of origin use (Yang et al., 2010). They drew from genome-wide

replication profiling experiments from previously published work to estimate the probability of origins' firing. One of the highlighted findings from their probabilistic model is that late-firing origins should be less efficient than early-firing origins. They ascribe all variation in origin activation in their model to a single variable, writing that "We found that we could replace these empirical firing programs with a universal firing program that describes the behavior of each origin by a single parameter *n*, which suggests that a fundamental underlying mechanism regulates firing at all origins. Moreover, *n* can intuitively be interpreted as the number of initiators loaded at an origin in this [multiple-initiator model]." (Yang et al., 2010). In other words, the association of a specific replication protein at an origin increases its intrinsic probability of firing, so the more of that protein loaded at a single origin, the more likely that origin is to fire. They propose the MCM2-7 helicase complex to be this regulating initiator. It should also be noted that at the time this modelling study was completed, there was no *in vivo* evidence to suggest that more than one MCM2-7 double hexamer loads at an origin, although more recent studies suggest that this is a possibility (Gros et al., 2015; Ticau et al., 2015).

To prove that multiple MCM2-7 loading increases the likelihood of an origin firing, the Rhind group carried out a ChIP-seq study on the MCM2-7 complex and compared time of origin firing to ChIP signal (Das et al., 2015). They reported finding a correlation between ChIP signal and the previously-defined timing parameter *n* at known origins, which they concluded confirmed their hypothesis that the more MCM2-7 complexes loaded at an origin the higher the probability of origin firing (Das et al., 2015). However, this interpretation of ChIP data is troublesome because ChIP-seq measures the occupancy of a particular protein, not necessarily the number of molecules of that protein at specific loci (Pugh, 2010; Zentner and Henikoff, 2014). Additionally, the ChIP data themselves are somewhat questionable as they are not normalized to an input control, and

they report only the absolute read count from a single ChIP experiment. The MCM2-7 complex is challenging to ChIP with high confidence, probably because the complex slides freely on dsDNA (Gros et al., 2015). Additionally, no cross-validation of their findings using other MCM2-7 ChIP datasets or other measurements of replication time, besides their modelling-based parameter *n*, was shown, casting doubt on the universality of their findings. A second experiment using pull-down of a chromatinized plasmid is meant to support this finding, but it actually suffers from the same problem that plagues the interpretation of the ChIP data--it is challenging to quantify the number of molecules binding a DNA molecule without single molecule methods. The overreach in interpretation of these data stems primarily from assuming that high ChIP signal means more molecules of a protein complex. While I think it is possible that the strength of interaction between MCM2-7 and an origin could impact an origin's firing, these data do not in any way support that conclusion. In summary, while the stochastic model of origin firing is pleasing in its simplicity and parsimony, the evidence for a mechanism based on the number of MCM2-7 helicase complexes loaded is less so.

1.3.2 *Opposing evidence*

While, in my opinion, most of the published experimental evidence disagrees with a purely stochastic model for origin firing, I will highlight a few studies that I think illustrate why the details of this model are inaccurate. The main prediction of the stochastic origin firing model is that all late-firing origins are also inherently inefficient. However, the high efficiency of *ARS501*, the first origin demonstrated to fire late in S phase, directly contradicts that prediction (Ferguson et al., 1991). *ARS501*'s behavior may be an exception—what holds true on a genome-wide level?

According to the Rhind model for stochastic origin firing, in which the number of MCM2-7 molecules loaded at an origin determines both firing time and efficiency, efficiency and MCM2-

7 occupancy should be correlated. Until recently, no genome-wide origin efficiency data were available since most whole genome replication profiling methods are unable to definitively distinguish between efficiency and timing. McGuffee et al. (2013) developed a method to measure efficiency at every origin by deep sequencing Okazaki fragments and preserving the strand information, so that transition zones between leading and lagging strand synthesis contain capture the efficiency of an origin's firing. When McGuffee et al. (2013) compared their efficiency measurements with MCM2-7 ChIP data, they did not find any correlation. If origin efficiency and origin firing time are both related to the degree of MCM2-7 interaction at an origin, it is unexpected that no link between efficiency and MCM2-7 occupancy could be established.

A new study of DNA replication during zebrafish embryogenesis also provides an interesting example of uncoupled origin firing time and efficiency (Siefert et al., 2017). A comparison of whole genome sequencing-based replication profiles from pre-midblastula transition embryos and post-MBT embryos seemed to reveal no variation in origin firing time in the pre-MBT cells, which was in concurrence with previously published studies of pre-MBT DNA replication (Hyrien et al., 1995; Sasaki et al., 1999). However, when the replication profiles from the pre-MBT cells were scaled to reflect the extremely short length of S phase, Siefert et al. (2017) found that there are differences in replication time, and the pattern of earlier and later-replicating regions is very similar to the post-MBT origin firing pattern. Recall that prior to the MBT, origin firing efficiency is very high, which allows rapid passage through S phase. Thus the existence of variable replication time even when origin efficiency is uniformly very high hints that time and efficiency are independent types of DNA replication variation.

1.4 A Limiting Factor-Based Model for Variable Replication Time and Efficiency

If time and efficiency of origin activity are not simply explained by the number of MCM2-7 complexes loaded at each origin, then what is the mechanism of variable origin activity? In 2011, Mantiero et al. presented a new model for how variation in origin efficiency and timing is enforced across the yeast genome. Additionally, this model suggests a system in which more thorough tests of the interplay between origin time and efficiency can be carried out. From their work Mantiero et al. concluded that the abundance of four limiting replication initiation proteins combined with the varying ability of different parts of the genome to efficiently recruit those factors results in the pattern of origin use observed during DNA replication. Rather than hunting down locally-acting features of the genome that impact replication activity, as had been the approach of many previous replication time studies, Mantiero et al. began their study by asking whether there is enough of every replication protein required to initiate replication at every potential origin. They compared the relative cellular abundance of different replisome components and found that the initiation factors Sld2, Sld3, Dbf4, and Dpb11 are present at much lower concentration than other replication factors. Each of these four proteins, collectively termed the SSDD factors, must function at the assembling replication complex for an origin to fire, although none of them are required for replisome activity once it begins to synthesize dsDNA. In other words, these factors are required only for the initiation of DNA replication, not for the progression of replication forks as dsDNA is synthesized, i.e., the elongation phase of DNA replication. The interactions between the SSDD factors and the assembling replication machinery are depicted in [Figure 1.3]. The SSDD factors are shown in bold. The factors Sld2 and Sld3, the focus of my work, are highlighted in color. The relevant S phase kinases and their targets are also illustrated.

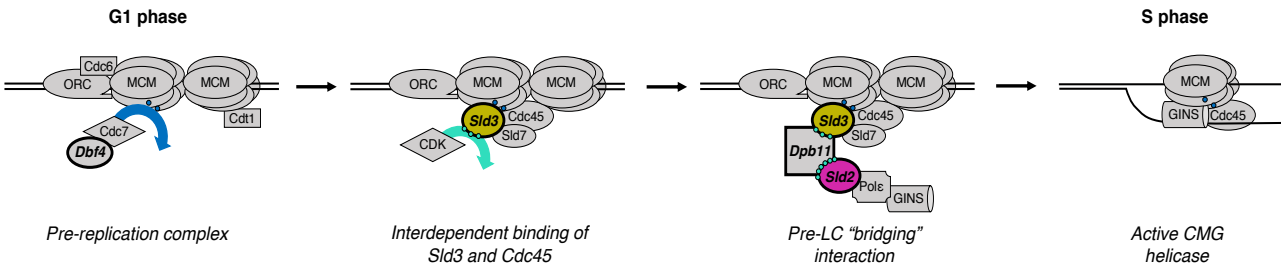

Figure 1.3. Sld2 and Sld3 at the assembling replisome.[3]

After identifying these low abundance proteins they tested whether the low abundance restricts origin firing by overexpressing them and assaying origin activity. Only when all four proteins were overexpressed simultaneously was replication timing advanced for a late-firing origin. They expanded upon this observation by determining the time of replication at six different loci using a density transfer experiment during SSDD overexpression and found that the time of replication was advanced at each location [Figure 1.4]. Intriguingly, even when the SSDD proteins are overexpressed there are still some observable differences in time of replication measured between those loci, meaning that there is still some variation in origin firing time. Also, the relative order of replication time is preserved between these loci, even though the time of replication relative to the start of S phase is advanced for each. Based on the fact that two additional replication proteins, Cdc45 and Sld7, associate preferentially with early firing origins, and that

[3] The progression from the pre-replication complex (pre-RC) to the active replicative CMG helicase (Cdc45 – MCM2-7 – GINS) is illustrated. Sld2 and Sld3, the two initiation factors that are the focus of my work, are shown in purple and gold, respectively. The other limiting initiation factors, Dbf4 and Dpb11, are labeled in bold italic type. The main kinase complexes required for replication initiation, DDK and CDK, and their phosphosites are shown as small blue and aqua circles on targeted replisome components. DDK is required first to phosphorylate MCM2-7, which allows for the interdependent interaction of Sld3, Cdc45, and Sld7 with the replication complex. Next, S-CDK phosphorylates Sld3 and Sld2 (which is not depicted here), to promote their interactions with Dpb11. Through the bridging interaction of Dpb11 with Sld2 and Sld3, the pre-loading complex components (Sld2, Dpb11, Polε, and GINS) are brought into association with the replisome. Through this interaction with the pre-LC, the GINS complex is integrated into the replisome and the CMG helicase is assembled. The mechanism of CMG assembly from the pre-LC phase is not known. CMG is the active form of the replicative helicase and is the commitment step to initiation of replication. Note that some of the essential replisome components, such as Mcm10 and RPA, are excluded from this illustration. Also, all phosphorylation events and initiation factor interactions occur at both MCM2-7 helicase hexamers, but in the interest of simplicity, I am showing only the interactions at one hexamer.

their association depends on Sld3, they tested whether the low levels of these two additional proteins also limit origin activity (Itou et al., 2014; Kamimura et al., 2001; Tanaka et al., 2011a). [Again, see Figure 1.3 for how Cdc45 and Sld7 interact with the replication machinery.] The combination of overexpressing Cdc45 and Sld7, in addition to the primary limiting SSDD proteins, increased efficiency of origin firing, although the overexpression of these additional factors did not advance replication time more than what was already observed when only the four main SSDD proteins were overexpressed.

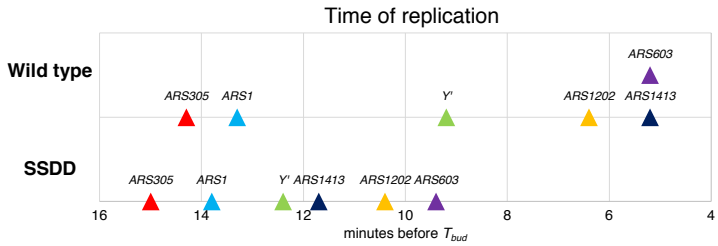

Figure 1.4. Advancement of replication time when SSDD factors are overexpressed.[4]

Despite the overall advancement of origin firing time and increased efficiency observed when the six initiation factors, together referred to as SSDDCS, were overexpressed, the few origins that reside in silenced regions of the yeast genome were still inactive. To determine whether this dormancy was caused by the silent chromatin state of those regions, they deleted the histone deacetylase *RPD3* and found that, when SSDDCS were overexpressed, even those normally inactive origins were able to fire. From this series of observations, Mantiero et al. concluded that the combination of chromatin state, which could modify the accessibility of the

[4] Time of replication at six specific loci as determined by density transfer analysis. Replication time is shown relative to time of budding. The disparity in replication time observed in WT is reduced when the SSDD factors are overexpressed simultaneously. While the timeframe for replication time is compressed, the relative order of replication is broadly the same between the two conditions. Figure adapted from (Mantiero et al., 2011).

limiting initiation factors to interact with the replication complex at origins, and the abundance of the limiting initiation factors result in variation in origin firing time and efficiency [Figure 1.5].

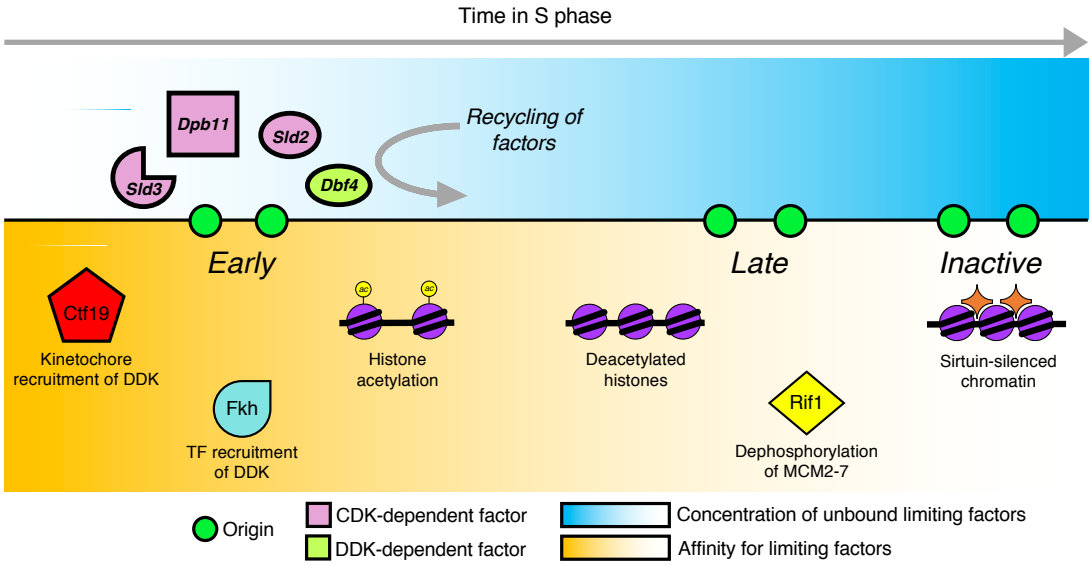

Figure 1.5. The limiting SSDD factor model for variable origin firing time and efficiency.[5]

1.5 Do Individual SSDD Factors Influence Both Origin Firing Time and Efficiency?

Based on the model for variation in replication origin firing time and efficiency presented by Mantiero et al., for my thesis work, I wanted to determine whether the association of individual SSDD factors with the assembling replisome contributes to both time of origin activation and origin efficiency. Considering that each of the SSDD factors interacts with the replisome at

[5] I have combined the model presented by Mantiero et al., with current knowledge of genome features that influence origin firing time and efficiency. In the limiting SSDD model, Mantiero et al. suppose that different parts of the genome have a higher affinity for recruitment of the SSDD proteins than others. For example, in early S phase, only origins with a high affinity for SSDD factors, such as those near centromeres, with Fkh sites, and more open chromatin state are able to recruit the limiting proteins. Since the limiting factors do not travel with the replication fork, the SSDD proteins are released from the active replisome, presumably increasing the concentration of freely available limiting factors as the earliest firing origins become active. The limiting factors can then be re-phosphorylated and recycled to promote origin firing in parts of the genome with lower affinity for those proteins, such as regions with deacetylated histones, high local Rif1 activity, or silenced chromatin.

different times and with different components of the complex [Figure 1.3] (reviewed by Bell and Labib, 2016), it seemed possible that individual limiting factors have different roles in contributing to time of origin activation and origin efficiency (Mantiero et al., 2011). My goal was to reduce the abundance of specific SSDD factors, one at a time, then assay DNA replication genome-wide to test whether those factors contribute to both time and efficiency of origin activity. These genome-wide assays for changes to replication time and efficiency would also allow me to test one of the main predictions of the stochastic model for origin firing—that origin efficiency and timing are interlocked features, and a change to one will necessarily impact the other.

Due to technical considerations, I focused my work on reducing the abundance of a subset of initiation factors—Sld2 and Sld3. (See Methods for more information.) However, given that Sld2 and Sld3 associate with the replisome at different points during the cell cycle and interact with distinct proteins within the replication complex (Kamimura et al., 2001; Tanaka et al., 2011a), I was satisfied that a study of just those factors could provide insights into how the SSDD proteins contribute to variation of replication initiation. In the following section, I will provide more detailed information on the different roles of Sld2 and Sld3 in promoting replisome assembly and activation.

1.6 The Roles of Sld2 and Sld3 in Promoting DNA Replication Initiation

The *SLD2* and *SLD3* genes were identified in the same forward genetic screen for suppressors of a temperature sensitive mutant of *DPB11* which is an essential DNA replication protein (Araki et al., 1995; Kamimura et al., 1998). The initial characterization of Sld2 revealed that it interacts directly with Dpb11, its expression is upregulated during S phase, and it is required for normal DNA replication (Kamimura et al., 1998). Sld3 was not the focus of that initial paper, but later

work revealed that Sld3 interacts directly with Cdc45 and that it is also required for normal DNA replication (Kamimura et al., 2001). Like Cdc45, Sld3 preferentially associates with early-firing origins as cells transition from G1 to S phase (Aparicio et al., 1997; Kamimura et al., 2001). Kamimura et al. (2001) also found that as cells progress through S phase, Sld3 is no longer present at early firing origins but instead associates with later-firing origins. That time-dependent variation in origin association first suggested that Sld3 is involved in executing the time of DNA replication (Kamimura et al., 2001).

Later work established that Cdc45 and Sld3 are recruited to origins at the same time, because DDK-dependent phosphorylation of the MCM2-7 complex results in interdependent recruitment of Sld3 and Cdc45 to the helicase [Figure 1.3] (Heller et al., 2011; Kanemaki and Labib, 2006). Sld7, a non-essential replication initiation factor, stabilizes the interaction between Sld3 and the MCM2-7 complex, while simultaneously destabilizing the interaction between Cdc45 and Sld3 (Tanaka et al., 2011b). These opposing functions suggest that Sld7 facilitates the dissociation of Sld3 from the replisome, as Sld3 does not travel with the active replication complex at replication forks, but Cdc45 does (Tanaka et al., 2011b). Instead, the dissociated Sld3 may coordinate assembly and initiation of replication complexes at later-firing origins. It should be noted that while Sld3's association with the MCM2-7 complex depends solely on DDK phosphorylation of MCM2-7, Sld3 itself is phosphorylated by the S-CDKs (Zegerman and Diffley, 2007).

Both Sld2 and Sld3 are targets of the S phase CDKs, and phosphorylation of the two factors is essential to replication initiation (Masumoto et al., 2002; Tanaka et al., 2007; Zegerman and Diffley, 2007). Phosphorylation of Sld2 results in the formation of the pre-loading complex, which consists of Sld2, Dpb11, Polε, and the GINS complex (Muramatsu et al., 2010). Phosphorylation

of Sld3 promotes its interaction with Dpb11 and, through that interaction, the rest of the pre-loading complex (Tanaka et al., 2007; Zegerman and Diffley, 2007). It is thought that the S-CDK-dependent interaction between Sld3, Dpb11, and Sld2 brings the GINS complex into association with the replisome, although the specifics of how GINS is ultimately coordinated into the replisome are unknown. This "bridging" interaction is depicted in Figure 1.3. Regardless, GINS must be integrated into the replisome, in complex with Cdc45 and MCM2-7, for an origin to fire (Ilves et al., 2010).

Once the complex of Cdc45, MCM2-7, and GINS (known as the CMG helicase) is assembled, it immediately begins to unwind DNA [Figure 1.3], thus regulation of its assembly is crucial for ensuring that initiation of DNA replication occurs only during S phase (Douglas et al., 2018; Ilves et al., 2010). The abundance of Sld2 and its phosphorylation state are important regulatory mechanisms that prevent aberrant activation of the CMG helicase in other phases of the cell cycle (Bloom and Cross, 2007; Reusswig et al., 2016; Tanaka and Araki, 2011). Sld3 also serves as an important point for regulation of initiation. Sld3, along with Dbf4, is a target of the S phase checkpoint, and inhibition of those factors in response to checkpoint activation prevents late-origin firing during DNA replication stress [Zegerman and Diffley, 2010; Lopez-Mosqueda, 2010] (Lopez-Mosqueda et al., 2010; Zegerman and Diffley, 2010). See the following section for more details about the S phase checkpoint.

Both Sld2 and Sld3 have metazoan orthologs. Sld2, while not as highly functionally conserved as other replication proteins, is known as RecQ4 or RecQL4 in higher eukaryotes (Sangrithi et al., 2005). RecQ4 is present in humans and, in addition to having helicase function, plays a role in replication initiation (Capp et al., 2009; Matsuno et al., 2006; Sangrithi et al., 2005). Unlike Sld2, Sld3 and its role at the replisome seem to be more conserved between yeast and

metazoans (Boos et al., 2011; Sanchez-Pulido et al., 2010). In humans, the Sld3 ortholog is known as Treslin, and it interacts with the human Dpb11 ortholog, TopBP1, to promote initiation of DNA replication in much the same way that those two proteins interact in yeast (Boos et al., 2011; Mueller et al., 2011).

1.7 Additional Background Information

My thesis work deals mostly with questions about timing and efficiency of origin firing, but also how origin timing and efficiency impact genome stability. In this section, I will provide some background information relevant to genome stability as well as the rDNA locus of the yeast genome.

1.7.1 *The S phase checkpoint*

The DNA replication process, while of fundamental importance to actively proliferating cells, is a risky prospect as it provides a window of opportunity for genome instability (reviewed in Branzei and Foiani, 2010). The regions of single-stranded DNA at each replication fork are particularly susceptible to damage that can lead to the formation of double stranded breaks (Feng et al., 2007). Uncoupling of the replicative helicase from the rest of the replication complex, which can occur as a consequence of replication stress, exposes larger single-stranded regions at the replication fork than are found during an uninterrupted S phase (Byun, 2005; Sogo et al., 2002). Cells have evolved an S phase checkpoint that, when activated, delays the onset of mitosis, presumably until cells are able to resolve the problem inhibiting normal passage through S phase (Paulovich and Hartwell, 1995; reviewed by Segurado and Tercero, 2009). Activation of the checkpoint depends on accumulation of RPA-coated ssDNA at replication forks, which is sensed at the fork by Mec1.

Mec1 signaling is transduced by Mrc1, leading to phosphorylation of the main S phase checkpoint effector, Rad53 (Segurado and Tercero, 2009). Testing for the phosphorylation of Rad53 is a reliable method for determining if the S phase checkpoint has been activated.

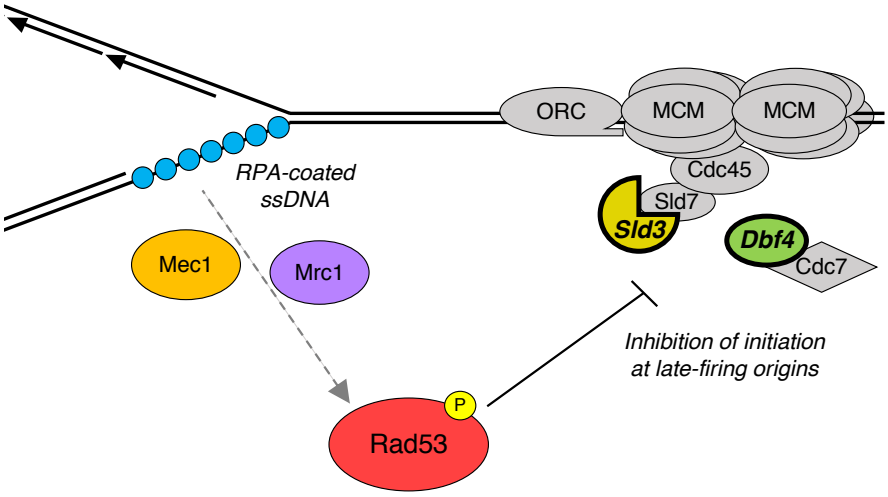

Figure 1.6. Phosphorylation of Rad53 in response to activation of the S phase checkpoint.[6]

One important feature of the S phase checkpoint is that its activation requires a threshold of replication forks be present in a cell for the checkpoint to become triggered (Shimada et al., 2002; Tercero et al., 2003). Another important feature of the checkpoint is that it prevents later-firing origins from initiating DNA replication (Santocanale and Diffley, 1998). This inhibition is accomplished by inhibitory phosphorylation of Sld3 and Dbf4, two of the SSDD limiting initiation factors, as a result of Rad53 phosphorylation (Zegerman and Diffley, 2010). It should also be noted that, at this time, there does not seem to be a mechanism to prevent onset of mitosis in the case of incomplete DNA replication. Cells in which the S phase checkpoint is constitutively active will eventually die (Foiani et al., 2000; Zhang and Hunter, 2014). Cells that cannot activate the S

[6] Accumulation of RPA-coated ssDNA at replication forks triggers activation of the S phase checkpoint, which results in phosphorylation of Rad53. Rad53 phosphorylation status is a useful indicator of whether the checkpoint has been activated. S phase checkpoint activation inhibits Sld3 and Dbf4 activity, thereby preventing late-firing origins from firing. Figure adapted from Segurado and Tercero (2009).

phase checkpoint will continue through mitosis, regardless of whether or not chromosomes are fully replicated, resulting in double-stranded breaks and mitotic catastrophe (Feng et al., 2011).

1.7.2 *The rDNA locus and its role in DNA replication*

The highly repetitive nature of the rDNA locus in *S. cerevisiae* renders it an unusual landscape for DNA replication compared to the rest of the yeast genome. All ribosomal DNA repeats are found at a single locus on the right arm of Chromosome XII (Petes, 1979; reviewed by Venema and Tollervey, 1999; Woolford and Baserga, 2013). Yeast strains typically carry 100 – 250 copies of the 9.1 kb tandem repeats, each of which codes for the 5S, 5.8S, 25S, and 18S ribosomal RNAs (Venema and Tollervey, 1999). Each repeat also contains an origin of replication in the non-transcribed region found between the divergently transcribed rDNA coding genes [Figure 1.7]. A replication fork barrier (RFB) sequence is found at the 3' end of the large 35s rDNA unit and is bound by the protein Fob1 (Brewer and Fangman, 1988; Kobayashi, 2003). The RFB impedes replication forks that would pass through the rDNA genes in the direction that is opposite to 35s transcription, thereby preventing replication-transcription conflicts (Brewer and Fangman, 1988; Kobayashi, 2003).

Outside of the rDNA locus, the yeast genome has very few repetitive DNA elements compared to other eukaryotes (Goffeau et al., 1996). In terms of genome content, the rDNA accounts for ~10% of the yeast genome, but rather large variations in terms of copy number are tolerated with very few discernible biological costs (French et al., 2003; Kobayashi et al., 1998). The high density of potential sites of DNA replication initiation is also unique—one origin every 9.1 kb, and hundreds of origins packed into 1-2 Mb of DNA where elsewhere in the yeast genome,

origins are found more sparsely [Figure 1.7] (Ferguson et al., 1991; Friedman et al., 1997; Venema and Tollervey, 1999). In addition to the unusually high density of origins within the rDNA, each rDNA origin resides in the same sequence context as all of the other rDNA origins. This organization means that any replication defects related to the sequence of the rDNA origin would impact every rDNA origin, potentially destabilizing a huge portion of the largest yeast chromosome.

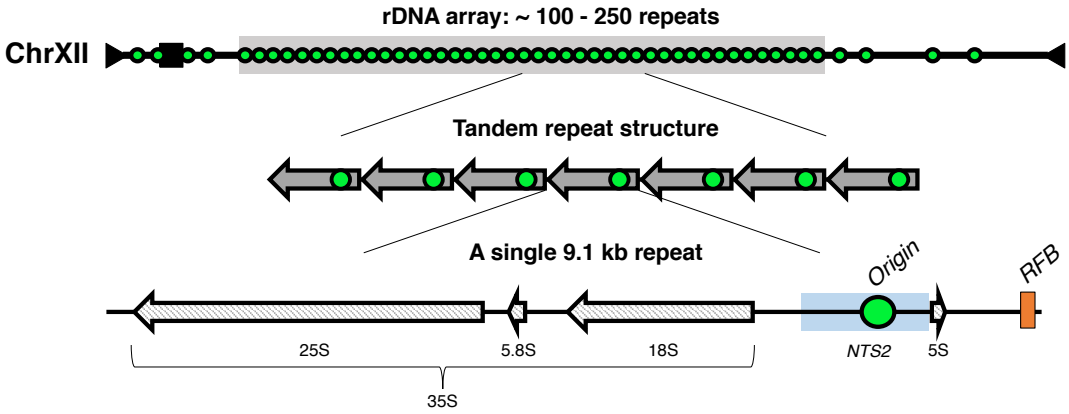

Figure 1.7. The rDNA locus in *Saccharomyces cerevisiae*.[7]

Indeed, partial loss of function mutations in replication initiation proteins have been shown to disrupt the stability of chromosome XII through their effect on the rDNA locus (this study; Ide et al., 2007; Sanchez et al., 2017). Moreover, mounting evidence suggests that features of the rDNA locus can influence DNA replication as a whole. For example, rDNA origin sequence and silencing of rDNA chromatin, may influence how DNA replication is carried out throughout the rest of the yeast genome (Kwan et al., 2013; Yoshida et al., 2014). The full impact of the unusual

[7] The rDNA locus is shown approximately to scale on this illustration of ChrXII. Origins are shown as green circles. Not all known origins are depicted on ChrXII. The number of rDNA repeats varies by strain background. The tandem repeat structure of the locus is shown below the full-length chromosome. The arrow indicates the direction of replication and transcription, and the location of the origin within each repeat. A single 9.1 kb rDNA unit is shown at the bottom. rDNA genes are labeled, as is the origin and the RFB. The origin resides within one of the non-transcribed spacers, *NTS2,* also shown here. All Southern blots of the rDNA region in this thesis are probed for *NTS2*.

structure of the rDNA locus on DNA replication of the non-repetitive parts of the genome is still unclear. Ongoing work in our lab is aimed at dissecting the influence that rDNA origin sequence and rDNA copy number may exert over DNA replication across the entire yeast genome.

Chapter 2. EXPERIMENTAL METHODS

The model organism *Saccharomyces cerevisiae* is a powerful tool for studying the interplay between *cis*- and *trans*-acting features that influence DNA replication. The budding yeast genome is compact, at 12.1 Mb, and well-annotated. There are bountiful and effective molecular tools for manipulating that genome and its translational products, the proteome. The cell cycle is easily synchronized, and generation time is short, which allows for the study of coordinated S phase progression in a large population of cells on a practical timescale. The high degree of conservation of DNA replication factors across Eukarya further justifies yeast as an ideal model system for the study of DNA replication. For my work, budding yeast provided an ideal biological framework for manipulating the abundance of specific replication initiation factors and following changes in replication origin activity across the genome.

To reduce the cellular pools of the essential Sld2 and Sld3 initiation factors, I used the auxin inducible degron (AID) system. Introduction of a C-terminal degron domain to the target protein and galactose-induced expression of an E3 ubiquitin ligase derived from *Oryza sativa* enables inducible ubiquitylation of the degron domain in response to the addition of the plant hormone auxin, resulting in proteasomal degradation of the protein [Figure 2.1] (Nishimura et al., 2009). I also attempted to construct Dbf4 and Dpb11 auxin inducible degron strains but was not successful; I suspect that the degron tag interfered with the important biochemical features of the C-termini of those proteins (Natsume et al., 2013; Zegerman and Diffley, 2007). While temperature sensitive alleles of the SSDD factors are available, I favored uniformity in the mechanism of depleting these proteins. Additionally, in engineering my own strains, I would be assured of a consistent genetic background. My main resource for constructing, verifying strains, and determining growth conditions was the *Current Protocols in Cell Biology* chapter “Rapid

Depletion of Budding Yeast Proteins via the Fusion of an Auxin-Inducible Degron (AID)" (Nishimura and Kanemaki, 2014). However, I empirically determined the time of galactose and auxin induction most appropriate for my experiments, which often required α-factor synchronization of S phase. See Appendix A for more information on how these parameters were established.

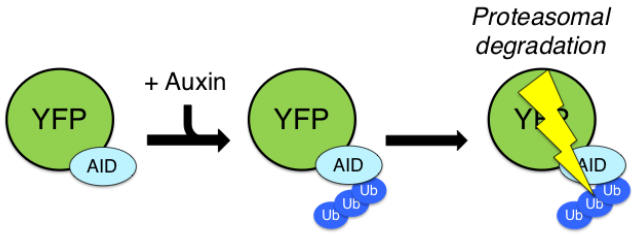

Figure 2.1. Targeted protein degradation using the auxin inducible degron (AID) system.[8]

I used two different genome-wide DNA replication assays in this study to classify how reduced replication initiation resources impact the pattern of origin firing. Initially, I used the single-stranded DNA mapping assay, which reveals the pattern of origin use in early S phase and also provides information about replication fork dynamics (Feng et al., 2006, 2011). Since cells are treated with hydroxyurea (HU) before a synchronous S phase, this method captures initiation activity at origins that fire in HU, which corresponds roughly to the first half of S phase. As this project progressed, I realized that a genome-wide assay for replication activity would also be necessary. Consequently, I followed up the ssDNA assay method with a whole-genome sequencing (WGS) approach. While the spatiotemporal resolution of the WGS-based method, which is based on genome-wide differences in copy number that are due to differences in origin firing time and efficiency, is not as precise as the ssDNA method, the trade-off was that WGS

[8] The presence of the C-terminal auxin inducible degron domain (AID) on a target protein is the basis of inducible degradation at the proteasome. Additionally, an E3 ubiquitin ligase, TIR1, which is derived from *Oryza sativa,* must be expressed under the GAL1-10 promoter in order for recognition and ubiquitylation of the AID domain.

allowed me to assay replication activity for all of S phase. Methodological details for both techniques are described below.

2.1 Strain Construction and Verification

I constructed all strains for this study from *S. cerevisiae* strain W303 *rad5*Δ *MATa.* W303 is used as a wild-type (WT) control throughout. I used a standard yeast lithium acetate transformation for all genetic transformations. I constructed the auxin inducible degron (AID) strains by integrating a linearized plasmid containing a cassette with *Os*TIR1-9myc under the *GAL1-10* promoter at the *URA3* locus. Using homologous recombination, I then C-terminally tagged the Sld2 and Sld3 proteins with the 3xmini-AID domain. I confirmed correct integration of the AID domain both by PCR and Southern blot. Where appropriate, I performed parallel experiments using a strain containing only the *GAL1-10-Os*TIR1-9myc component of the AID system (referred to as the "AID parent strain") to confirm that there were not off-target effects on DNA replication, cell cycle progression, etc. caused by expression of the foreign ubiquitin ligase. Takashi Kubota and Anne Donaldson at the University of Aberdeen generously gave me the auxin degron plasmids. I tested the effects of protein degradation by spot-testing strains on yeast synthetic complete medium (YC) + 1% raffinose + 2% galactose + 0.5 mM auxin plates, and then confirmed those results by flow cytometry experiments for delayed or slowed S phase in auxin-treated cultures. My attempts to detect degron-tagged protein abundance by western blot were unsuccessful, likely due to the low abundance of Sld2 and Sld3 and poor anti-degron antibody specificity. I constructed the *RAD53*-2xHA tagged versions of the AID strains by integrating linearized plasmid containing a partial copy of *RAD53* with the HA tag at the endogenous locus. The Bedalov lab at the Fred Hutchinson

Cancer Research Center shared the *RAD53*-2xHA tagging plasmids with our lab. See Table 2.1 for complete list of strains used in this work.

Table 2.1. Yeast strains

Strain name	Background Strain	Ploidy	Genotype	Mating type	rDNA copy number
WT	W303	Haploid	*ura3-1 leu2-3,112 his3-11 trp1-1 can1-100 ade2-1 bar1-1*	a	~250
AID Parent	W303	Haploid	*leu2-3,112 his3-11 trp1-1 can1-100 ade2-1 bar1-1 ura3-1*::*GAL1*-OsTIR1-9myc-*URA3*	a	~250
SLD2-AID	W303	Haploid	*leu2-3,112 his3-11 trp1-1 can1-100 ade2-1 bar1-1 ura3-1*::*GAL1*-OsTIR1-9myc-*URA3 SLD2*-3xminiAID-*KANMX6*	a	~250
SLD3-AID	W303	Haploid	*leu2-3,112 his3-11 trp1-1 can1-100 ade2-1 bar1-1 ura3-1*::*GAL1*-OsTIR1-9myc-*URA3 SLD3*-3xminiAID-*KANMX6*	a	~90
AID Parent *RAD53*-2xHA	W303	Haploid	*leu2-3,112 his3-11 trp1-1 can1-100 ade2-1 bar1-1 ura3-1*::*GAL1*-OsTIR1-9myc-*URA3 RAD53*-2xHA-*TRP1*::*RAD53*	a	~190
SLD2-AID *RAD53*-2xHA	W303	Haploid	*leu2-3,112 his3-11 trp1-1 can1-100 ade2-1 bar1-1 ura3-1*:: *GAL1*-OsTIR1-9myc-*URA3 SLD2*-3xminiAID-*KANMX6 RAD53*-2xHA-*TRP1*::*RAD53*	a	~115
SLD3-AID *RAD53*-2xHA	W303	Haploid	*leu2-3,112 his3-11 trp1-1 can1-100 ade2-1 bar1-1 ura3-1*:: *GAL1*-OsTIR1-9myc-*URA3 SLD3*-3xminiAID-*KANMX6 RAD53*-2xHA-*TRP1*::*RAD53*	a	~140
SLD3-AID *Os*TIR1⁻ Clone #1	W303	Haploid	*leu2-3,112 his3-11 trp1-1 can1-100 ade2-1 bar1-1 ura3-1 SLD3*-3xminiAID-*KANMX6*	a	~70
SLD3-AID *Os*TIR1⁻ Clone #2	W303	Haploid	*leu2-3,112 his3-11 trp1-1 can1-100 ade2-1 bar1-1 ura3-1 SLD3*-3xminiAID-*KANMX6*	a	~60
AID Parent *clb5Δ*	W303	Haploid	*leu2-3,112 his3-11 trp1-1 can1-100 ade2-1 bar1-1 ura3-1*::*GAL1*-OsTIR1-9myc-*URA3* clb5Δ::*TRP1*	a	~200
SLD2-AID *clb5Δ*	W303	Haploid	*leu2-3,112 his3-11 trp1-1 can1-100 ade2-1 bar1-1 ura3-1*:: *GAL1*-OsTIR1-9myc-*URA3 SLD2*-3xminiAID-*KANMX6* clb5Δ::*TRP1*	a	Not determined
SLD3-AID *clb5Δ*	W303	Haploid	*leu2-3,112 his3-11 trp1-1 can1-100 ade2-1 bar1-1 ura3-1*:: *GAL1*-OsTIR1-9myc-*URA3 SLD2*-3xminiAID-*KANMX6* clb5Δ::*TRP1*	a	<90

2.2 Galactose and Auxin Induction of AID Strains

Unless noted, all liquid culture was in yeast synthetic (YC) medium. For asynchronous growth experiments, I grew the cells in YC + 1% raffinose (YCR) medium until early log phase growth and transcriptionally induced with 2% galactose for 3 hours before inducing depletion of the degron-tagged target protein by adding 0.5 mM auxin (IAA) for 2 hours. I collected samples at relevant time intervals and then compared them to the no-auxin control [Figure 2.2]. Unless specified, negative controls are the degron strain without auxin treatment. As required, I diluted cultures to a lower cell density during galactose induction to maintain mid-log phase growth. For synchronous S phase experiments, I grew cultures in YCR media to early log phase, then synchronized them with 3 μM α-factor for 3.5 hours. Thirty minutes after α-factor, I added galactose at 2% concentration. One hour before release, I split the cultures in half and treated one portion with 0.5 mM auxin. I released the two cultures simultaneously by adding

pronase to a final concentration of 0.3 mg/ml. I collected flow cytometry samples for every experiment, both synchronized and asynchronous cultures, to verify G1 arrest, release from arrest, and S phase progression.

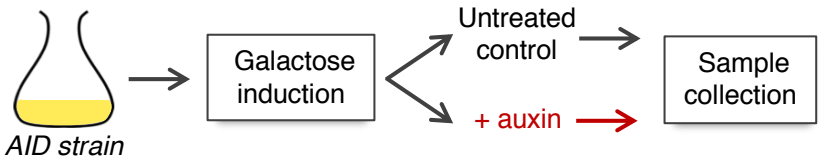

Figure 2.2. General outline for AID strain experiments.

2.3 Flow Cytometry

I collected one mL of culture per sample by treating the cells with 5 µl 10% sodium azide and fixing them in 70% EtOH. I washed the fixed cells with 20 mM sodium citrate, then sonicated them. When required, I set aside a portion of fixed cells for budding analysis to confirm release from α-factor arrest. I treated the remaining washed cells with 10 µg/ml RNase A for one hour at 50°C, then 0.5 mg/ml proteinase K for one hour at 50°C before adding SYTOX Green Dead Cell Stain (ThermoFisher). I measured 10,000 events per sample on an BD FACSCanto flow cytometer, and analyzed the resulting data using FlowJo software. In general, I gated all samples from a single time course experiment based on the uninduced asynchronous culture of an individual strain.

2.4 Growth and Viability Assays

To determine viability by plating for colony-forming units (CFUs) at timed intervals during asynchronous growth experiments, I plated 300 cells in triplicate on YEPD and grew the plates for 2 days before counting colonies. For spot-testing, I suspended the cells in water, sonicated them,

then serially diluted them in a 1:3 ratio. I pipetted 5 μl spots of each dilution onto appropriate plates and grew them at 30°C. I photographed the plates each day until the spots were overgrown.

2.5 Western Blotting

I grew the AID strains containing the *RAD53*-2xHA construct to mid-log phase and collected ~4.0 x 10^7 cells for each sample. I treated the strains with 0.1% MMS as a positive control for Rad53 phosphorylation. I extracted protein by bead beating in SUMEB pH 6.8 (1% SDS, 8 M Urea, 10 mM MOPS pH 6.8, 10 mM EDTA, and 0.01% bromophenol blue) plus ThermoFisher protease inhibitor cocktail and 5% 2-Mercaptoethanol. I loaded ~15 μg protein from each sample per lane. I ran 7% tris-acetate protein gels in tris-acetate SDS running buffer for 1 hour and 25 minutes, then transferred the gels in ThermoFisher NuPAGE transfer buffer for 1 hour and 10 minutes at 4° C. I confirmed transfer and protein loading by Ponceau stain. I blotted the membranes overnight at 4°C with 1:2500 α-HA primary antibody conjugated to HRP or 1:5000 α-GAPDH primary antibody conjugated to HRP as a loading control. I developed the blots using ThermoFisher SuperSignal West Dura Extended Duration Substrate and exposed them to film.

2.6 ssDNA Mapping Assay for Origin Activity

I used the ssDNA mapping assay used to detect replication activity genome-wide in the *SLD2*-AID and *SLD3*-AID strains (Feng et al., 2006, 2011). I performed a parallel experiment on a WT control (W303). I grew the cultures to OD_{660} = 0.25, then α-factor arrested them, induced ligase expression with galactose, and added auxin as above. I grew the WT cells in YC + 2% glucose, not in raffinose medium. I collected an equivalent volume of G1-arrested cells before release from

α-factor arrest as was collected during S phase. At the time of collection, I chilled the cells with frozen 0.1% sodium azide + 0.025 M EDTA (final concentrations), pelleted them, and then embedded them in 1% low melt agarose plugs. To the remaining culture, I added 200 mM final concentration hydroxyurea (HU) ten minutes before release. I collected 50 mls of culture volume at each time interval—30, 60, 90, and 120 minutes after release. I prepared the G1 and S phase samples for *in gelo* ssDNA labeling as detailed by Feng et al., (2011). For each timed sample, I co-hybrized one G1 and one S phase sample to an Agilent ChIP-on-chip 4x44 *S. cerevisiae* microarray [Figure 2.3]. I processed and normalized the array data as described in Feng, et al. 2006, and then Loess smoothed over a 6 kb window to generate replication profiles [Figure 2.3].

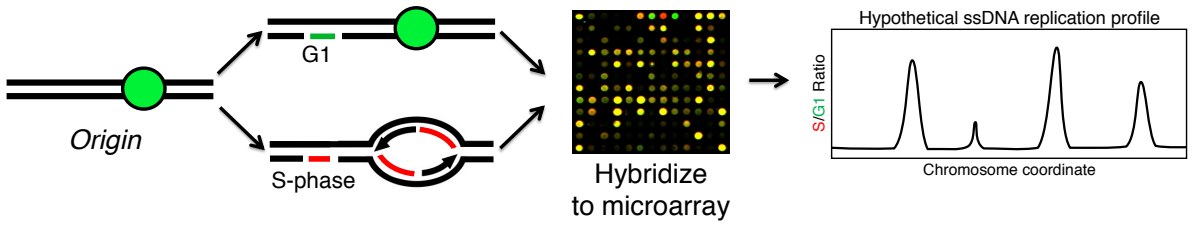

Figure 2.3. ssDNA mapping assay.[9]

2.6.1 *ssDNA Assay Peak Area and Peak Width*

To detect changes in origin usage during initiation factor-depleted S phase, I calculated the areas under the curve at known origins for each ssDNA mapping assay dataset. The pairwise comparisons of the origin peak areas between control and reduced initiation factor datasets revealed whether the same set of origins were active under the different conditions. I used a custom Python script written by Elizabeth Kwan, Ph.D., to calculate the origin peak areas (Sanchez et al.,

[9] Small regions of ssDNA are present at the replication fork during S phase. Co-hybridization of fluorescently-labelled S phase ssDNA (shown in red) and G1 ssDNA (shown in green) to microarray reveals enrichment of ssDNA at active origins. Mapping the S/G1 ssDNA ratio along each chromosome reveals peaks where origins are active.

2017). Additionally, I determined the peak width at half the maximum peak height for each of the origins detected in the ssDNA assay data. Peak width indicates replication fork movement (Sheu et al., 2014). To determine whether significant changes in replication fork movement occurred after depletion of initiation factors, I compared the distributions of two sets of peak width data using an unpaired Wilcoxon rank sum test in R. Peak widths are rounded to the closest 500 bp interval in the Python script, so some width values are rounded down to 0 bp. I excluded those 0 values from the distribution analysis.

2.6.2 *Defining the Set of Origins Used in the Peak Area and Peak Width Analysis*

For the peak area and width calculations, I started with the list of known origins from the DNA Replication Origin Database OriDB (http://cerevisiae.oridb.org/) (Siow et al., 2012). OriDB is an online database of all known origins, approximately 700 loci, in *S. cerevisiae*. Since not all origins fire during S phase in HU, this full list OriDB origins was not appropriate to use for the peak area and peak width analysis as peaks would be "overcalled". To exclude inactive origins from this analysis, I created a reduced set of origins to use based on the WT control data. I excluded origin peaks with maximum height less than 3 standard deviations above the average S/G1 ssDNA ratio in the WT dataset. I confirmed this cutoff by comparing the origin peak area values from the uninduced *SLD2*-AID dataset with the WT peak areas, as well as between the *SLD3*-AID no auxin and WT sets of peak areas [Figure 2.4]. If a subset of origins were unable to fire in the uninduced degrons strains, a number of peak area data points would be located along the X axis. Few origins fall into this category, and the correlations between the uninduced degron strains and WT origin peak values were high, I therefore concluded that the WT-derived set of origins was appropriate for subsequent analysis.

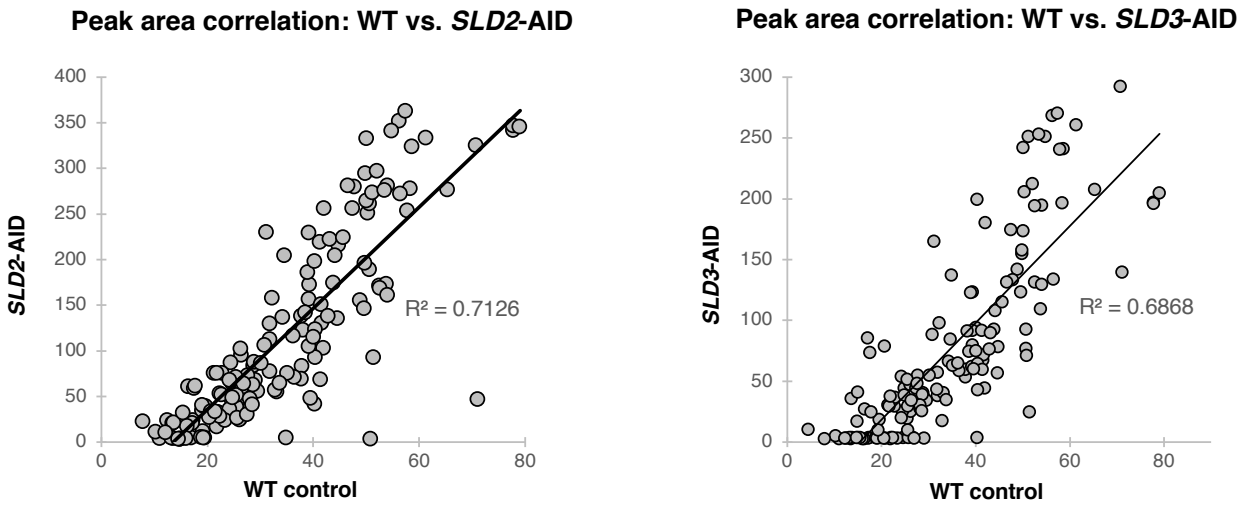

Figure 2.4. ssDNA peak area correlation between WT and uninduced AID strains.

For some ssDNA assay peaks, more than a single origin is identified in the database. I manually excluded these multiple origins from the list. The full list of origins used for the ssDNA peak area and width analysis is in Appendix B. In curating this list of origins, I found that even though the microarray probes for Ty elements are excluded from my data processing, there is often artefactual labeling of ssDNA at Ty-adjacent loci. The peaks formed near Ty elements do not reflect origin activity, so I have specially marked those loci on all ssDNA replication profiles. The list of Ty-adjacent peak loci is in Appendix B.

2.7 Whole Genome Sequencing Replication Analysis

I also used whole genome sequencing to profile DNA replication for all of S phase by determining copy number variation across the genome in an asynchronous population of cells [Figure 2.5]. In Figure 2.5, a flow cytometry profile from an asynchronous cell population is shown on the right side of the illustration to indicate variable DNA content in those cells. For haploid yeast, all cells

in the G1 population contain one copy of the single chromosome shown in this example, and the G2 cells, having gone through S phase, contain two copies of the chromosome. In S phase cells, copy number varies due to partial replication of the chromosome. Origins will result in local maxima in read depth, while regions where replication forks converge (termini), will result in local minima. Read depth at origins that fire early in S phase will be high, while read depth at late-firing as well as inefficient origins will be lower. Large-scale chromosomal regions that are replicated early in S phase (for example, *CEN*-proximal regions) will have a higher average read depth, while regions that are replicated late in S phase (for example, subtelomeric regions) will be underrepresented in average read depth.

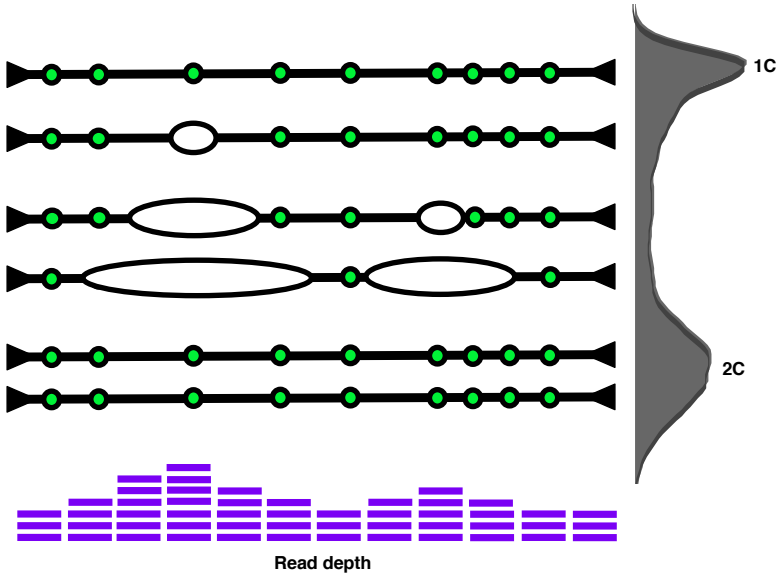

Figure 2.5. Whole genome sequencing of asynchronous cells to profile DNA replication.[10]

For each experimental condition, I collected a 50 ml culture sample when cells reached mid-log phase ($OD_{660} \approx 0.5$). I also collected a G1-arrested control sample at a comparable culture

[10] Copy number is used to assay replication activity based on variation in origin efficiency and firing time. The earlier-firing origin on the left side of the hypothetical chromosome produces a higher peak in read depth than the later-firing origin on the right. The terminal region between the two origins results in a local minimum in read depth. Figure adapted from Müller et al., 2014.

density after 120 minutes in α-factor. I purified genomic DNA by the standard Smash & Grab protocol (Rose, 1990). I sheared the DNA to an average length of 260 bp using a Covaris ultrasonicator, then removed RNA nucleotides by treating the sample with 0.01 mg/ml RNAse A final concentration before subjecting the DNA to a Zymo Research DNA Clean and Concentrator-25 kit. I end-repaired and adapter ligated 100 ng of the resulting DNA using the KAPA Biosystems Hyper Prep Kit and the KAPA Single-Indexed Adapter Kit. I then sequenced the libraries on the Illumina NextSeq 550 platform.

I aligned single-end reads at least 35 basepairs long to the Saccer1 *S. cerevisiae* genome assembly using Bowtie2, and then binned the reads into 1 kb windows using custom Python scripts written by Elizabeth Kwan, Ph.D. If the libraries had been sequenced over multiple runs, I combined the reads by 1 kb bin. I aimed to recover at least 10,000,000 usable reads per library, which, assuming a 35 bp read, provides a minimum of 28X coverage of the yeast genome. One library sequenced from the *SLD3*-AID no auxin condition collection did not meet this requirement and I generated replication profiles based on ~5,000,000 reads, which is still adequately high read coverage.

After verifying that I had sufficient read depth for each sample, I normalized the read depth in each 1 kb bin to the average read depth per bin for the entire library. However, I excluded the read depth of the rDNA locus, the 2-micron plasmid, and the mitochondrial DNA when calculating the average read depth per bin. Next, I corrected for sequencing bias by dividing the read depth of each bin by the corresponding read depth of that bin in the G1-arrested sample. The data, at that point, reflected copy number variation across the genome for the asynchronous population of cells relative to G1 cells, or marker frequency.

Before smoothing the data to generate replication profiles, I needed to exclude outlying data points. I determined that most outlying marker frequency values were due to the poor mappability of repetitive subtelomeric DNA sequences, transposable elements, and highly conserves paralogous genes descended from the whole genome duplication event. I excluded these three types of outlying marker frequency values. Tables of the 1 kb bins I excluded are included in Appendix E. Finally, I used the same Loess smoothing program applied to the ssDNA assay microarray data to smooth the marker frequency values in 50 kb windows and generated replication profiles.

2.8 2-D Gel Electrophoresis of Replication Intermediates

I performed 2-D gel electrophoresis to determine replication activity at both single copy origins and the high copy rDNA origin. I used different DNA purification and restriction digest conditions depending on the type of origin analyzed. For single copy origins, I collected 300 ml of mid-log phase culture (OD_{660} = 0.5 – 0.7) after galactose induction and auxin addition as detailed above. I chilled the sample on frozen sodium azide and EDTA, as above, then washed, pelleted, and froze the cells at -20° until I obtained flow cytometry results to confirm depletion of the AID-tagged protein. If the cells exhibited the expected S phase phenotype, I purified genomic DNA using a variation of the "NIB (nuclear isolation buffer) & Grab" DNA purification protocol detailed on the Brewer/Raghuraman lab website (Brewer). Instead of using bead-beating along to lyse the cells, I used a combination of zymolyase treatment and short bead-beating, which I determined to preserve replication intermediates better than multiple rounds of vortexing. Details are available in Appendix D.

For each gel, I used all of the DNA purified from a single sample, a few micrograms, for restriction digestion. I used the enzyme BanI for *ARS1209* (4.8 kb fragment) and *ARS1213* (3.7 kb fragment) analysis. Due to a polymorphism within the BanI site in the *SLD3*-AID strain, I used a different enzyme (BspHI) to cut a 4.9 kb fragment containing *ARS1209* in that strain. For the *ARS501* gels, I used XbaI to cut a 3.2 kb origin-containing fragment. For the first dimension, I ran the entire mass of digested DNA on a 0.4% agarose gel at 1 V/cm for 18 hours without ethidium bromide. I cut the resulting gel slice at least 1 cm below the enzyme-dependent fragment size, then transferred each gel slice to a casting tray and poured the 2nd dimension gel. I ran the 1.1% agarose 2nd dimension gel with ethidium bromide at 7 V/cm for 4 – 5 hours, depending on the size of the origin fragment. I transferred the gels to GeneScreen nylon membrane by standard Southern blotting methods, then probed the blots with a DNA fragment containing the origin of interest.

Figure 2.6A illustrates the expected patterns produced by the different forms of replication intermediates that are separated and analyzed on 2-D gels. This figure demonstrates how changes in signal intensity at certain regions on these blots reflect differences in origin efficiency. The top panel shows hypothetical migration patterns of partially replicated DNA structures, with arrows pointing out the replication bubble and Y arc portions of each blot. The gray boxes illustrate the most abundant replication intermediates found over the course of a single S phase at a single origin (closed green circle) that is either active or inactive. At active origins, the signal from the bubble arc is high compared to the signal from the Y arc. If the origin is off-center on the restriction fragment (restriction sites indicated as scissors and dotted line), then the partially replicated DNA molecule will transition from a replication bubble to a Y structure over time, as the restriction enzyme will cut interior to the replication fork on a proportion of partially replicated molecules. This transition from bubble to Y molecules accounts for the high signal along the portion of the Y

arc descending to the 2N spot accompanied by high signal along the bubble arc (shown in the "active origin" Figure 2.6.A). In contrast, at an inactive origin, where the origin is most often replicated by replication forks initiated from other origins, the bubble arc signal will be low, and the intensity of the Y arc will be more uniform along its length, as there will not be a transition from bubble to Y structure at that locus.

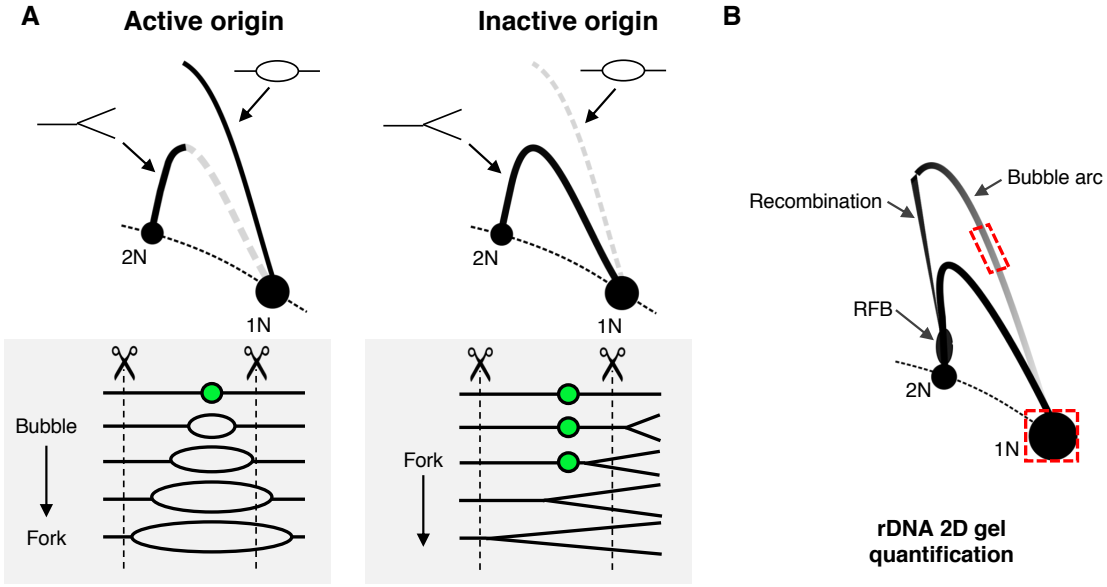

Figure 2.6. Example 2D gels for active and inactive origins, and rDNA 2D gel quantification.[11]

For the timed rDNA 2D gels, I prepared the DNA in agarose plugs and digested the DNA *in gelo* (Wenyi Feng, personal communication). To collect the timed samples, I arrested the cells at OD_{660}= 0.25, and then released them after galactose induction and auxin treatment, as described in Section 2.2. I collected a 50 ml culture volume for each timed sample and embedded the cells

[11] (A) In the top section, the relative Y and bubble arc intensities are shown for an active and an inactive origin. The 1N spot is the size of the unreplicated origin restriction fragment, and the 2N spot is the almost completely replicated origin fragment. The gray panels show the different replication intermediates present at the origin over the course of S phase. The scissors and dotted line indicate the restriction sites near the origin. (B) Expected 2-D gel pattern for NheI digest for analysis of the rDNA origin. The red dotted boxes indicate the parts of each gel that were quantified. The bubble arc intensity is shown as a proportion of the 1N spot.

in 0.5% low melt (SeaPlaque) agarose plugs before spheroplasting [reference lab website]. Immediately after spheroplasting, I washed the half plug in 10 mM Tris three times in excess buffer, then equilibrated the piece by pipetting 200 µl NEBuffer 2.1 onto the agarose and incubating on ice gentle shaking. I repeated this equilibration twice more before removing all the buffer from around the plug and pipetting 3 µl NheI (10,000 units/ml) directly onto each plug. NheI generates a 4.7 kb fragment containing the rDNA origin. The restriction digest continued for 4-5 hours at 37°C. After the enzyme digest finished, I loaded each piece of plug onto a comb and poured the first dimension 0.5% agarose gel around the gel slices. The first dimension ran for 20 hours at 1V/cm. I cut the gel slices and ran the 2nd dimension for 6 hours using the same parameters as before. I probed the membranes with an *NTS2* fragment [Figure 1.7] and quantified the rDNA 2D gels as shown in Figure 2.6B. The bubble arc signal, or hybridization due to active replication origins, is shown as a proportion of the 1N spot.

2.9 Pulsed Field Gel Analysis of Chromosome Stability

I used contour-clamped homogeneous electric field (CHEF) gel electrophoresis to determine rDNA copy number for all strains used in this study by measuring ChrXII size compared to chromosome size standards from *Hansenula wingei*. I also used CHEF gel analysis to assay chromosome instability. For copy number determination, I embedded stationary phase cells in agarose plugs and ran slices of each sample on a 1% agarose gel on Bio-Rad CHEF electrophoresis apparatus at 100 V for 68 hours, switch time ramped from 300 to 900 seconds (Kwan et al., 2016).

Additionally, I used CHEF gel analysis to assay chromosome integrity and stability during synchronous S phase (Cha and Kleckner, 2002; Feng et al., 2011; Hennessy et al.). I collected 5 ml culture volume to make agarose plugs at the varying time intervals. I ran the gels above, then

transferred them using standard Southern blotting protocols. I probed the membranes for single copy chromosome sequences and stripped the probes before re-probing with another sequence. I used a BioRad PMI and QuantityOne software to quantify the probed blots. See Figure 2.7 for diagram of how I quantified the resulting Southern blots.

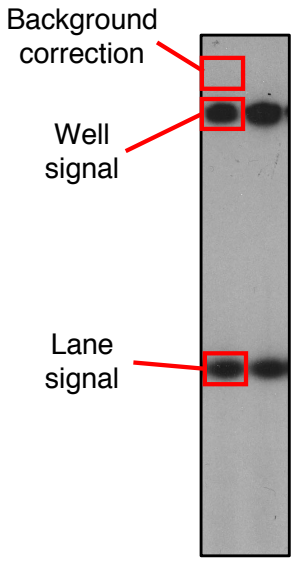

Figure 2.7. Quantification of well signal on CHEF gel Southern blots.[12]

To confirm that branched molecules stemming from incomplete replication of the rDNA prevent proper migration of ChrXII, I treated the plugs with I-Ppo1 before loading them onto a CHEF gel. I-Ppo1 cuts each rDNA repeat, but not elsewhere in the yeast genome. Again, I washed the plugs three times in 10 mM Tris, but did not equilibrate them in I-Ppo1 buffer. Instead, I pipetted 75 µl of I-Ppo1 buffer + 0.5 µl I-Ppo1 enzyme onto each plug slice, then incubated the

[12] I calculated the total signal for a sample by adding the hybridization volume in the well at the top of the gel and the corresponding part of the lane region where I expected the chromosome to run (based on the untreated control sample). A background hybridization correction was taken from an equal-sized region on the membrane above the well. All quantification data shown are the signal derived from the lane compared total total signal for a single sample as an indicator of the proportion of branched chromosome structures unable to migrate under CHEF gel conditions.

plugs for 1 hour at 37°C. After the I-Ppo1 digest finished, I loaded the plugs onto a 1% CHEF gel and ran the samples using the same parameters as described above. See Appendix G for how I determined the desired I-Ppo1 digest conditions.

Chapter 3. RESULTS

3.1 Independent Depletion of Two of the SSDD Limiting Replication Initiation Factors Slows S Phase Progression, Decreases Growth Rate, and Reduces Cellular Viability

Using the 3x-mini-AID version of the auxin inducible degron system, I set out to engineer strains with a C-terminal degron tag on each of the SSDD factors (Kubota et al., 2013; Nishimura et al., 2009). I recovered Sld2 and Sld3 auxin degron strains (*SLD2*-AID and *SLD3*-AID) but was unable to construct AID-tagged versions of Dbf4 or Dpb11, likely due to important biochemical features at the C-terminus of those proteins (Natsume et al., 2013; Zegerman and Diffley, 2007).

The *SLD2*-AID and *SLD3*-AID strains were tested for an S phase phenotype by comparing synchronized S phase using flow cytometry for DNA content without and with the presence of 0.5 mM auxin to induce depletion of the target protein [Figure 3.1]. Compared to the uninduced condition, in which the cells reached 2C DNA content 60 - 80 minutes following release from α-factor arrest, the Sld2-depleted cells were still in mid-S phase 100 minutes after release [Figure 3.1]. Progress into and through S phase was even slower in the Sld3 depleted culture [Figure 3.1]. The uninduced *SLD3*-AID cells reached 2C content 80 minutes after release, although the uninduced cells progressed through mid S phase more slowly than the uninduced *SLD2*-AID strain (compare to no auxin T60 in Figure 3.1). I suspected that the presence of the degron tag on Sld3 was inhibiting its normal function, which will be addressed in greater detail below. The Sld3-depleted cells had an extreme defect in S phase progression compared to the Sld2-depleted cells [Figure 3.1]. I attribute this difference compared to Sld2 depletion to two factors: Sld3 is less abundant than Sld2, even without induced depletion of either protein, and because it associates with the replication complex before S phase begins, so its depletion might prevent all but a very

few early-firing origins from firing (Ghaemmaghami et al., 2003; Kamimura et al., 2001; Mantiero et al., 2011). To test for possible off-target effects of inducing expression of the plant-derived E3 ubiquitin ligase, I carried out a synchronous arrest and release experiment with a strain harboring the *GAL1-Os*TIR1-9myc construct alone, without a degron domain-tagged target protein (referred to hereafter as the "AID parent strain"). Cell cycle progression was identical regardless of the presence or absence of auxin from which I concluded that any off-target effects of the AID system have minimal consequences for cell cycle progression [Figure 3.1].

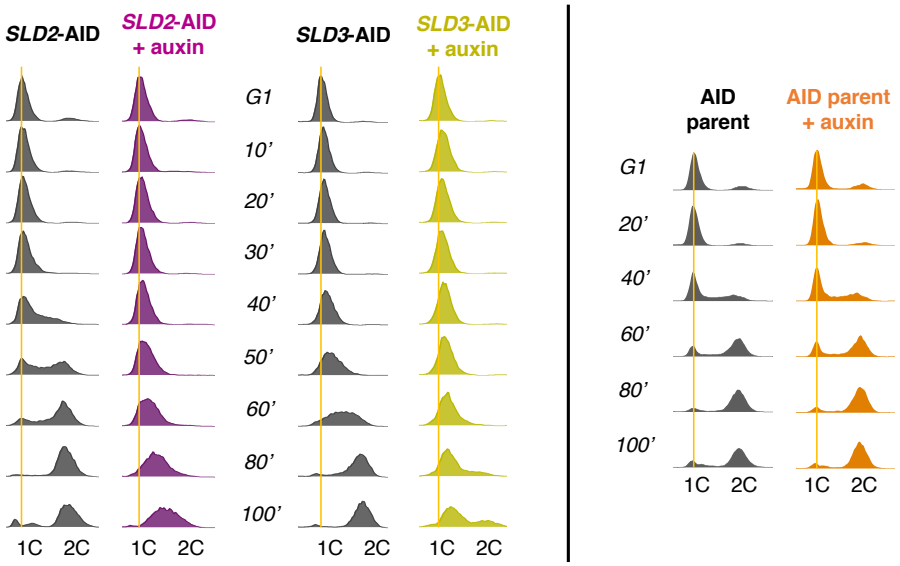

Figure 3.1. Flow cytometry analysis of α-factor synchronized cell cycle progression of auxin degron strains.[13]

To determine whether the increased time in S phase observed in the Sld2- and Sld3-limited strains is due to decreased growth rate or reduced cellular viability, I analyzed log-phase growth and plated cells for viability, with and without the addition of auxin. Both *SLD2*-AID and *SLD3*-AID strains had increased population doubling times when the target proteins were degraded

[13] Orange line indicates 1C DNA content. AID parent strain flow cytometry samples were collected in a different experiment, hence the different time intervals.

[Figure 3.2]. In agreement with the more severe S phase phenotype observed by flow cytometry, the Sld3-depleted cells exhibited a greater increase in doubling time compared to cells depleted for Sld2. Both strains experienced an approximately 40% decrease in viability as assayed by colony-forming ability. While auxin treatment did slightly slow growth in the AID parent control strain, it was not due to decreased viability [Figure 3.2].

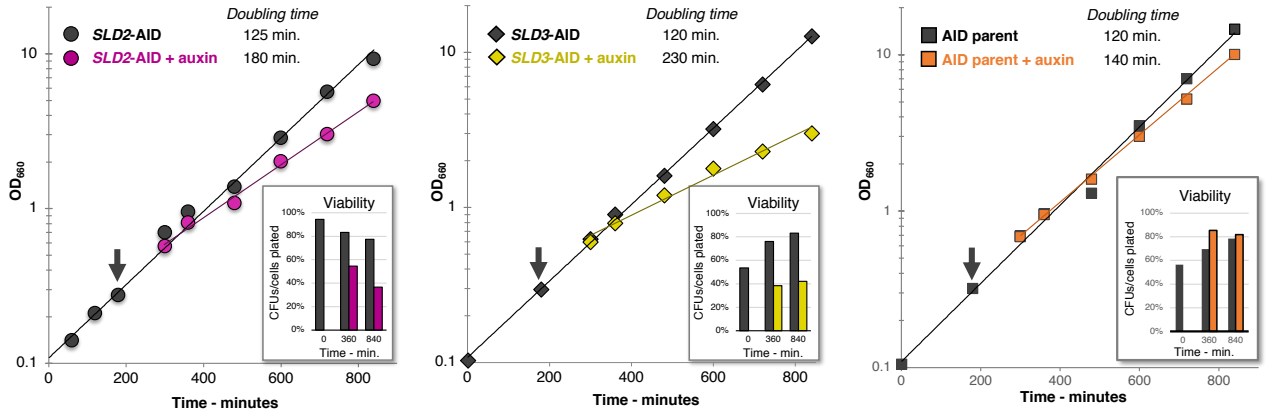

Figure 3.2. Log-phase growth and viability of auxin degron strains.[14]

The rapid onset of decreased viability suggested that the S phase checkpoint might be activated in response to initiation factor depletion, thus preventing the cells from completing the cell cycle, and resulting in a loss of viability (Foiani et al., 2000; Zhang and Hunter, 2014). I tested whether the checkpoint was active by western blotting for phosphorylated Rad53. I HA-epitope tagged Rad53 in the *SLD2*-AID, *SLD3*-AID, and AID parent strains, then tested for

[14] Log phase growth of *SLD2*-AID, *SLD3*-AID, and AID parent strains, with and without auxin, in YC + 1% raffinose + 2% galactose media. After 180 minutes in 2% galactose, the cultures were split (noted by arrow in figure), and auxin was added to one portion. After 360 minutes, the cultures were cut back to maintain log phase growth and fresh auxin added to the appropriate culture. Depletion of either Sld2 or Sld3 increased doubling time, with depletion of Sld3 resulting in a more severe growth defect (92% doubling time increase) compared to the increase in doubling time caused by Sld2 depletion (44% increase). At the three indicated times, an aliquot of the culture was removed, and plated on glucose-containing medium lacking auxin to measure viability (i.e., ability of the cells to recover from Sld2 or Sld3 depletion and form colonies).

phosphorylation of Rad53 in an asynchronous population of cells for 3 hours of galactose induction followed by 2 hours of auxin treatment. The Sld2- and Sld3-depleted cells had a clear S phase progression phenotype as assayed by flow cytometry, while the AID parent did not [Figure 3.3]. However, the stalled S phase was not due to activation of the S phase checkpoint, as no phosphorylation of Rad53 was detected in the auxin-treated samples for either the *SLD2*-AID or *SLD3*-AID strains [Figure 3.3]. Likewise, no Rad53 phosphorylation was detected in the AID parent strain following auxin treatment [Figure 3.3].

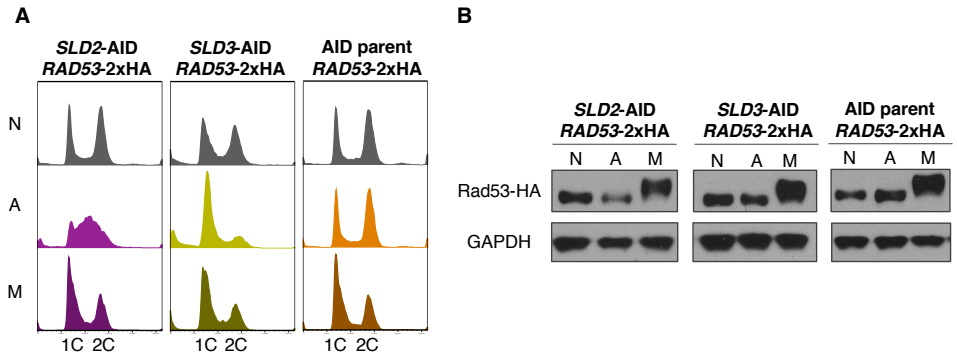

Figure 3.3. Western blot to detect Rad53 phosphorylation in Sld2- or Sld3-depleted cells.[15]

3.2 Differentiating Between Changes in Origin Efficiency and Time of Origin Firing by Genome-Wide Replication Assay

Given that depletion of either Sld2 or Sld3 impairs S phase progression, I next sought to classify how the pattern of replication initiation might change under those conditions and determine whether those changes are linked to differences in origin firing time, efficiency, or both. Furthermore, given the differences in S phase progression observed by targeting the two different

[15] (A) Flow cytometry profiles from asynchronous culture western blot collection. Cells were left untreated (sample N), treated with 0.5 mM auxin (sample A), or treated with 0.1% MMS (sample M). (B) Western blots for Rad53 phosphorylation. Yeast GAPDH (Tdh1) was used as a loading control. Neither depletion of Sld2 nor of Sld3 resulted in phosphorylation of Rad53 compared to the MMS control. Adding auxin to the AID parent strain does not induce phosphorylation of Rad53.

proteins, it was possible that the changes in origin firing pattern may differ depending on the protein targeted. I imagined two models, which are not mutually exclusive, for alterations in origin use during reduced Sld2 or Sld3 S phase [Figure 3.4 and described below]. I will frame the two models around changes to origin activity occurring in early S phase since that is the time interval resolved by the ssDNA mapping assay for replication initiation.

In the first model, depletion of a limiting initiation factor would result in a global reduction of origin firing efficiency compared to WT. In the hypothetical WT population of four yeast cells illustrated in Figure 3.4A, in which four out of six potential origins fire during early S phase, reduced origin efficiency would result in overall fewer origins firing per cell. If the reduction in efficiency is widespread across the genome, each cell might fire a different subset of origins in relation to the other cells in the population [Figure 3.4B]. However, considering the population of cells in aggregate, initiation would be detected at all the same origins as in WT, although each origin would be used in fewer cells than in WT [Figure 3.4B]. Based on previous studies, I predicted that a widespread reduction in origin efficiency would result in increased replication fork movement from a reduced number of active origins per cell (Zhong et al., 2013).

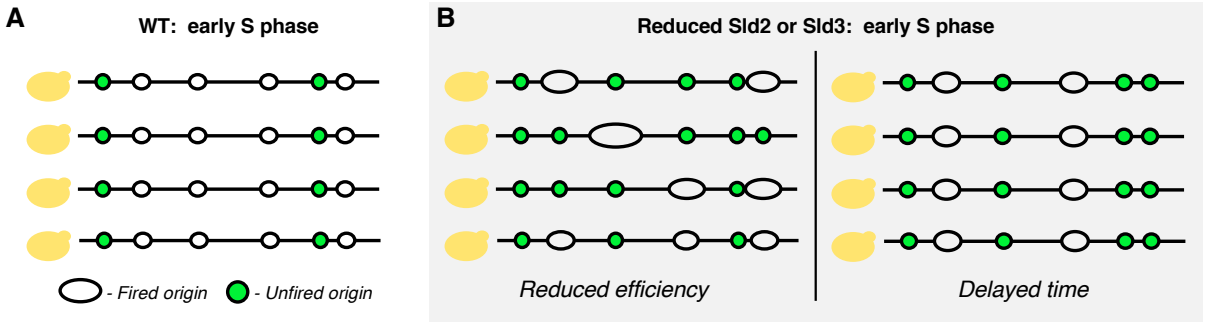

Figure 3.4. Models for changes to origin firing when Sld2 or Sld3 are depleted.[16]

[16] (A) In the hypothetical population of WT cells, four out of six potential origins fire. (B) Two possible types of changes to origin firing due to Sld2 or Sld3 depletion. Reduced origin efficiency, shown on the left, would result in fewer origins firing per cell, although in the population, the same set of origins are active as in wildtype. Changes in efficiency would change replication fork movement, as previous work has shown that fewer active origins per cell allows for greater fork movement from fired origins (Zhong et al., 2013). In contrast, delays in origin firing time,

In the second model, reduced abundance of a limiting initiation factor would delay firing time for some origins, but not for others. The model for recycling of limiting SSDD factors presented by Mantiero, et al. (2011) suggests that late-firing and inefficient origins are least able to compete for and recruit these factors, so less competitive origins may not be able to recruit the extremely limited initiation factors when Sld2 or Sld3 are depleted. In that case, a timed genome-wide replication assay would reveal that, in early S phase, a subset of origins is not initially active in the population of cells [Figure 3.4B]. Initiation at those origins may be delayed or they may fail to fire completely.

To test for such changes in origin firing, I used a single-stranded DNA mapping assay, in which enrichment of ssDNA at replication forks is detected genome-wide by microarray hybridization (Feng et al., 2006, 2011). Active origins produce peaks in the ratio of S phase ssDNA compared to G1 phase ssDNA. In this method, cells are synchronously released into S phase in hydroxyurea (HU) which activates the S phase checkpoint and therefore restricts the resolution of the experiment to origins whose activity is not inhibited by activation of the checkpoint. This method can differentiate between my two predicted models. For example, widespread reduction in origin efficiency resulting in increased replication fork migration would generate wider ssDNA peaks on the replication profiles [Figure 3.5A]. Due to lower firing efficiency, the replication forks may be able to move far enough from each other that two small peaks corresponding to individual replication forks (termed "split peaks") are evident at some origins [see the leftmost origin peak on the hypothetical profile in Figure 3.5A] (Feng et al., 2011). Furthermore, if origin efficiency is lower across the genome, but initiation time is unchanged, I

---

shown on the right, would result in a subset of origins firing outside of the time frame in which those origins normally fire in WT cells.

would expect that the same set of origins would fire in the control and initiation factor depleted condition. By calculating the area under the curve at each origin for the two conditions, I can use the correlation between those two sets of peak data to ask whether the same origins are active in both conditions. If the cells use the same set of origins, the two sets of peak area values will be well-correlated [Figure 3.5A].

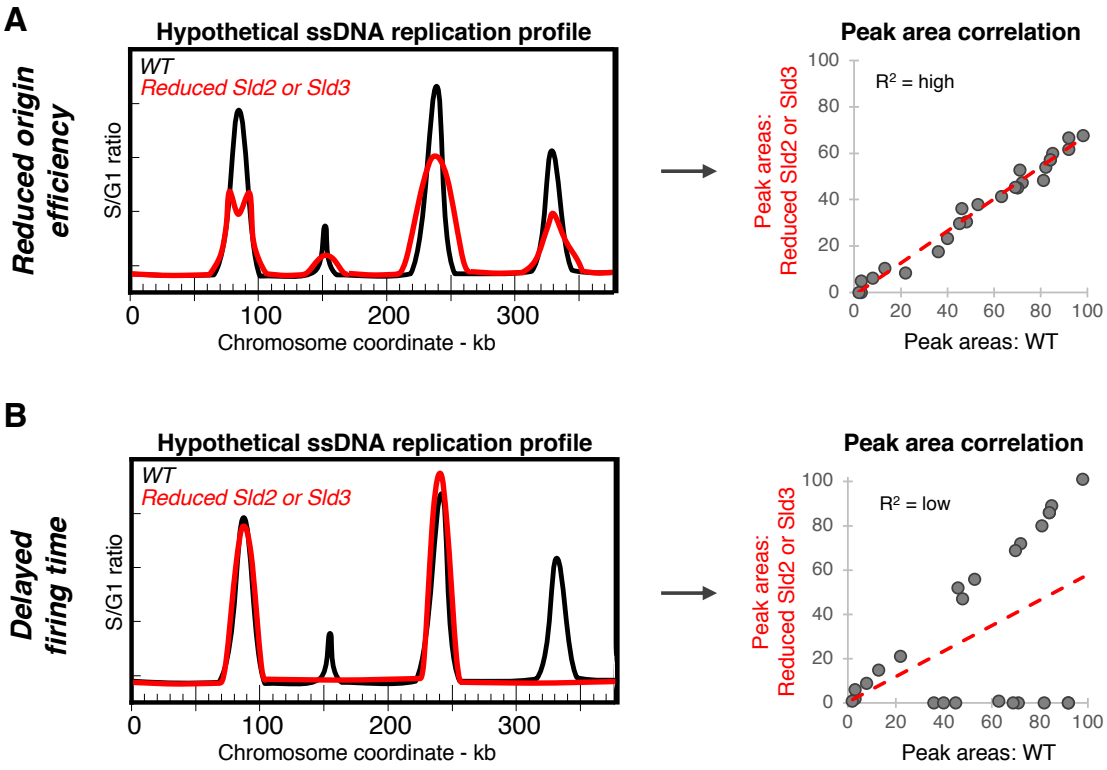

Figure 3.5. Hypothetical ssDNA replication profiles reflecting changes in origin efficiency or delayed time, and corresponding predicted peak area correlation.[17]

[17] Changes to time of origin firing and firing efficiency are discernable using a genome-wide assay for ssDNA accumulation at replication forks during S phase in hydroxyurea. These two sets of hypothetical replication profiles illustrate how these changes would be detected. Hypothetical WT profiles are shown in black and reduced initiation profiles are shown in red. (A) If depleting Sld2 or Sld3 causes widespread reduction in origin firing efficiency, replication forks will move farther from each other, resulting in broader peaks compared to WT replication profiles. The presence of two small adjacent peaks at a single origin, as shown at the leftmost origin peak in the reduced efficiency example profile, is also due to greater replication fork movement, because at those loci, replication forks have moved far enough to resolve them separately from each other. Overall, the same set of origins are used during S phase, which is confirmed by calculating the area under curve at each origin in each condition and determining how well correlated the two sets of area values are (hypothetical peak area correlation shown to the right of the ssDNA replication profile). (B) If time of origin firing is delayed, some origin peaks would be absent or extremely reduced in peak height in the reduced factor condition. Since the area under the curve at those origins would be very

In contrast, delayed firing of a subset of origins would result in absent peaks at some origins [Figure 3.5B]. In that case, the number of origins detected by ssDNA assay would be lower in the replication profiles from Sld2- or Sld3-depleted cells and the sets of areas under the ssDNA peaks would not be expected to correlate as well since any origins that fail to fire would be low on the Y axis [Figure 3.5B]. It should be noted that, if some origins are delayed in firing and fewer origins are active in early S phase, there may also be changes in replication fork movement.

Additionally, changes to origin efficiency under the two different conditions can be confirmed by measuring changes in replication fork movement, as highlighted in Figure 3.6. The ssDNA peak width at half maximum height indicates how far replication forks have moved from each other. A broad ssDNA peak, as shown in red in Figure 3.6, results from the replication forks moving farther away from each other compared to the control condition. As a consequence, the labeled regions of ssDNA at each fork are spaced farther apart along the length of the chromosome. Comparing the distribution of peak width at half maximum height for all origins under the two different conditions would confirm genome-wide changes in replication fork movement due to reduced origin efficiency, both globally or at specific origins.

low compared to WT, there would be less correlation between the sets of peak values. Individual origins that fail to fire could be identified as data points that fall at 0 on the Y axis.

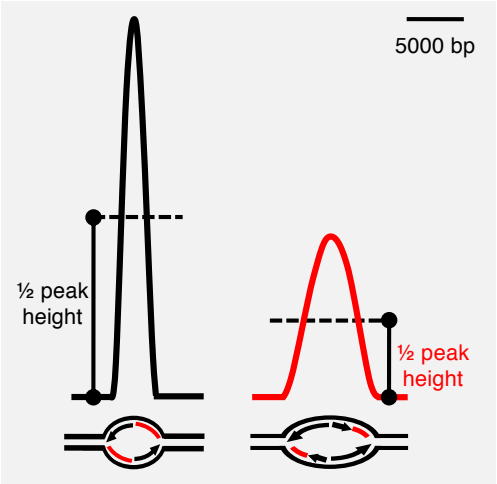

Figure 3.6. Variation in ssDNA peak width reflects variation in replication fork movement.[18]

3.3 Depletion of Sld2 or Sld3 Reduces Origin Efficiency Genome-Wide during S Phase in HU

Origin activity was assayed genome-wide in the *SLD2* and *SLD3*-AID strains, uninduced and induced, using the ssDNA assay method. Samples were also collected for a WT control—the strain W303, that is the background for all degron strains used in this study. For the WT experiment, cells were grown in synthetic complete medium containing dextrose, which results in a faster transition to S phase from G1 arrest than the degron strains. Because of these metabolic differences, an earlier timed sample from the WT experiment (30 minutes after release) is compared to a slightly later time (60 minutes after release) for the auxin degron strains.

Initially, I surveyed differences in origin activity between the uninduced degron strains and the WT control. Visual inspection suggested that origins detected in the WT condition were also

[18] Reduction in origin efficiency is confirmed by determining ssDNA peak width at half maximum peak height as a proxy for changes in replication fork movement (Sheu et al., 2014). The replication bubble associated with either a narrow or broad ssDNA assay peak is shown below each peak. In the WT example shown, restricted replication fork movement results in the fluorescent labelling of ssDNA (the red lines at each fork) at replication forks that are near one another, giving rise to a very narrow peak in the ssDNA replication profile. When efficiency is reduced, ssDNA accumulates at replication forks that are farther apart, resulting in a broader ssDNA peak at the origin. Scale bar represents 5000 bp.

active in the *SLD2*-AID [Figure 3.7]. This observation was confirmed by comparing the origin peak area values from the uninduced *SLD2*-AID dataset with the WT peak areas [Figure 2.4]. If a subset of origins were unable to fire in the uninduced *SLD2*-AID strain, a number of peak area data points would be located along the X axis since there would not be a corresponding area under the curve calculated at those loci. Since the correlation between the two sets of origin peak values was high, I concluded that the WT-derived set of origins was appropriate for subsequent analysis. This same list of origins was used in all subsequent analyses of the degron strains. (See Methods for more details, and Appendix B for the complete list of origins derived from the WT data.)

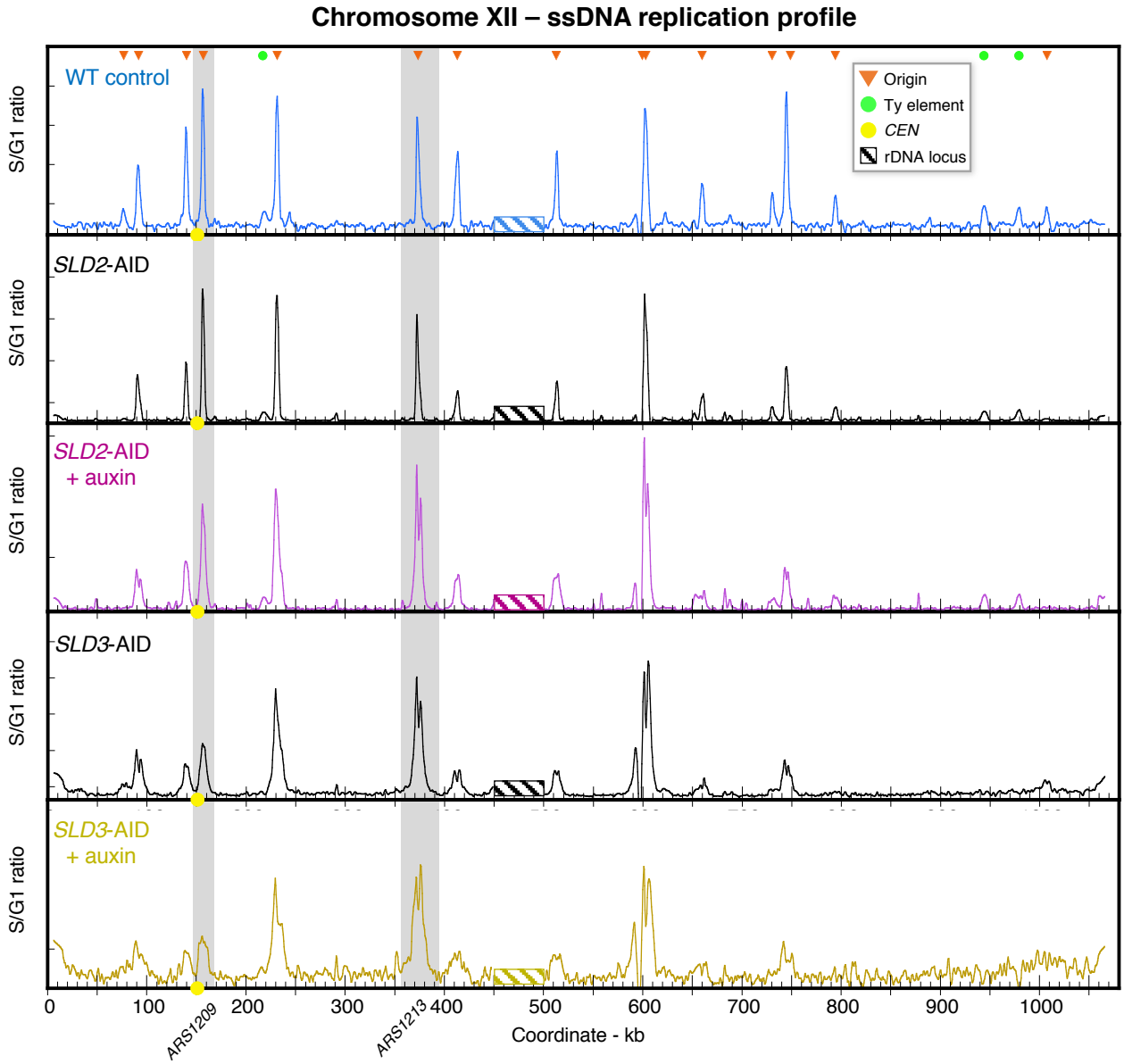

Figure 3.7. Chromosome XII ssDNA replication profiles for WT control and degron strains.[19]

The WT-based origin set also captured origin activity in the *SLD3*-AID (uninduced) strain [Figure 2.4]. However, the ssDNA peaks in the *SLD3*-AID strain appeared broader or "split"

[19] Chromosome XII replication profiles for T30 of WT control, and T60 for the auxin degron strains. Orange triangles denote origin peaks with S/G1 ssDNA ratio maxima that are 3 SD above the average S/G1 ratio in the W303 control. Green dots denote regions around Ty elements, which have elevated S/G1 ssDNA ratios, but are not origins of replication. Yellow dots on the X axis indicate the centromere. Values at the rDNA locus,between coordinates 450- 500 kb, are excluded and indicated by the striped bar. Two origins, ARS1209 and ARS1213, have been highlighted in gray as they were subjected to further analysis, shown in Figure 3.10. ssDNA assay profiles for all other chromosomes are in Appendix C.

[Figure 3.7]. These differences in replication fork movement suggested that even without the addition of auxin, the degron-tagged version of Sld3 has a partial loss of function resulting in reduced origin firing efficiency. Note that because of this broadening of peaks, origins that have very small peak area to begin with in the WT strain may escape being scored as peaks in our area measurement algorithm [Figure 2.4, Figure 3.7].

To test the idea that the degron-tagged version of *SLD3*-AID is a hypomorph, I constructed a second version of the *SLD3*-AID strain that does not contain the plant-derived E3 ubiquitin ligase. Two independent isolates of this strain (denoted *SLD3*-AID$^{OsTIR1-}$) exhibited a larger population of cells in S phase compared to the WT control [Figure 3.8]. Furthermore, I found by 2D gel electrophoresis that the presence of the AID tag corresponded with lower replication bubble signal at the rDNA origin [Figure 3.8]. Together, these data show that the presence of the degron tag on Sld3 reduces origin efficiency.

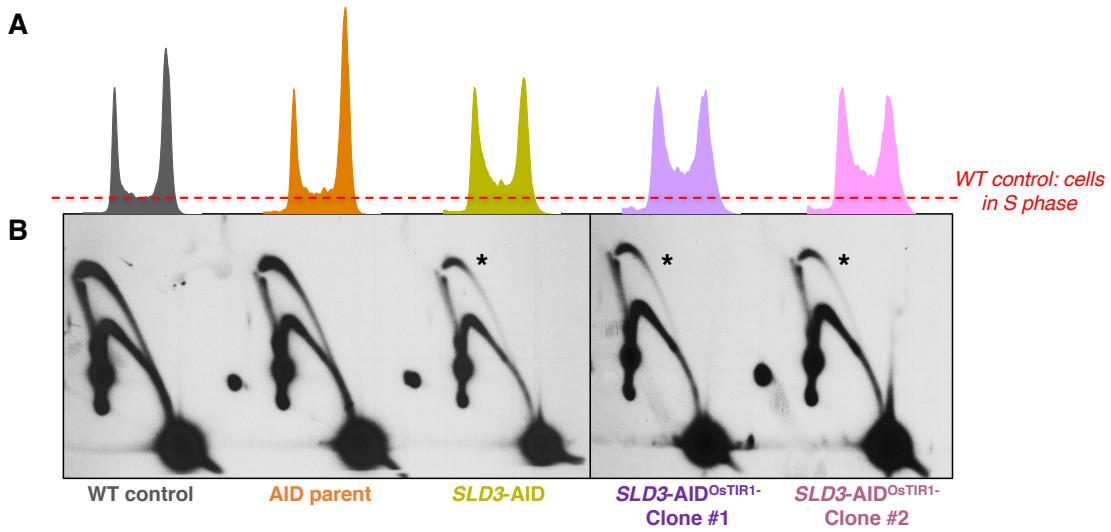

Figure 3.8. The C-terminal AID domain reduces Sld3 function.[20]

[20] A. Flow cytometry profiles based on DNA content for log-phase growth WT control, AID parent, *SLD3*-AID, and two clones with AID-tagged Sld3 in the WT background. The G1 peaks have been matched for height between profiles, and the dashed red line shows the proportion of S phase cells in the WT control. B. 2D gel analysis of the rDNA origin in the same cultures shown in (A). Samples were collected from log-phase growth cells. Blots are probed with *NTS2* sequence. The reduced signal intensity of the replication bubble arc, indicated by the asterisk, in all of the *SLD3*-AID strains indicates reduced rDNA origin efficiency in the degron-tagged strains.

Confident that I was able to analyze the appropriate set of origins across these datasets, I next determined how activity among that set of origins changed in response to depletion of Sld2. I compared the replication profiles for the *SLD2*-AID control condition and the auxin-treated cells. Peak areas were strongly correlated between the two conditions [Figure 3.9A]. Therefore, I concluded that the same origins that fire in the *SLD2*-AID no auxin condition are active when Sld2 is depleted. In addition, the peaks on the *SLD2*-AID plus auxin profiles were slightly wider or resolved as split peaks [Figure 3.7]. To quantify these differences in peak widths, I calculated peak width at half maximum peak height for each origin [Figure 3.9B]. The distributions of peak widths were found to be significantly different between the control *SLD2*-AID condition and the auxin-treated cells (Wilcoxon rank sum test $p < 2.2x10^{-16}$). The median peak width in the uninduced strain was 4000 bp but increased to 6000 bp following Sld2 depletion. Overall, these findings are consistent with the model of a general decrease in origin efficiency upon Sld2 depletion and are not consistent with the model of delayed firing of some origins.

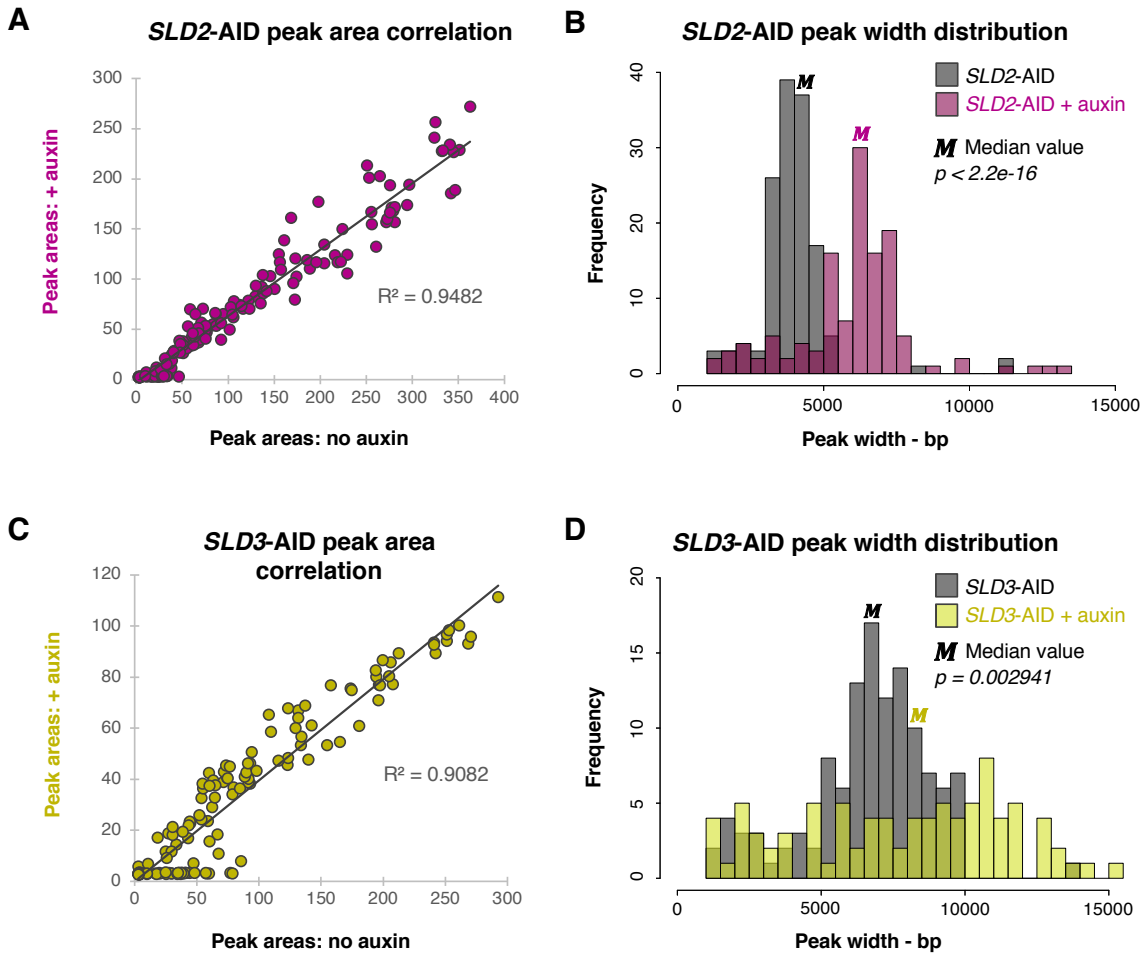

Figure 3.9. Correlation between ssDNA peak areas and distribution of ssDNA peak width for Sld2 and Sld3 degron strains.[21]

As with the *SLD2*-AID strain, upon depletion of Sld3 I observed origin activity at the same locations as in the control condition, indicated by a high correlation of peak areas between the two

[21] (A) Correlation between ssDNA peak areas at all active origins for *SLD2*-AID vs. *SLD2*-AID plus auxin condition. (B) Distribution of origin peak width at half the maximum peak height for *SLD2*-AID vs. *SLD2*-AID plus auxin ssDNA assay replication profiles. Peak widths are calculated in 500 bp intervals. The median peak width for *SLD2*-AID was 4000 bp and for *SLD2*-AID plus auxin, 6000 bp. Some peak widths were rounded down to zero and excluded from distribution analysis. An unpaired Wilcoxon Rank Sum test was performed, and distributions of peak width were found to be significantly different ($p < 2.2x10^{-16}$). (C) Origin peak area correlation for *SLD3*-AID vs. *SLD3*-AID plus auxin. (D) Distribution of peak widths at half maximum peak height for *SLD3*-AID vs. *SLD3*-AID plus auxin. *SLD3*-AID median peak width was 7000 bp and *SLD3*-AID plus auxin median was 8500 bp. Unpaired Wilcoxon Rank Sum test was used to test for significant difference in distribution of peak widths ($p = 0.002941$).

conditions [Figure 3.9C]. As was the case for the comparison between the *SLD3*-AID no auxin and WT ssDNA peak area values, origins with very small peaks in the uninduced condition escape reliable detection and measurement in the depletion condition when the peaks are broader and split [Figure 3.9]. I concluded that overall, as with Sld2, the same set of origins are active both in the control *SLD3*-AID condition and the auxin-treated *SLD3*-AID cells. Depletion of Sld3 did correspond with a shift in median peak width--7000 bp in the no auxin control vs. 8500 bp in the plus auxin condition [Figure 3.9D]. While the difference between the two sets of peak widths is significant (Wilcoxon rank sum p-value = 0.002941), it is notable that the p-value is much higher than observed with the *SLD2*-AID data. I attribute this difference to origin efficiency being lower in the uninduced *SLD3*-AID strain, giving rise to broader ssDNA peaks even before Sld3 is depleted. While the severity of the effect on replication fork movement is slightly different depending on which initiation factor is targeted for degradation, the results are consistent with the idea that depletion of either Sld2 or Sld3 causes an overall reduction in origin efficiency, at least at the origins that fire under HU treatment conditions.

3.4 2D Gel Electrophoresis of Individual Origins Confirms Reduced Efficiency

To confirm that depletion of either Sld2 or Sld3 reduces origin efficiency, I performed 2D-gel electrophoresis of replication intermediates was asynchronously growing cells to assay origin efficiency at individual origins. A decrease in efficiency at an origin would result in reduced replication bubble signal relative to Y signal on the Southern blot of the 2D gel (see illustrations of hypothetical gels in Figure 2.6 for more details). S phase phenotypes in the induced degron strains were confirmed by flow cytometry before DNA purification and 2D gel electrophoresis

[Figure 3.10]. *ARS1209* and *ARS1213* were selected as representative origins as both were active in the ssDNA replication profiles from both *SLD2*-AID and *SLD3*-AID strains (highlighted in gray in Figure 3.7). In the control condition, both *ARS1209* and *ARS1213* are efficient origins, as evidenced by the intensity of replication bubble signal and relative dearth of signal in the ascending Y-arc for each origin [Figure 3.10]. Upon depletion of Sld2, the replication bubble signal is reduced, and the Y arc signal is more pronounced, indicating reduced efficiency at both *ARS1209* and *ARS1213* [Figure 3.10]. Both *ARS1209* and *ARS1213* were likewise analyzed under reduced Sld3 conditions. Analysis of *ARS1209* in the Sld3-AID strain was less conclusive, but also hinted at reduced efficiency [Figure 3.10]. However, at *ARS1213*, the replication bubble signal was reduced in the auxin-treated cells, with an increase in Y arc signal [Figure 3.10]. In addition to the early-firing origins *ARS1209* and *ARS1213*, efficiency of a late-firing origin of replication, *ARS501* (*ARS522*), was measured. Depletion of Sld2 or Sld3 also diminished origin efficiency at *ARS501*—at that locus, the replication bubble signal was weak in the control conditions and undetectable in depletion conditions [Figure 3.10].

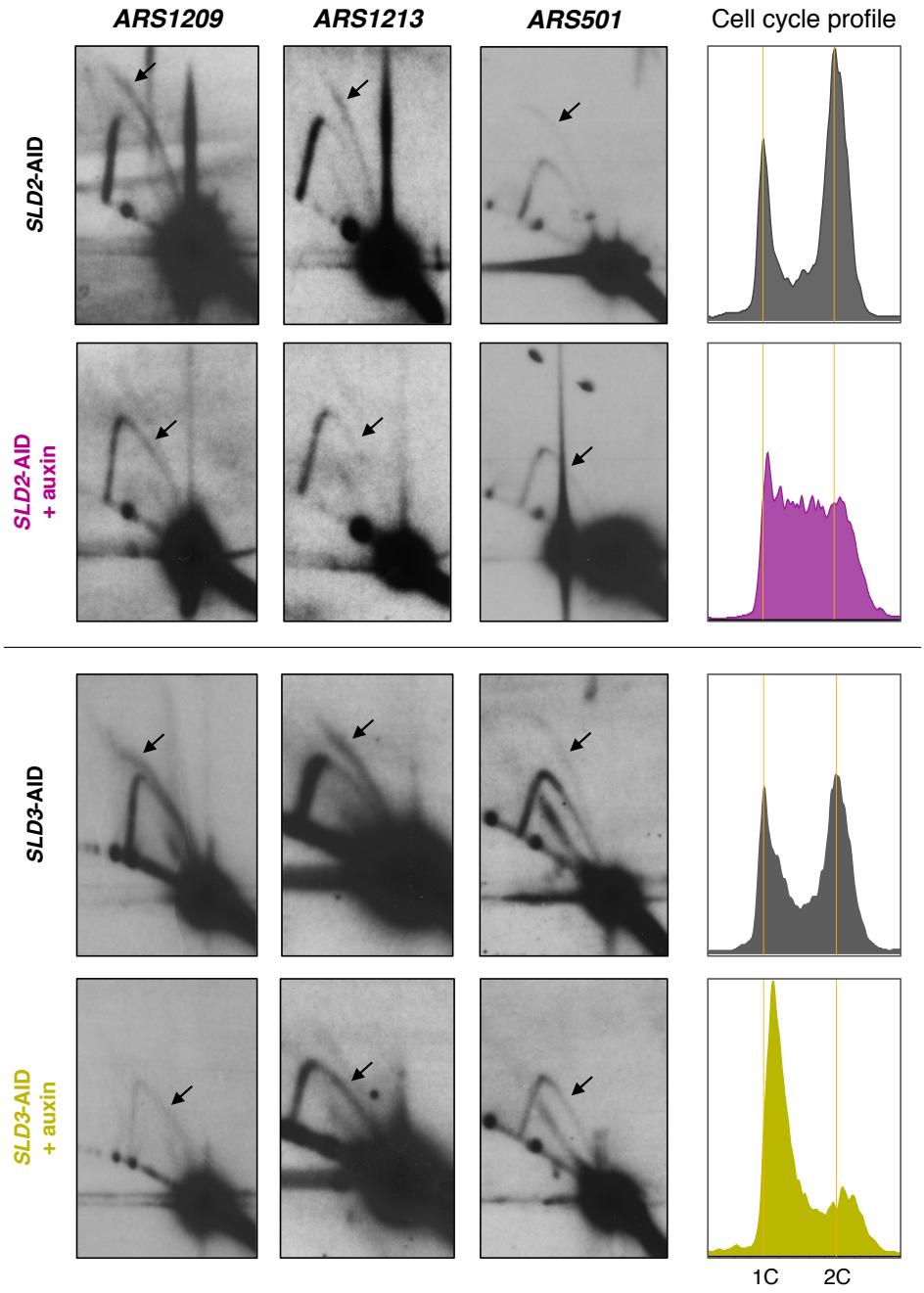

Figure 3.10. 2D gel analysis of *ARS1209*, *ARS1213,* and *ARS501*. [22]

[22] Black arrows indicate replication bubble signal for the uninduced condition gels and replication fork signal on the auxin induced conditions gels. Based on the ssDNA assay replication profiles, two early-firing origins, *ARS1209* and *ARS1213*, were selected for analysis by 2D gel in both the *SLD2*-AID and *SLD3*-AID strains. There is replication bubble signal at both *ARS1209* and *ARS1213* in the uninduced strains. There is also intense signal on the portion of the Y arc that descends from the 2N spot. The bubble arc is less clear on the *SLD3*-AID no auxin *ARS1209* blot. In the auxin-treated samples, the bubble arc signal is lower and the signal intensity along the length of the Y arc is more uniform at both origins, indicating that origin efficiency is reduced. There are fewer replication intermediates in the *SLD3*-AID plus auxin condition at *ARS1209*. A late-firing origin, *ARS501*, was also analyzed by 2D gel. The bubble arc signal is lower and Y arc signal is more consistent along its entire length, confirming

3.5 Late-Firing Origins Are Active When Origin Efficiency is Reduced

If the time an origin fires and its efficiency are two sides of the same coin, then a further reduction in efficiency by depleting Sld2 or Sld3 may prevent late-firing origins from becoming active at all. The outcome of the 2D gel analysis of *ARS501*, a late origin, was consistent with this possibility. However, a genome-wide approach to assay initiation at more late-firing origins would be necessary to determine whether or not late origins fire when efficiency is reduced. I used two different approaches to survey late origin activity.

First, I attempted to delete *CLB5* in the Sld2 and Sld3 degron strains. Deleting *CLB5* interferes with late-origin firing (Donaldson et al., 1998). If deletion of *CLB5* did not worsen the effects of Sld2 or Sld3 depletion on growth rate, cell cycle progression, or viability, it would indicate that late-firing origins are inactive during reduced Sld2- or Sld3-S phase. Deletion of *CLB5* in the *SLD2*-AID strain, attempted both by gene replacement with standard lithium acetate transformation and by crossing *SLD2*-AID with a *clb5Δ* strain, was only somewhat successful. A single, very sick clone was recovered through gene replacement by transformation, but it could not be grown to high enough culture density for experimentation. Instead, I spot-tested the *SLD2*-AID *clb5Δ* strain and found that it has a serious growth defect, even when not galactose-induced or treated with auxin [Figure 3.11]. Deletion of *CLB5* in the *SLD3*-AID strain was, however, successful. The different tolerance for *CLB5* deletion between the two strains was unexpected since the uninduced *SLD2*-AID strain has no S phase phenotype, while *SLD3*-AID is a hypomorph. However, Sld2 has six CDK-dependent phosphosites, while Sld3 has only three (Masumoto et al.,

---

lower firing efficiency at *ARS501*. Flow cytometry profiles for asynchronously-growing degron strains collected for DNA purification and 2D gel electrophoresis are shown on right. Orange lines indicate 1C and 2C DNA content based on the uninduced strain profiles. Depletion of Sld2 in an asynchronous population of cells enriches the number of S phase cells, and depletion of Sld3 causes cells to stall in early S phase and reduces the number of cells in late S/G2 phase.

2002; Zegerman and Diffley, 2007). I suspect that the combination of the degron tag on Sld2 and the restricted window for S-CDK activity in a *clb5Δ* background prevents adequate phosphorylation of Sld2 for initiation of DNA replication.

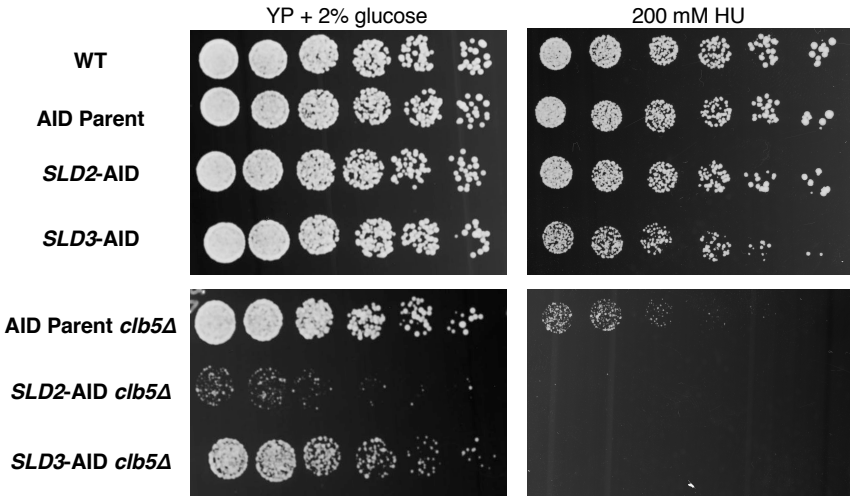

Figure 3.11. Spot test of AID strains and corresponding *clb5Δ* strains on rich media and 200 mM hydroxyurea.[23]

As with the deletion of *CLB5* in the *SLD2*-AID strain, deletion of *CLB5* in the *SLD3*-AID strain caused a growth defect even without auxin-induced depletion of Sld3, as shown by spot-testing cell growth on rich media [Figure 3.11]. Deleting *CLB5* in the AID parent strain did not impact cell growth and viability [Figure 3.11]. The *clb5Δ* versions of the *SLD2*-AID and *SLD3*-AID strains are inviable on media containing 200 mM hydroxyurea [Figure 3.11]. The combination of the degron tag on either of the two initiation factors and inhibition of late-origin firing is more detrimental to cell growth than either effect on its own. This additive effect suggests that late origins are still active, even when Sld2 or Sld3 are depleted from cells.

[23] 1:3 serial dilutions of each strain were spotted onto YP + 2% glucose media and YC + 200 mM hydroxyurea, then incubated at 30°C. YPD plates were photographed after 2 days. HU plates were photographed after 6 days.

Second, to confirm these genetic results, I used whole genome sequencing (WGS) of asynchronous cell cultures to profile DNA replication. This method uses copy number variation across the genome to approximate origin location and activity, allowing me to survey origin firing for all of S phase, as opposed to the ssDNA mapping method [Figure 2.5]. On the WGS replication profiles, there are local maxima in read depth at both early- and late-firing origins, although the absolute height of the peaks at the late-firing origins will be lower than those at early-firing origins (see section 2.7 for more details). If late-firing origins fail to fire completely, there will no longer be peaks in read depth at those origins.

I generated WGS replication profiles for both the *SLD2*-AID and *SLD3*-AID strains, uninduced and treated with auxin. The right arm of ChrXV from ~ 550 - 850 kb contains a series of late-firing origins (McCune et al., 2008) and is highlighted in blue in [Figure 3.12]. This late-replication region provides a clear example of how late-firing origins respond to changes in replication initiation induced by depletion of Sld2 or Sld3. In the control condition for both degron strains, there are peaks in read depth indicating origin activity in the late-replicating region of ChrXV, although the heights of those peaks are lower than the peaks from origins that fire earlier in S phase, such as those nearer the centromere [Figure 3.12]. The lower absolute peak heights on that part of the chromosome is expected since the origins located here are known to fire later in S phase and will therefore be underrepresented in read depth.

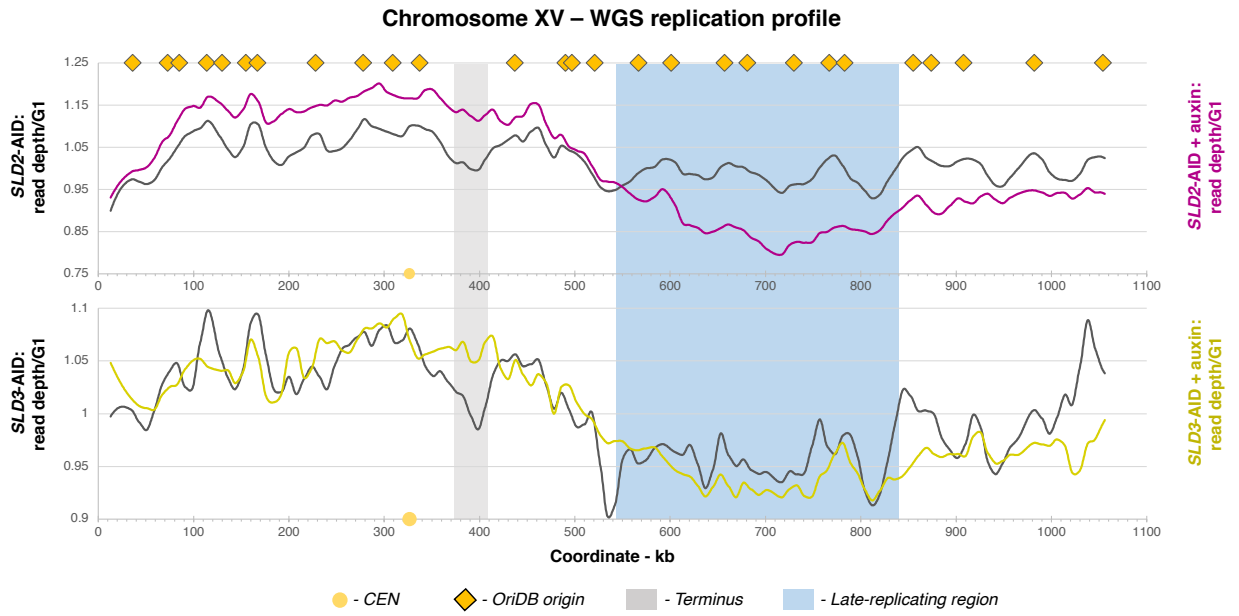

Figure 3.12. ChrXV WGS replication profiles for *SLD2*-AID and *SLD3*-AID strains.[24]

For both the Sld2- and Sld3-depleted cells, there are still peaks in read depth at late-firing origins, indicating that late-firing origins do fire even when origin efficiency is reduced genome-wide [Figure 3.12]. The presence of these peaks confirms the observations made after deleting *CLB5* in the *SLD2*-AID and *SLD3*-AID strains—that late firing origins are active even when efficiency is reduced. While there are peaks at late-firing origins when Sld2 or Sld3 is depleted, the height of those peaks is much lower compared with the control profiles [Figure 3.12]. In fact, the entire late-replicating region on ChrXV is underrepresented in read depth [Figure 3.12]. Lower read depth can be caused either by late-replication or reduced efficiency, but it is difficult to determine whether the lower read depth in this region when Sld2 or Sld3 is depleted is caused by a delay in time of firing or reduced efficiency, or both. However, based on the results of the ssDNA

[24] ChrXV is shown here because of the large, late-replicating region on the right arm of the chromosome—indicated by the blue box. The origins in that region tend to fire late in S phase. Origins classified as "confirmed" in OriDB are indicated on the top X axis as orange diamonds. The origin loci do not line up perfectly with peaks in read depth but are helpful to show where the origins are located, as well as where there are regions that are origin-poor. The gray box indicates a terminus. That region is largely devoid of origins and there is a local minimum in read depth.

mapping replication assay, I suspect that reduced efficiency is more likely to be responsible for underrepresentation of read depth of the late-replicating region of ChrXV.

Moreover, I suspect that changes elsewhere on ChrXV observed on Sld2- or Sld3-depleted replication profiles reflect changes in origin efficiency. On the left arm of ChrXV, the difference in height between peaks and valleys of read depth are not as clear when Sld2 or Sld3 are depleted [Figure 3.12]. This loss in amplitude of read depth variation seems to be driven mostly by "filling in" between peaks that correspond to where origins are located, i.e., loss of replication termini [Figure 3.12]. For example, the local minimum observed at coordinate ~400 kb reflects that there are few origins in that region and replication forks converge in that region—it is a replication terminus. When Sld2 or Sld3 are depleted, that local mimimum in read depth is not as distinct and the read depth across that region is almost completely uniform [Figure 3.12]. A reduction in origin efficiency, which results in increased fork movement as observed by ssDNA mapping assay, could cause replication forks to converge in different places compared to the control condition and produce a replication profile such as those generated from Sld2- or Sld3-depleted cells. See discussion section 4.4 for more information.

3.6 Depletion of Sld2 or Sld3 Reduces Origin Efficiency but Does Not Delay Firing Time of the rDNA Origin

Having tentatively determined that depleting Sld2 and Sld3 reduces origin efficiency, but not time of initiation for both early- and late-firing origins, I realized that there was a part of the genome that I had not yet assayed—the repetitive rDNA locus. Neither of the genome-wide replication assays I had used thus far were appropriate for measuring replication activity at the rDNA locus due to its high copy number. For example, the assembly of the *S. cerevisiae* genome which is used

for aligning sequencing reads contains only two copies of the 9.1 kb rDNA repeat. The disparity between actual rDNA copy number and copy number in the genome assembly results in overrepresentation of rDNA-aligned sequencing reads, rendering analysis of replication activity based on copy number variation ineffective for the rDNA.

Most importantly, I could assay both time of initiation and origin efficiency by performing a timed collection for 2D gel analysis of the rDNA locus during synchronous S phase. Unlike timed 2D gels, neither of the genome-wide methods I had used could allow me to distinguish definitively between time of origin firing and firing efficiency. If reducing origin efficiency delays its time of initiation, as one would predict from the stochastic model for origin firing, then reducing the efficiency of the rDNA origin should also result in a delay in time of origin firing.

I collected DNA samples for 2D gel analysis every 10 minutes following release into S phase until 90 minutes after release. For auxin-treated cells, I continued to collect samples, although less frequently, until 180 minutes after release, to compensate for the extended S phase I observed both under Sld2- and Sld3-depleted conditions [Figure 3.1]. Flow cytometry confirmed that the progression from 1C to 2C DNA content was fully captured by the timed samples [Figure 3.13A & B]. In the uninduced *SLD2*-AID cells, no rDNA origin activity was detected in the G1-arrested control or 20 minutes after the addition of pronase [Figure 3.13A]. Starting 30 minutes after release from α-factor, replication intermediates resulting from both active and passive replication of the rDNA were seen, indicating that the rDNA origins begin to fire 20-30 minutes after release. The signal from the bubble arc is prominent for the subsequent timed samples, but by 90 minutes after release, as the majority of cells reached 2C DNA, the signal from both the bubble arc and Y arc were reduced, indicating the end of new initiation events [Figure 3.13A]. To compare active replication between timed samples, I quantified the blots by calculating the bubble

arc signal as a proportion of the 1N spot (see Figure 2.6 for schematic). The signal from replication bubbles was gradually reduced at the 70-, 80-, and 90-minute samples [Figure 3.13C].

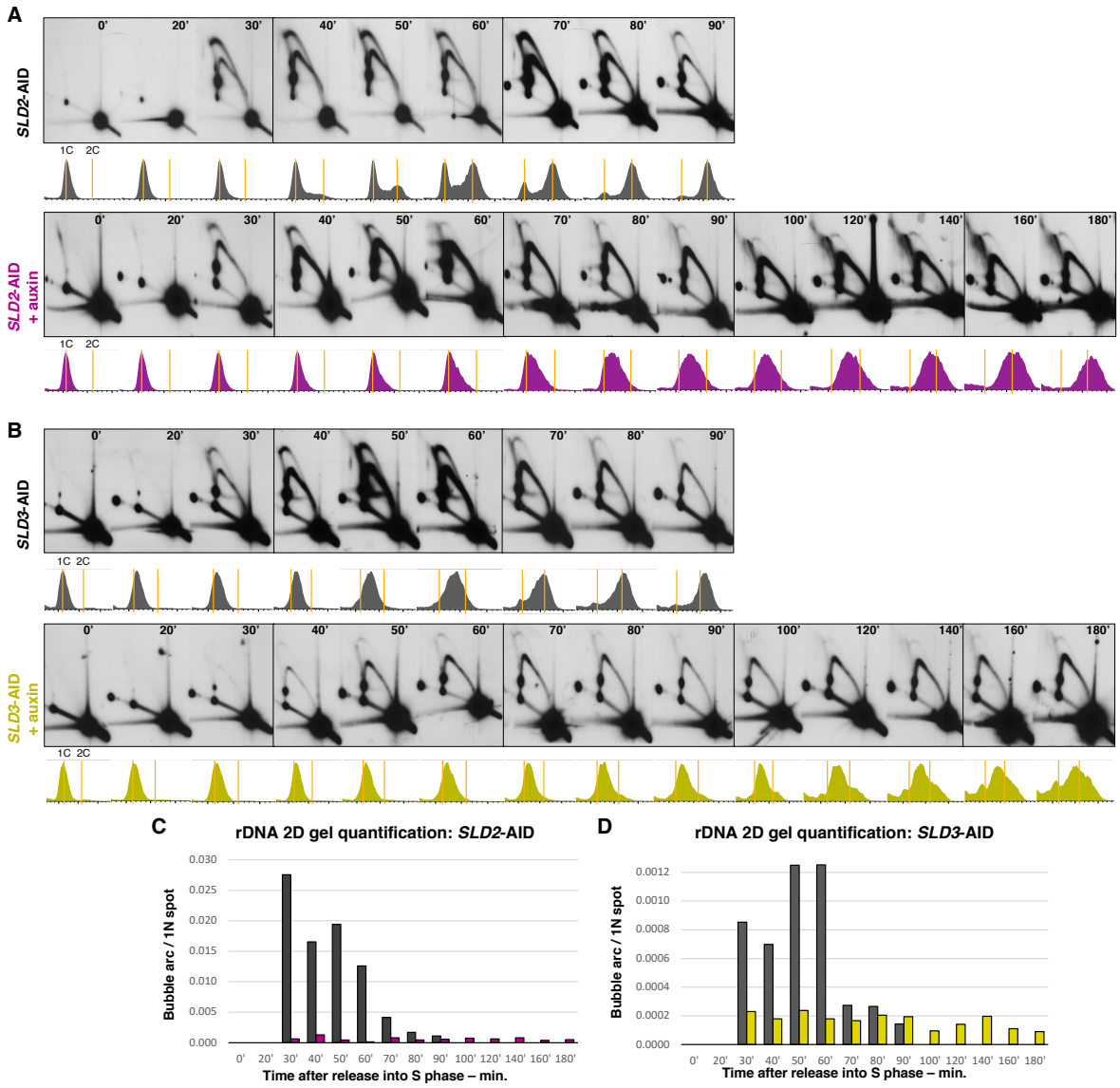

Figure 3.13. 2D gel analysis of the rDNA origin during synchronous S phase.[25]

[25] (A) rDNA 2D gels for *SLD2*-AID vs. *SLD2*-AID plus auxin. Southern blots are probed for one of the non-transcribed spacer regions, *NTS2-2*. Time relative to release from α-factor arrest is indicated in top right corner of each panel. Flow cytometry profiles corresponding to each timed sample are shown below each blot. Orange lines indicate 1C and 2C DNA content. (B) rDNA 2D gels for *SLD3*-AID vs. *SLD3*-AID plus auxin. Flow cytometry profiles are also shown. (C) Quantification of rDNA 2D gels for *SLD2*-AID vs. *SLD2*-AID plus auxin. The bubble arc signal, or hybridization due to active replication origins, is shown as a proportion of the 1N spot signal. No values were calculated for T(0') and T(20') as very little hybridization was present where the bubble arc would be located. (D) Quantification of rDNA 2D gels for *SLD3*-AID vs. *SLD3*-AID plus auxin using bubble arc signal as proportion of 1N spot.

For the Sld2-depleted cells, timed samples were collected up to 180 minutes after release to compensate for the longer time that it takes these cells to reach 2C DNA content (see flow cytometry profiles in Figure 3.13A). Even though Sld2 is depleted, replication intermediates appear at the same time relative to the start of S phase as in the control [Figure 3.13A]. However, the bubble arc signal is reduced compared to the Y arc across the time course [Figure 3.13A]. Quantification of the bubble arc over time confirms that, unlike the control condition, the signal from active DNA replication bubbles is consistently lower than the control and does not decrease as the cells reach 2C [Figure 3.13C].

The same experiment was carried out in the *SLD3*-AID strain, again capturing the cells' passage from 1C to 2C DNA, which required collecting the Sld3-depleted cells for a longer time course (see flow cytometry profiles in Figure 3.13B). Replication intermediates were first detected in the 30-minute sample whether or not Sld3 was depleted. The maximum bubble arc signal occurred between the 50 – 60 minute intervals, but that by the time the population of cells reached 2C DNA at ~90 minutes, the bubble signal had decreased [Figure 3.13B & D]. Upon depletion of Sld3, the replication bubble signal was much lower and, as in the induced *SLD2*-AID strain, persisted for the duration of the longer time course [Figure 3.13B & D]. This result confirms that, like in the Sld2-depleted cells, rDNA origin efficiency is reduced upon Sld3 depletion and suggests that new initiation events continue over a longer timeframe. Thus, the changes in rDNA origin firing efficiency due to depletion of these two limiting initiation proteins echo our findings at single copy origins.

3.7 Chromosome XII is Specifically Destabilized as a Result of Reduced Origin Efficiency

Although the S phase checkpoint is not active when Sld2 or Sld3 is depleted, the rapid onset of viability defects observed in asynchronous growth experiments suggested that genome stability may nonetheless be compromised. Since origin efficiency is reduced genome-wide, I hypothesized that genome instability, in the form of chromosome breakage, may occur as a result. To assay chromosome breakage, I used CHEF gel electrophoresis to resolve whole yeast chromosomes during synchronous S phase. I anticipated that random breakage within chromosomes would manifest as chromosome bands with a smeared appearance on the CHEF gels and that subsequent Southern blotting for individual chromosomes would reveal a distribution of fragments smaller than the full-length chromosome. Additionally, I expected that slowed or partial replication of chromosomes would be observable using this method. Branched DNA structures due to the presence of replication bubbles fail to migrate under CHEF gel conditions, so quantification of chromosome signal from partially replicated chromosomes stuck in the well of each lane is an indicator of delayed or incomplete replication (Cha and Kleckner, 2002; Hennessy et al., 1991).

SLD2-AID and *SLD3*-AID cultures were synchronized with α-factor, then released into S phase, with and without auxin treatment. Flow cytometry samples were collected for each timed sample to verify slowed S phase progression in the Sld2- and Sld3-depleted cells [Figure 3.14]. Asynchronous culture samples were also collected before α-factor was added to the cells to provide a "baseline" measurement for impaired chromosome migration due to partial replication of chromosomes in S phase cells. After arrest and release, samples were collected at varying intervals over 420 minutes (7 hours) to determine how long cells took to complete replication of

all chromosomes when origin efficiency was reduced. Following the 420-minute sample collection, cells were grown to stationary phase overnight, and recovered for a final sample.

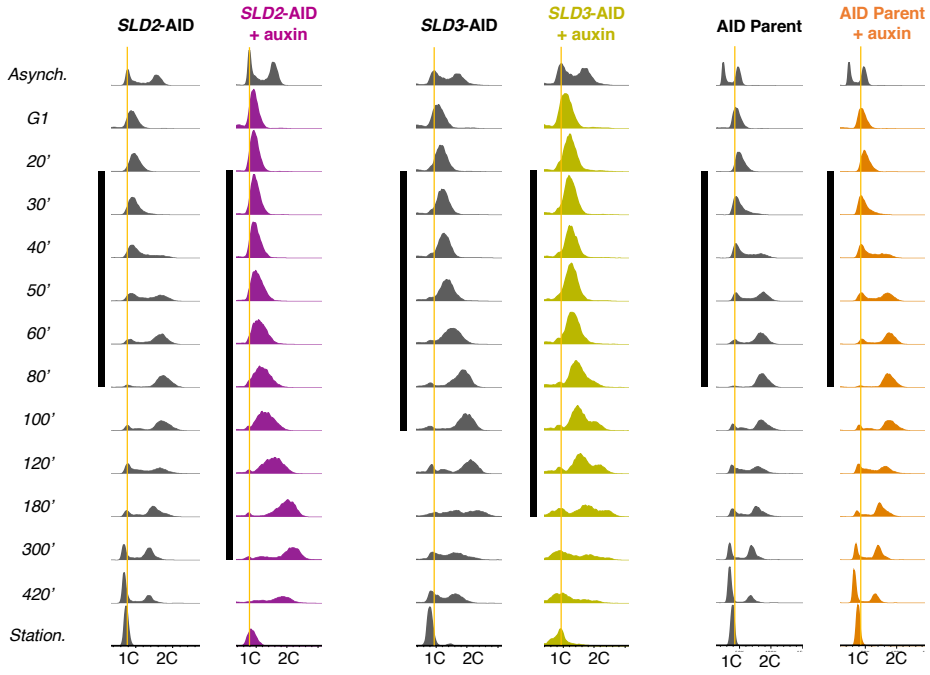

Figure 3.14. Flow cytometry profiles from CHEF gel analysis of genome stability in the degron strains.[26]

Blots were first probed for a single copy chromosome IV sequence. Impairment in DNA migration due to the onset of S phase is evident in the earliest no auxin control samples [Figure 3.15A]. Chromosome signal in the well was low for the G1-arrested control samples, but as the cells enter S phase, more signal is present in the well and depleted from the gel [Figure 3.15A]. As DNA replication finishes and there are fewer partially-replicated DNA molecules (80 - 100 minutes after release in the no auxin samples) there is less signal in the well and chromosomes reappear at their expected positions in the gel [Figure 3.15A]. Quantification of well signal as a

[26] CHEF gel samples were collected during synchronized S phase. Profiles for asynchronously growing cultures as well as stationary phase cells used in this analysis are shown. Orange lines indicate 1C DNA. Vertical black bar indicates estimated duration of S phase. Cells, in both conditions, were allowed to continue through the cell cycle until cells lost synchrony. Note that, in the Sld2- or Sld3-depleted cultures, at the later time points, the cells eventually divide and there are cells present in all phases of the cell cycle.

proportion of total chromosomes signal highlights the changes in chromosome well-retention over the course of S phase [Figure 3.15C]. The samples collected from stationary phase cultures, in which almost no cells are actively proliferating, had very little signal restricted in the well [Figure 3.15A & C]. At the latest times (180, 300, and 420 minutes), when the no-auxin control cells had lost synchrony but were still in log-phase growth, the ratio of signal from partially-replicated and fully-replicated chromosomes was constant [Figure 3.15A & C].

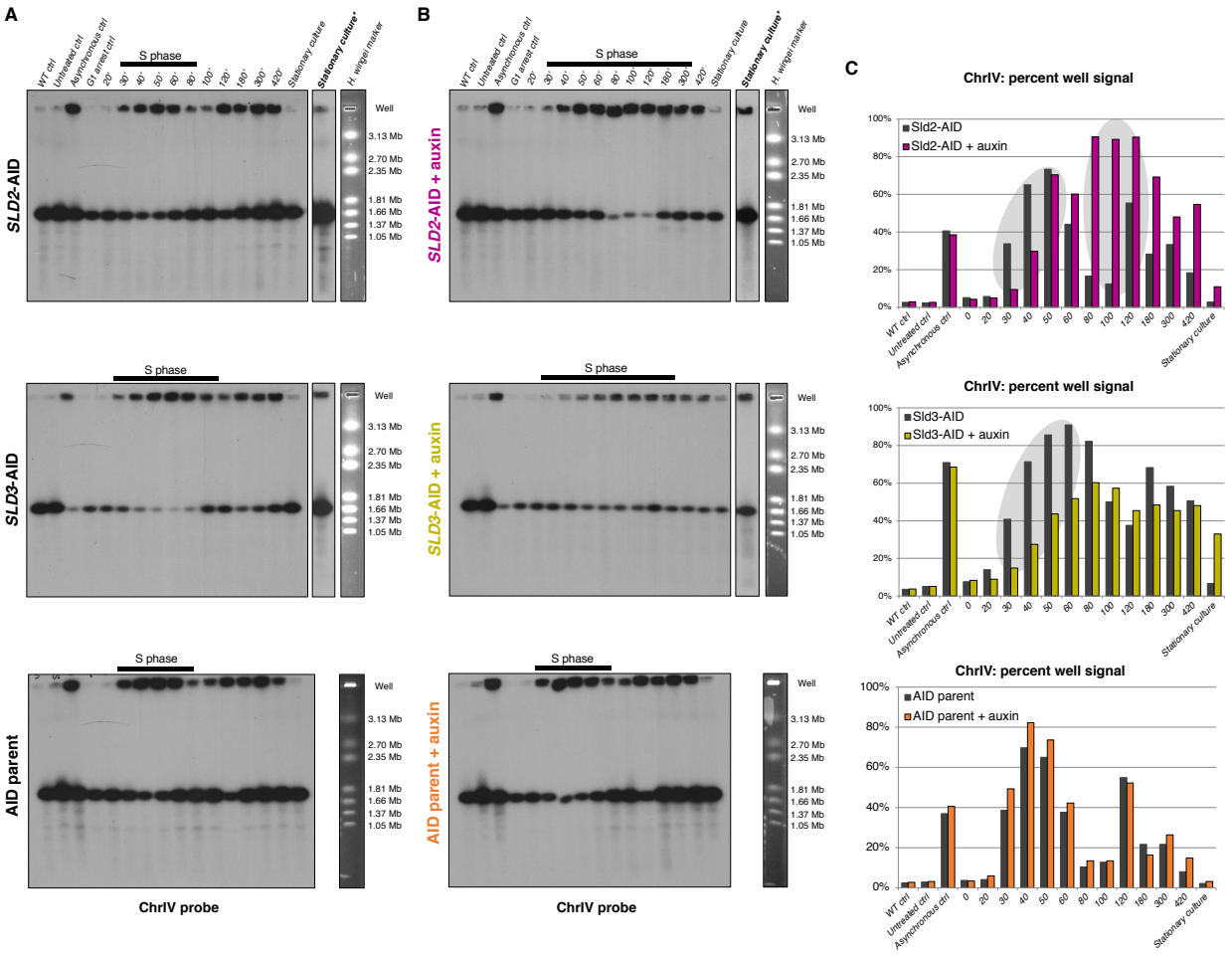

Figure 3.15. ChrIV Southern blots and quantification for degron strain CHEF gels.[27]

[27] (A) No auxin degron strain samples. (B) Auxin-treated degron strain samples. Both sets of blots were probed for *GAL3*. Agarose embedded-*Hansenula wingei* chromosomes were used as a marker for DNA migration and images from the EtBr-strained gels are included to the right of the blots along with chromosome size. The DNA trapped at the top of the gel in the wells is indicated. In addition to the samples shown above, a WT control sample is included, as is a sample from saturated cells that did not undergo galactose induction nor auxin treatment (labelled "Untreated control"). "Saturated culture" are cells that were subjected to the entire time course experiment and then

When Sld2 or Sld3 is depleted, the accumulation of ChrIV signal in the wells after release into S phase was delayed [Figure 3.15B & C]. The peak in well retention for ChrIV in the auxin-treated samples occurred 80 – 100 minutes after release, compared to 50 – 60 minutes after release in the control [Figure 3.15B & C]. Signal in the well persisted for longer in the auxin-treated samples, presumably as it took longer for chromosomes to replicate fully when origin efficiency was reduced [Figure 3.15B & C]. I did not see evidence of random breakage for ChrIV in the timed samples or the stationary phase samples for either *SLD2*-AID or *SLD3*-AID plus auxin [Figure 3.15B & C]. Overexposure of the ChrIV-probed blots to detect chromosome fragments in stationary phase cells revealed no appreciable differences in sub-chromosomal sized fragments between the no auxin and plus auxin samples [Figure 3.15B]. The AID parent strain was also subjected to the same pulsed field gel collection, with and without auxin. The ChrIV-probed blots, and their subsequent quantification, revealed no off-target consequences for chromosome migration in the background strain resulting from the addition of auxin [Figure 3.15A, B, C].

Reduced replication efficiency resulted in very different patterns of migration for chromosome XII [Figure 3.16A, B, C]. For the uninduced strains, the migration pattern of ChrXII over time was very similar to that of ChrIV, although there was generally more ChrXII signal trapped in the well at all times [Figure 3.16A]. I also noted that ChrXII in the *SLD3*-AID strain is reduced in size due to fewer rDNA repeats [Figure 3.16A]. Based on the *H. wingei* marker migration, I estimated that there are ~250 rDNA repeats in the Sld2-AID strain vs. ~90 copies in

---

allowed to grow to stationary phase overnight. The separate images of "Saturated culture" indicated by bold type and an asterisk are over-exposed blots included to reveal chromosome breakage. The black bar indicates the samples estimated to be in synchronous S phase after release, as denoted in Figure 3.14. (C). Bar charts show the hybridization signal in the well relative to total signal for a single sample (see Figure 2.7 for more). Highlighted regions on bar charts indicate the disparity in well signal due to depletion of Sld2 or Sld3.

the *SLD3*-AID strain. Upon induction of the *SLD2*-AID strain, the intensity of the ChrXII band was lost over time [Figure 3.16B]. After 80 minutes, nearly all ChrXII signal was present only in the wells [Figure 3.16B & C]. Longer exposure of the saturated culture samples reveals evidence of ChrXII breakage—a smear of hybridization signal migrating at a smaller size than ChrXII [Figure 3.16B]. These broken chromosome fragments are not present when the no auxin ChrXII-probed blot is overexposed [Figure 3.16A]. The persistence of ChrXII signal in the well followed by chromosome breakage suggests that reduced origin initiation prevents ChrXII from completing replication before cells enter mitosis, causing random breakage along ChrXII.

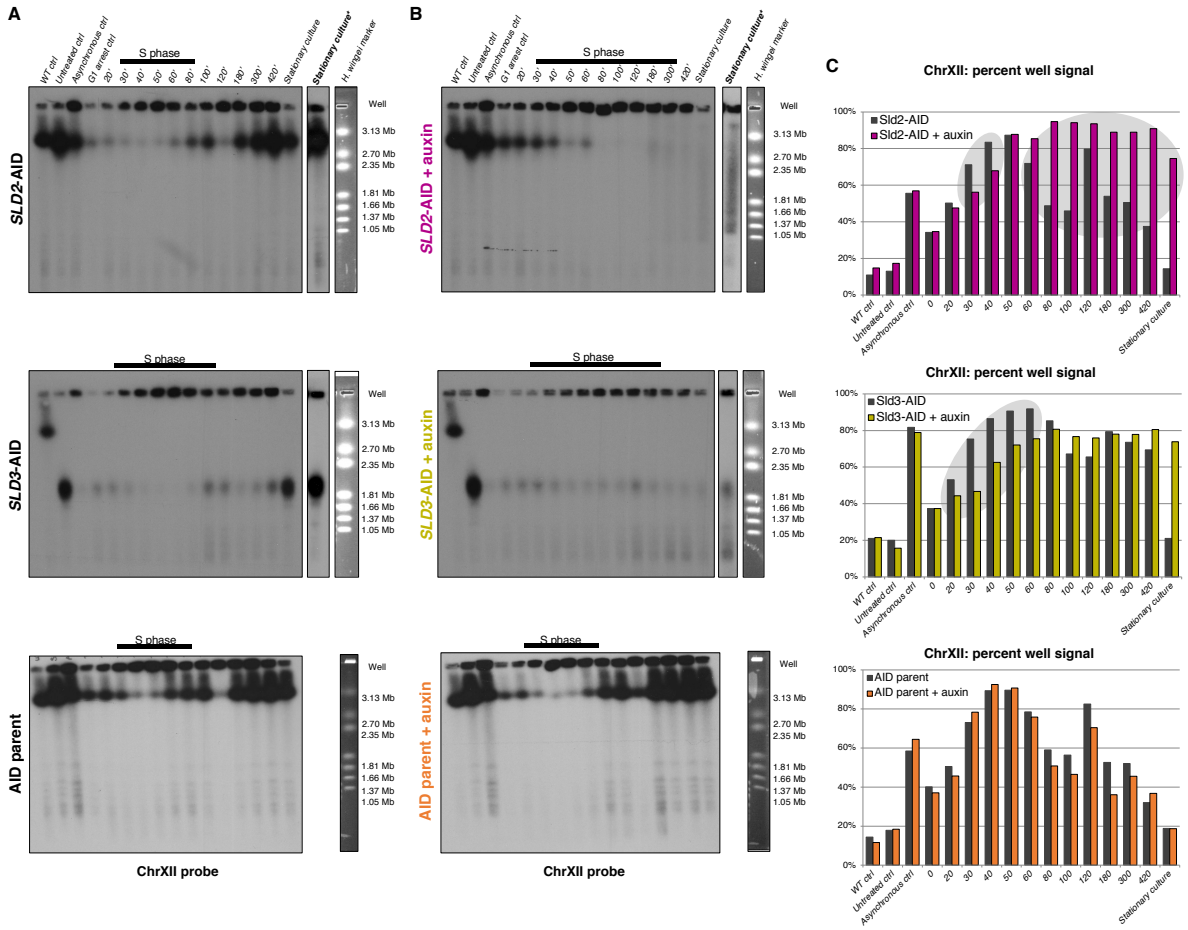

Figure 3.16. ChrXII Southern blots and quantification for degron strain CHEF gels.[28]

[28] (A) No auxin degron strain samples. (B) Auxin-treated degron strain samples. Southern blot for a single copy sequence on ChrXII (*CDC45* gene) of the same blots shown in Figure 3.15. *H. wingei* chromosome marker

The dynamics of ChrXII migration are similar upon Sld3 depletion but the terminal effect is slightly different than with Sld2 depletion [Figure 3.16B & C]. As with *SLD2*-AID, ChrXII signal persisted in the well for longer in the auxin-treated samples, but there was some signal from ChrXII in the lane in every sample, although it is very faint at later times [Figure 3.16B & C]. Based on the flow cytometry analysis of cell cycle progression over the course of this experiment, I suspect that the subpopulation of cells remaining in G1 gives rise to the consistent low ChrXII signal retained in the wells. This effect would confound the differences between the Sld3 depleted vs. control conditions. The reduced rDNA copy number in *SLD3*-AID may also impact how ChrXII is replicated (see Discussion). Probing the AID parent blots for ChrXII revealed that the incomplete replication of ChrXII is specific to Sld2- or Sld3-depleted cells [Figure 3.16A, B, C].

Incomplete replication of ChrXII, but not of ChrIV, suggested that ChrXII is uniquely susceptible to reduced origin firing efficiency. To verify this supposition, I stripped these blots and re-probed for a selection of other chromosomes. The following chromosomes were chosen: chromosome XV, another large chromosome which contains a large late-replicating region that might prove a challenge for completing DNA replication before the onset of mitosis; chromosome X, an intermediate-sized yeast chromosome; and chromosome III, which is one of the smaller yeast chromosomes (See Appendix E for blots and quantification). None of these other chromosomes exhibited as severe a defect in completing replication as ChrXII, indicating that ChrXII is unique among the tested chromosome in its sensitivity to reduced origin efficiency. Chromosome XII is unique in the yeast genome due to the rDNA locus, and we suspected that the rDNA remains

---

migration is shown to the right of each blot and a separate image of an overexposed Southern blot for "Saturated culture" is shown for each strain in both conditions. (C) Bar charts show the hybridization signal in the well relative to total signal. Highlighted regions on bar charts indicate the disparity in well signal due to depletion of Sld2 or Sld3.

unreplicated for much longer than the rest of the genome when replication efficiency is reduced and eventually destabilizes the entire chromosome.

3.8 Incomplete Replication and Breakage Within the rDNA Array Destabilizes ChrXII

To test whether the rDNA locus causes instability of ChrXII, I repeated the CHEF gel collection, this time using asynchronous cultures of the *SLD2*-AID strain and collecting cells 120 minutes and 240 minutes after adding auxin, as well as allowing the cells to grow to saturation overnight as before. Flow cytometry showed an enrichment of S phase cells as had been observed previously [Figure 3.17A]. In addition to running the agarose-embedded chromosomes under the standard conditions, I also treated one portion of each agarose-embedded sample with the intron-encoded endonuclease I-Ppo1, which cuts once within each yeast rDNA repeat, but not elsewhere in the yeast genome (Ellison and Vogt, 1993). If incomplete replication of the rDNA is indeed causing persistent branched structures on ChrXII that prevent the chromosome from migrating in the gel, then cutting the DNA molecule within the rDNA should release the fully replicated regions of the chromosome on either side of the rDNA, which can detected by hybridization of the Southern blot with unique single copy probes [Figure 3.17B].

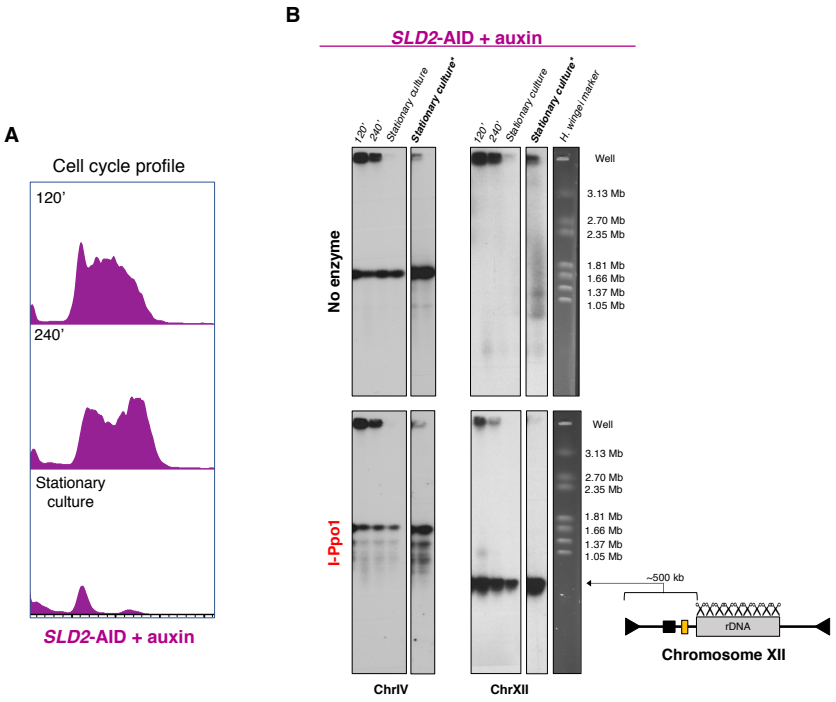

Figure 3.17. I-Ppo1 digest of CHEF gel samples from Sld2-depleted cells reveals incomplete replication of the rDNA.[29]

ChrXII failed to migrate from the top of the gel in Sld2-depleted cells [Figure 3.17B]. In the saturated culture sample, breakage of ChrXII, but not ChrIV, was evident upon longer exposure of the film [Figure 3.17B]. Migration of the ~500 kb portion of ChrXII to the left of the rDNA was restored in the I-Ppo1-treated samples, confirming that incomplete replication of the rDNA array causes the well retention of ChrXII in Sld2-depleted cells [Figure 3.17B]. In the saturated culture sample, in which ChrXII shows evidence of breakage, the released part of ChrXII (left of the rDNA) once again migrates as a band after I-Ppo1 digestion Figure 3.17B]. The migration of an intact portion of chromosome generated from the broken chromosome reveals that all the

[29] (A) Flow cytometry profiles from asynchronous *SLD2*-AID plus auxin cells used for I-Ppo1 digested CHEF gel experiment. (B) Southern blots were probed with *GAL3,* stripped, and re-probed with *CDC45*. ChrIV migration did not change when samples were treated with I-Ppo1. ChrXII does not migrate from the top of the gel in the control condition, but the portion of ChrXII left of the rDNA does migrate after I-Ppo1 digest. The schematic of ChrXII to the right of the blot shows where I-Ppo1 cuts on Chr XII (the scissors symbol) in relation to the *CDC45* probe shown in orange.

breakage evident in the undigested sample occurred within the rDNA locus. The unusual structure of the rDNA array renders ChrXII more sensitive to reduced origin efficiency while, in contrast, the unique parts of the genome are not as catastrophically destabilized.

Chapter 4. DISCUSSION AND CONCLUSIONS

4.1 Origin Efficiency Can Vary Without Impacting Time of Initiation

My work demonstrates that the efficiency of origin firing is independent of time of initiation. My success in manipulating origin efficiency independently of origin firing time does not support the recently proposed stochastic model for origin firing. The stochastic model predicts that any changes to origin efficiency will result in a change to time of origin firing (Rhind, 2006; Yang et al., 2010). In the course of my work, I depleted two different limiting replication initiation factors, Sld2 and Sld3, which reduced origin firing genome-wide, both at early- and late-firing origins of replication. The stochastic model predicts that reducing the efficiency of late-firing origins would delay their firing, which could result in their being unable to fire at all if efficiency is reduced to an extreme degree. In contrast to these predicted changes, I observed that late-firing origins are active in the *SLD2*-AID and *SLD3*-AID strains, both by a genetic test and genome-wide replication assay [see section 3.5].

It is particularly striking that deleting *CLB5* in either degron strain, which prevents late origins from firing, results in a severe growth phenotype and sensitivity to HU even without auxin-induced depletion of the degron-tagged proteins [Figure 3.11]. The additive effects of *CLB5* deletion and presence of the auxin degron make it clear that both the *SLD2*-AID and *SLD3*-AID strains require that late origins fire, even at a lower efficiency, to carry out complete DNA replication. The two strains, however, did not tolerate the deletion of *CLB5* equally [Figure 3.11]. Before attempting to construct the *clb5Δ* degron strains, I predicted that the *SLD3*-AID strain would not tolerate deletion of *CLB5*. This prediction was based on finding that the auxin degron on Sld3 causes a partial loss of function and that replication initiation in the uninduced *SLD2*-AID strain was nearly indistinguishable from WT as measured by the ssDNA assay [Figure 3.7, Figure

3.8]. I expected that further inhibition of origin firing caused by the deletion of *CLB5* would be a problem for the *SLD3*-AID strain, but not for the *SLD2*-AID strain. The opposite was true, and the *SLD2*-AID *clb5Δ* strain was so unhealthy that I could not even grow adequate amounts of it to perform many experiments besides the spot-tests [Figure 3.11]. This severe growth defect was yet another example of how, while both Sld2 and Sld3 depletion reduced origin efficiency, the phenotypes were slightly different depending on which initiation factor was being targeted with the AID system.

4.2 The Abundance of Sld2 and Sld3 Influences Origin Efficiency, But Not Time of Origin Firing

Of the four limiting SSDD factors, the cellular availability of two of those factors, Sld2 and Sld3, primarily determines the efficiency of origin firing. Since the relative time of origin activation is maintained even when efficiency is lower due to depletion of Sld2 or Sld3, it seems that some prior-acting component of this system is already in play to determine when origins become active. This supposition is in agreement with previous work showing that time of origin activity is established during G1 phase (Dimitrova and Gilbert, 1999; Raghuraman et al., 1997). Considering that Mantiero et al. (2011) found that overexpression of the SSDD factors advanced both replication time and efficiency, I suspected that the abundance of one of the other limiting factors is responsible for the advancement in replication time and that it likely acts upstream of Sld2 and Sld3 at the replisome. Since phosphorylation of the MCM2-7 helicase by the Dbf4-dependent kinase is required for Sld3 to bind to the replisome, and Dpb11 is brought into the replication complex simultaneously with Sld2, it seemed possible that Dbf4 abundance is responsible for the changes in time of origin firing [Figure 1.3] (Deegan et al., 2016; Muramatsu et al., 2010). In fact,

a recent study has established a mechanistic link between Dbf4, the regulatory subunit of DDK that phosphorylates the MCM2-7 helicase, and Fkh1/2 transcription factor binding near origins as a determinant of origin firing time (Fang et al., 2017). If I were to continue working on this project, I would want to deplete cells of Dbf4 (perhaps using a temperature-sensitive mutant, since my attempts to construct a degron stain were unsuccessful), and assay changes to replication genome-wide.

In thinking more about how my own work relates to this new Dbf4 study, I returned to the question of how all of the cell cycle-dependent regulatory steps of DNA replication are interleaved with one another. For example, upstream of DDK phosphorylation of the MCM2-7 helicase is pre-replication complex assembly, which is regulated by the reduction in CDK activity that occurs during G1 phase (Remus and Diffley, 2009). If pre-RC assembly at early-firing origins is reduced to a subset of cells in the population, the recruitment of DDK via Dbf4's interaction with Fkh1/2 to those early-firing origins would still promote their early time of firing, but efficiency would be reduced. Considering these different phosphorylation-dependent steps involving key replisome components, I wondered to what extent CDK and DDK may be regulating the distinct processes of origin firing time and efficiency. In the next section, I will describe my model for how CDK- and DDK-influenced interactions determine replication time and efficiency in greater detail.

4.3 A Unifying Model for the Determination of DNA Replication Timing and Efficiency

In the course of my work, I developed a more unified model for how replication time and efficiency are separately regulated. I propose that the cellular availability and preferential interaction of the Dbf4-dependent kinase (DDK) with certain parts of the genome give rise to differences in origin

firing time, while factors responding to the activity of CDK primarily impact origin efficiency. My model begins with the assumption that time of origin firing and origin efficiency are different features of DNA replication. However, since the main replication complex assembly steps leading to origin activation depend sequentially on low CDK activity (pre-RC assembly), then DDK activity (phosphorylation of MCM2-7), and then high CDK activity (phosphorylation of Sld2 and Sld3 leading to CMG assembly and activation), these features are somewhat interdependent, which has probably led to the mistaken conclusion that efficiency and timing are determined by the same features [Figure 4.1] (Bell and Labib, 2016). For example, histone acetylation near an origin may impact ORC-binding which is the basis for pre-RC assembly (pre-RC assembly occurs when CDK activity is low), the phosphorylation of MCM2-7 (DDK-dependent), as well as how well Sld2 or Sld3 can access the replisome (CDK-dependent). Consequently, deleting the histone deacetylase Rpd3 results in changes to both timing and efficiency of origin firing (Knott et al., 2012).

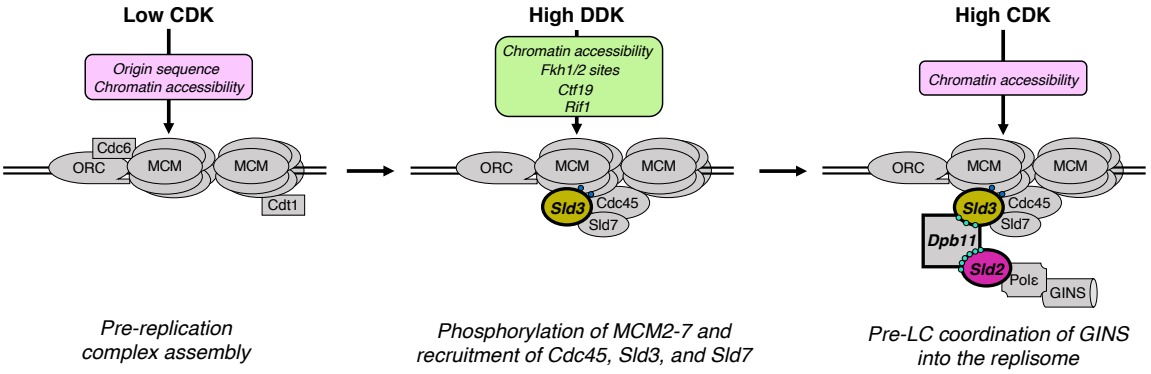

Figure 4.1. Model for CDK-influenced determination of origin efficiency and DDK-driven time of origin firing.[1]

[1] The steps leading to replisome assembly are sequential and interdependent. Some protein associations are influenced oppositely by CDK activity, such as pre-RC assembly and the pre-LC's interaction with the replisome. In my model, those CDK-influenced processes determine efficiency of origin activity, rather than firing time. The features of the genome that determine these CDK-influenced processes, described in the pink boxes, contribute to origin efficiency. This idea is supported by my own work on reducing the abundance of Sld2 and Sld3, as well as a genome-wide replication study of an Orc1 mutant (Zhong et al., 2013). In both studies, reducing the function of these CDK-influenced replisome assembly steps primarily reduced origin firing efficiency. From my model, I predict that DDK-dependent replisome assembly steps primarily impact time of origin firing, and any genomic features that influence DDK's association with origins (described in the green box) will likewise impact time of

In some cases, the features that influence timing or efficiency of replication have an evolutionarily selective advantage, but in other cases they may be incidental to the genome organization or chromatin state of a particular region of the genome. For example, Dbf4 is also recruited to centromeres by the kinetochore component Ctf19 and advances the time of origin firing within a certain distance of the centromere (Natsume et al., 2013; Pohl et al., 2012). If origins near the centromere are deleted to create a late-replicating centromere in a spindle pole checkpoint mutant, chromosome loss rate is increased (Natsume et al., 2013; Pohl, 2013). The increased genome stability imparted by early time of centromere replication may be the reason that early time of centromere replication is conserved across eukaryotes. In contrast, in the case of Rif1, its role in maintaining telomere structure may be more relevant, biologically, and its role in delaying time of DNA replication may be somewhat incidental (Hiraga et al., 2014; Smogorzewska and Lange, 2004).

My work demonstrates that two S-CDK targets, Sld2 and Sld3, act primarily to influence efficiency of origin firing. Since Dpb11 is also a target of S-CDK and it interacts specifically with Sld2 and Sld3, I would anticipate that its abundance also determines origin efficiency, rather than time of replication (Kamimura et al., 1998, 2001). I would also expect that Cdc45 acts as something of a nexus between DDK and CDK regulation of timing and efficiency. Its interaction with the replisome depends both on DDK phosphorylation of the MCM2-7 helicase along with Sld3, although its integration into the active CMG helicase depends on the CDK-driven interaction between Sld3, Dpb11, and Sld2 (Kamimura et al., 2001; Muramatsu et al., 2010). Experimental

---

origin firing. It is important to note that many aspects of genome organization, such as chromatin accessibility, can impact both the CDK- and DDK-influenced steps of replisome assembly. That overlap in influence on time and efficiency has likely contributed to conflating origin efficiency and firing time as being inherently the same characteristic.

evidence confirms that integration of Sld3, Cdc45, and Sld7 into the replisome, which depends on DDK phosphorylation of MCM2-7, is a key step for determining time of origin firing (Tanaka et al., 2011a). Additionally, my model would agree with the tenuous correlation between MCM2-7 occupancy at origins and time of origin firing, should the relationship between MCM2-7 and origin firing time hold up with better experimental evidence (Das et al., 2015). In my model, the more stable the interaction of MCM2-7 with an origin, the more likely it is to be phosphorylated by DDK, leading to an earlier time of initiation.

Given the interdependence of the replisome assembly steps, it would be challenging to test the individual contributions of CDK- and DDK-influenced steps to prove or disprove my model. However, I think that focusing on the mode through which Dbf4 influences time of origin firing would be an important place to start. In the first paper to identify that Fkh1/2 impact origin activity, the researchers found that simply integrating a Fkh binding site near an origin did not advance time of replication (Knott et al., 2012). However, if Fkh-dependent time of origin firing depends on its interaction with Dbf4, and Dbf4 is a limiting initiation factor, perhaps other origins with Fkh sites have a higher affinity for recruiting Dbf4 due to other characteristics, which would prevent the integration of a Fkh site alone from advancing time of firing (Fang et al., 2017; Mantiero et al., 2011). I would test this prediction by replacing all of the origins on a single yeast chromosome with the same Fkh-associated origin and assay replication activity for the entire chromosome when Dbf4 is overexpressed. In that scenario, I predict that all origins would advance in their time of replication, but due to the impact of other chromosome features in the surrounding chromatin context outside of the origin sequence itself, there would still be variation in time of origin firing. While my CDK/DDK model remains to be tested, I think that it is in agreement with much of the pre-existing work on regulators of origin timing and efficiency, as described in section 1.1.

4.4 Whole Genome Sequencing Also Reveals Changes in Fork Movement

Until now, the primary information provided by whole genome sequencing-based replication profiles has been location of origins and their relative time of origin firing and efficiency (Muller, et al. 2014). Due to the nature of WGS replication profiling, it is impossible to differentiate between late-firing and inefficient origins, since both will be underrepresented in sequencing depth (Müller et al., 2014). However, the WGS replication profiles I generated in this study suggest that that this assay can also provide information about changes in replication fork movement. I noticed that the main differences in the replication profiles between the control and auxin-treated *SLD2*-AID and *SLD3*-AID strain conditions came from the replication termini.

Termini are regions between origins where replication forks converge (Zhu et al., 1992). Due to variability in origin timing and efficiency as well as the fact that DNA sequence does not play a large role in termination, forks converge over much broader regions compared to site-specific origins (Hawkins et al., 2013; McGuffee et al., 2013). Despite their broad nature, termini are detectable by genome-wide replication profiling methods (Alvino et al., 2007; Raghuraman et al., 2001). For example, termini between two efficient origins would result in a very clear local read depth minimum on a WGS-based replication profile, because the replication forks would tend to converge in the same place in a population of cells [Figure 4.2]. In my WGS replication profiles, when Sld2 or Sld3 was depleted, I observed peaks in read depth due to origin firing, but I noticed that read depth was not as low at termini as it was in the WT condition [Figure 3.12]. The loss in contrast of read depth at termini gives the impression that the replication profiles for the *SLD2*-AID plus auxin and *SLD3*-AID plus auxin strains have been "smoothed-over" [Figure 4.2]. I suspect that the increased read depth at termini is caused by the global reduction in origin efficiency caused by depletion of Sld2 or Sld3. In contrast to WT, when origin efficiency is

reduced, and replication forks are able to travel farther from origins, the read depth is less varied between sites of initiation and termination, resulting in smoothed-over replication profiles [Figure 4.2].

Due to the noisiness of WGS replication profiles, I do not think it is appropriate to rely solely on that method to detect changes in replication fork movement. I do, however, think it is significant that both genome-wide replication profiling methods I used in this study imply changes in replication fork movement due to reduced origin efficiency. If I were I to continue working on this particular project, I would want to confirm these changes in replication termination caused by reduced origin efficiency using the Okazaki fragment sequencing method (McGuffee et al., 2013).

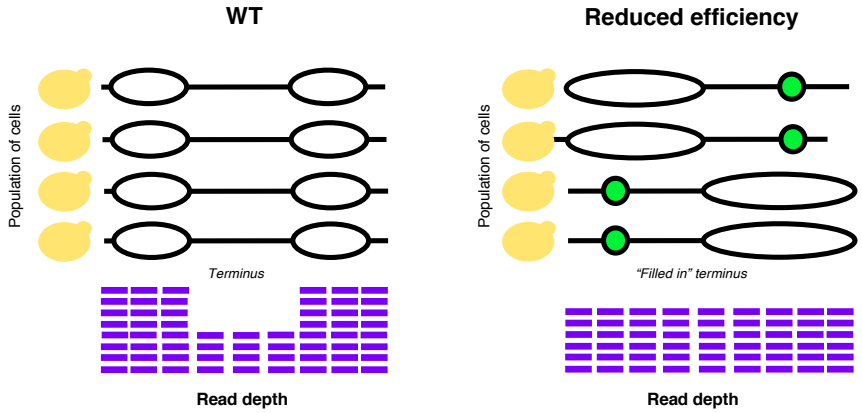

Figure 4.2. Changes in fork movement at replication termini as detected by WGS.[2]

[2] In the WT cells, high efficiency of the two origins results in a clear local minimum of read depth at the terminus between the two sites of initiation. In contrast, when origin efficiency is reduced, and replication forks move farther in each individual cell, the difference in read depth is not as distinct between the sites of initiation and the terminus. This loss of contrast in read depth results in the "smoothed-over" replication profiles generated from Sld2- or Sld3-depleted cells.

4.5 The rDNA Locus is an Achilles' Heel for Reduced Replication Efficiency

The implications of my CHEF gel experiments are that while most chromosomes are not destabilized by origin reduced efficiency, chromosome XII is an exception, likely due to the unusual replication characteristics of the rDNA array. The instability of the repetitive rDNA array compared to the stability of the unique parts of the genome I observed in my CHEF gel analysis lends some insight into why might cells maintain variability in origin activity. Outside of the rDNA locus, early- and late-firing, highly efficient and barely active origins are interspersed with one another on each chromosome. Even when challenged with depletion of Sld2 or Sld3, enough origins are able to fire on every chromosome in every cell to allow for passive replication of the origins that fail to fire, resulting in the eventual duplication of the entire chromosome. The non-uniformity in origin firing time and efficiency contributes to the stability of the non-repetitive parts of the genome. The rDNA locus, however, where every origin has the same sequence and the same sequence context, is clearly a problem for genome stability when replication efficiency is reduced. It should also be noted that the replication fork barrier (RFB) likely also plays a role in this instability. The RFB, which ensures that the replication forks move in the same direction as transcription from the rDNA genes, could also prevents replication forks from "rescuing" replication at inactive origins. During reduced origin efficiency in S phase, when very few active replication forks are responsible for duplicating the entire genome, the inability of incoming forks to rescue replication in the rDNA may contribute to the catastrophic and specific instability observed in that region.

While ChrXII-specific destabilization during compromised S phase has been observed previously, my observations of ChrXII instability emanating from the rDNA array suggest a

slightly different interpretation of that outcome than the conclusions drawn by Ide et al. (2007) when they observed a similar phenomenon. After shifting asynchronously-growing *orc1-4* cells to the non-permissive temperature, Ide et al. (2007) observed a ChrXII instability phenotype before instability of the other chromosomes. Primarily from this difference in time of onset of instability, they proposed that the rDNA array acts as a sensor for problems with DNA replication initiation, and that instability of the rDNA acts as something of a "canary in a coal mine" for the rest of the genome. No mechanism for transduction of such a signal was identified in their work, and I suspect that the time at which they first observed instability is misleading. In their study, Ide et al. (2007) never synchronized the cultures, so the actual time of onset of instability relative to the start of S phase was not determined. If the rDNA is the first part of the genome to experience initiation defects and, based on sensing those problems, it then relays that information to the rest of the genome, one would predict that replication initiation defects would be detected on ChrXII before the other chromosomes. However, in my synchronous CHEF gel experiments, ChrXII's problems migrating into the gel (evidence of partial replication or incomplete replication) are not detected any earlier than the migration issues experienced by other chromosomes (compare T0 - T60 for the plus auxin condition on the bar charts in Figure 3.15A and Figure 3.16A). I concluded that Chr XII is inherently less stable than other chromosomes due to the repetitive nature of the rDNA that prevents ChrXII from replicating completely before the onset of mitosis when replication initiation is reduced. Furthermore, the instability of ChrXII has no bearing on the stability of the other chromosomes; in my experiments, I did not detect instability of other chromosomes over the timeframe of my experiments.

This particular stress on the rDNA locus results in a preference for lower rDNA copy number in cells with persistent replication efficiency defects, as has been observed in previously

published work from our lab (Sanchez et al., 2017). The hypomorphic *SLD3*-AID strain exhibits reduced origin efficiency even before depletion of Sld3 and has a reduced rDNA copy number (~90 repeats vs. ~250 in the WT control). It is unclear whether this reduction is due to an active process on the part of the cell or, if in the course of strain construction, the only cells that could tolerate the degron tag on Sld3 already had reduced rDNA copy number. Further depressing the number of origins active during S phase by deleting *CLB5* in the *SLD3*-AID strain is associated with further reduction in rDNA copy number (data not shown here), a slower growth phenotype, and increased sensitivity to hydroxyurea. This particular problem of low efficiency also prevents the cell from sensing potential problems to genome stability because so few origins fire that the amount of RPA-coated ssDNA at replication fork may be too low for cells to sense (Shimada, 2002). Since the checkpoint is not activated, the cells likely continue into mitosis while the rDNA locus remains partially-replicated, leading to breakage specifically within the rDNA locus.

The instability of the rDNA in *S. cerevisiae* suggests that large spans of repeated DNA elements may likewise be a problem for genomes with much more repetitive content, such as the human genome. For example, the rDNA in humans, while divided into arrays on 6 different chromosomes, has a tandem repeat structure (Stults et al., 2008). Human centromeres, which are megabases long, also consist of tandem repeats primarily made up of α satellite DNA (Melters et al., 2013; Willard, 1990). The yeast rDNA locus is the only part of the yeast genome that approximates the structure of these long, tandemly-repeated parts of the human genome, and its sensitivity to replication initiation defects suggests that defective replication initiation may also impact the stability of similarly repetitive regions of metazoan genomes. Generally, it would be challenging to determine whether large repeated DNAs in metazoan cells are similarly sensitive to replication initiation defects because the requirements for origins are still unclear in those

organisms (reviewed comprehensively by Prioleau and MacAlpine, 2016). While the use of copy number-based WGS replication profiling experiments is rapidly expanding our understanding of the replication landscape in human cells, that particular method is difficult to apply to repeated sequences. DNA replication through repetitive sequence remains, for the most part, uninvestigated and, based on my work, a potential challenge for metazoans in terms of ensuring complete replication and maintaining genome stability.

4.6 Conclusions

In summary, reducing the cellular abundance of Sld2 and Sld3 results in changes in origin firing efficiency, but not time of initiation. Under Sld2 or Sld3 depleted conditions, I observed reduced origin efficiency genome-wide at both early- and late-firing origins. In contrast to recent proposals that firing time is a secondary consequence of origin efficiency, my work demonstrates that efficiency and time of initiation are separable features of the eukaryotic genome. My analysis of the high copy number rDNA origin, in which I assayed both the time of rDNA origin initiation and efficiency during synchronous S phase, provides the most concrete evidence that origin efficiency can be drastically reduced without affecting the time at which the origin fires. The reduction in origin efficiency caused by the depletion of Sld2 or Sld3 does compromise the stability of the yeast genome. In agreement with previous work from my lab and other groups, I found that the rDNA array on ChrXII is particularly sensitive to reduction in initiation efficiency, leading to ChrXII breakage and reduced viability. In contrast, the other chromosomes are stable throughout reduced initiation factor S phase.

REFERENCES

Alvino, G.M., Collingwood, D., Murphy, J.M., Delrow, J., Brewer, B.J., and Raghuraman, M.K. (2007). Replication in Hydroxyurea: It's a Matter of Time. Mol. Cell. Biol. *27*, 6396–6406.

Aparicio, J.G., Viggiani, C.J., Gibson, D.G., and Aparicio, O.M. (2004). The Rpd3-Sin3 Histone Deacetylase Regulates Replication Timing and Enables Intra-S Origin Control in Saccharomyces cerevisiae. Mol Cell Biol *24*, 4769–4780.

Aparicio, O.M., Weinstein, D.M., and Bell, S.P. (1997). Components and dynamics of DNA replication complexes in S. cerevisiae: redistribution of MCM proteins and Cdc45p during S phase. Cell *91*, 59–69.

Aparicio, O.M., Stout, A.M., and Bell, S.P. (1999). Differential assembly of Cdc45p and DNA polymerases at early and late origins of DNA replication. Proc Natl Acad Sci U S A *96*, 9130–9135.

Araki, H., Leem, S.-H., Phongdara, A., and Sugino, A. (1995). Dpb11, which interacts with DNA polymerase II (epsilon) in Saccharomyces cerevisiae, has a dual role in S-phase progression and at a cell cycle checkpoint. Proceedings of the National Academy of Sciences *92*, 11791–11795.

Bell, S.P., and Dutta, A. (2002). DNA Replication in Eukaryotic Cells. Annual Review of Biochemistry *71*, 333–374.

Bell, S.P., and Labib, K. (2016). Chromosome Duplication in Saccharomyces cerevisiae. Genetics *203*, 1027–1067.

Bell, S.P., and Stillman, B. (1992). ATP-dependent recognition of eukaryotic origins of DNA replication by a multiprotein complex. Nature *357*, 128–134.

Bloom, J., and Cross, F.R. (2007). Multiple levels of cyclin specificity in cell-cycle control. Nature Reviews Molecular Cell Biology *8*, 149–160.

Blow, J.J., Ge, X.Q., and Jackson, D.A. (2011). How dormant origins promote complete genome replication. Trends Biochem Sci *36*, 405–414.

Boos, D., Sanchez-Pulido, L., Rappas, M., Pearl, L.H., Oliver, A.W., Ponting, C.P., and Diffley, J.F.X. (2011). Regulation of DNA Replication through Sld3-Dpb11 Interaction Is Conserved from Yeast to Humans. Current Biology *21*, 1152–1157.

Bousset, K., and Diffley, J.F.X. (1998). The Cdc7 protein kinase is required for origin firing during S phase. Genes & Development *12*, 480–490.

Branzei, D., and Foiani, M. (2010). Maintaining genome stability at the replication fork. Nature Reviews Molecular Cell Biology *11*, 208–219.

Braun, R., and Wili, H. (1969). Time sequence of DNA replication in Physarum. Biochimica et Biophysica Acta (BBA)-Nucleic Acids and Protein Synthesis *174*, 246–252.

Brewer, B.J. NIB-n-grab DNA prep. http://fangman-brewer.genetics.washington.edu/nib-n-grab.html

Brewer, B.J., and Fangman, W.L. (1987). The localization of replication origins on ARS plasmids in S. cerevisiae. Cell *51*, 463–471.

Brewer, B.J., and Fangman, W.L. (1988). A replication fork barrier at the 3′ end of yeast ribosomal RNA genes. Cell *55*, 637–643.

Brewer, B.J., and Fangman, W.L. (1994). Initiation preference at a yeast origin of replication. Proc Natl Acad Sci U S A *91*, 3418–3422.

Byun, T.S. (2005). Functional uncoupling of MCM helicase and DNA polymerase activities activates the ATR-dependent checkpoint. Genes & Development *19*, 1040–1052.

Capp, C., Wu, J., and Hsieh, T. (2009). *Drosophila* RecQ4 Has a 3′-5′ DNA Helicase Activity That Is Essential for Viability. Journal of Biological Chemistry *284*, 30845–30852.

Cha, R.S., and Kleckner, N. (2002). ATR Homolog Mec1 Promotes Fork Progression, Thus Averting Breaks in Replication Slow Zones. Science *297*, 602–606.

Collart, C., Allen, G.E., Bradshaw, C.R., Smith, J.C., and Zegerman, P. (2013). Titration of Four Replication Factors Is Essential for the Xenopus laevis Midblastula Transition. Science *341*, 893–896.

Czajkowsky, D.M., Liu, J., Hamlin, J.L., and Shao, Z. (2008). DNA Combing Reveals Intrinsic Temporal Disorder in the Replication of Yeast Chromosome VI. J Mol Biol *375*, 12–19.

Das, S.P., Borrman, T., Liu, V.W.T., Yang, S.C.-H., Bechhoefer, J., and Rhind, N. (2015). Replication timing is regulated by the number of MCMs loaded at origins. Genome Research *25*, 1886–1892.

Deegan, T.D., Yeeles, J.T., and Diffley, J.F. (2016). Phosphopeptide binding by Sld3 links Dbf4-dependent kinase to MCM replicative helicase activation. The EMBO Journal *35*, 961–973.

Deshpande, A.M., and Newlon, C.S. (1992). The ARS consensus sequence is required for chromosomal origin function in Saccharomyces cerevisiae. Mol Cell Biol *12*, 4305–4313.

Diffley, J.F.X., and Cocker, J.H. (1992). Protein-DNA interactions at a yeast replication origin. Nature *357*, 169–172.

Diffley, J.F.X., Cocker, J.H., Dowell, S.J., and Rowley, A. (1994). Two steps in the assembly of complexes at yeast replication origins in vivo. Cell *78*, 303–316.

Dimitrova, D.S., and Gilbert, D.M. (1999). The Spatial Position and Replication Timing of Chromosomal Domains Are Both Established in Early G1 Phase. Molecular Cell *4*, 983–993.

Donaldson, A.D., Raghuraman, M.K., Friedman, K.L., Cross, F.R., Brewer, B.J., and Fangman, W.L. (1998). CLB5-dependent activation of late replication origins in S. cerevisiae. Molecular Cell *2*, 173–182.

Douglas, M.E., Ali, F.A., Costa, A., and Diffley, J.F.X. (2018). The mechanism of eukaryotic CMG helicase activation. Nature *555*, 265–268.

Ellison, E.L., and Vogt, V.M. (1993). Interaction of the intron-encoded mobility endonuclease I-PpoI with its target site. Mol Cell Biol *13*, 7531–7539.

Enserink, J.M., and Kolodner, R.D. (2010). An overview of Cdk1-controlled targets and processes. Cell Div *5*, 11.

Fang, D., Lengronne, A., Shi, D., Forey, R., Skrzypczak, M., Ginalski, K., Yan, C., Wang, X., Cao, Q., Pasero, P., et al. (2017). Dbf4 recruitment by forkhead transcription factors defines an upstream rate-limiting step in determining origin firing timing. Genes Dev. *31*, 2405–2415.

Farrell, J.A., and O'Farrell, P.H. (2014). From Egg to Gastrula: How the Cell Cycle Is Remodeled During the Drosophila Mid-Blastula Transition. Annual Review of Genetics *48*, 269–294.

Feng, W., Collingwood, D., Boeck, M.E., Fox, L.A., Alvino, G.M., Fangman, W.L., Raghuraman, M.K., and Brewer, B.J. (2006). Genomic mapping of single-stranded DNA in hydroxyurea-challenged yeasts identifies origins of replication. Nat Cell Biol *8*, 148–155.

Feng, W., Raghuraman, M.K., and Brewer, B.J. (2007). Mapping yeast origins of replication via single-stranded DNA detection. Methods *41*, 151–157.

Feng, W., Di Rienzi, S.C., Raghuraman, M.K., and Brewer, B.J. (2011). Replication Stress-Induced Chromosome Breakage Is Correlated with Replication Fork Progression and Is Preceded by Single-Stranded DNA Formation. G3 (Bethesda) *1*, 327–335.

Feng, W. Agarose plugs for yeast DNA. http://fangman-brewer.genetics.washington.edu/plug.html

Ferguson, B.M., and Fangman, W.L. (1992). A position effect on the time of replication origin activation in yeast. Cell *68*, 333–339.

Ferguson, B.M., Brewer, B.J., Reynolds, A.E., and Fangman, W.L. (1991). A yeast origin of replication is activated late in S phase. Cell *65*, 507–515.

Foiani, M., Pellicioli, A., Lopes, M., Lucca, C., Ferrari, M., Liberi, G., Muzi Falconi, M., and Plevani, P. (2000). DNA damage checkpoints and DNA replication controls in Saccharomyces cerevisiae. Mutation Research/Fundamental and Molecular Mechanisms of Mutagenesis *451*, 187–196.

French, S.L., Osheim, Y.N., Cioci, F., Nomura, M., and Beyer, A.L. (2003). In Exponentially Growing Saccharomyces cerevisiae Cells, rRNA Synthesis Is Determined by the Summed RNA Polymerase I Loading Rate Rather than by the Number of Active Genes. Mol Cell Biol *23*, 1558–1568.

Friedman, K.L., Diller, J.D., Ferguson, B.M., Nyland, S.V., Brewer, B.J., and Fangman, W.L. (1996). Multiple determinants controlling activation of yeast replication origins late in S phase. Genes & Development *10*, 1595–1607.

Friedman, K.L., Brewer, B.J., and Fangman, W.L. (1997). Replication profile of Saccharomyces cerevisiae chromosome VI. Genes to Cells *2*, Genes to Cells.

Ghaemmaghami, S., Huh, W.-K., Bower, K., Howson, R.W., Belle, A., Dephoure, N., O'Shea, E.K., and Weissman, J.S. (2003). Global analysis of protein expression in yeast. Nature *425*, 737–741.

Gilbert, C.W., Muldal, S., Lajtha, L.G., and Rowley, J. (1962). Time-Sequence of Human Chromosome Duplication. Nature *195*, 869–873.

Goffeau, A., Barrell, B.G., Bussey, H., Davis, R.W., Dujon, B., Feldmann, H., Galibert, F., Hoheisel, J.D., Jacq, C., Johnston, M., et al. (1996). Life with 6000 Genes. Science *274*, 546–567.

Gros, J., Kumar, C., Lynch, G., Yadav, T., Whitehouse, I., and Remus, D. (2015). Post-licensing Specification of Eukaryotic Replication Origins by Facilitated Mcm2-7 Sliding along DNA. Molecular Cell *60*, 797–807.

Hawkins, M., Retkute, R., Müller, C.A., Saner, N., Tanaka, T.U., de Moura, A.P.S., and Nieduszynski, C.A. (2013). High-Resolution Replication Profiles Define the Stochastic Nature of Genome Replication Initiation and Termination. Cell Reports *5*, 1132–1141.

Heller, R.C., Kang, S., Lam, W.M., Chen, S., Chan, C.S., and Bell, S.P. (2011). Eukaryotic Origin-Dependent DNA Replication In Vitro Reveals Sequential Action of DDK and S-CDK Kinases. Cell *146*, 80–91.

Hennessy, K.M., Lee, A., Chen, E., and Botstein, D. A group of interacting yeast DNA replication genes. (1991). Genes & Development *5*, 958-969.

Hiraga, S. -i., Alvino, G.M., Chang, F., Lian, H. -y., Sridhar, A., Kubota, T., Brewer, B.J., Weinreich, M., Raghuraman, M.K., and Donaldson, A.D. (2014). Rif1 controls DNA replication by directing Protein Phosphatase 1 to reverse Cdc7-mediated phosphorylation of the MCM complex. Genes & Development *28*, 372–383.

Hoggard, T., Shor, E., Müller, C.A., Nieduszynski, C.A., and Fox, C.A. (2013). A Link between ORC-Origin Binding Mechanisms and Origin Activation Time Revealed in Budding Yeast. PLoS Genetics *9*, e1003798.

Hyrien, O., Maric, C., and Méchali, M. (1995). Transition in Specification of Embryonic Metazoan DNA Replication Origins. Science *270*, 994–997.

Ide, S., Watanabe, K., Watanabe, H., Shirahige, K., Kobayashi, T., and Maki, H. (2007). Abnormality in Initiation Program of DNA Replication Is Monitored by the Highly Repetitive rRNA Gene Array on Chromosome XII in Budding Yeast. Molecular and Cellular Biology *27*, 568–578.

Ilves, I., Petojevic, T., Pesavento, J.J., and Botchan, M.R. (2010). Activation of the MCM2-7 Helicase by Association with Cdc45 and GINS Proteins. Molecular Cell *37*, 247–258.

Itou, H., Muramatsu, S., Shirakihara, Y., and Araki, H. (2014). Crystal Structure of the Homology Domain of the Eukaryotic DNA Replication Proteins Sld3/Treslin. Structure *22*, 1341–1347.

Jackson, A.L., Pahl, P.M., Harrison, K., Rosamond, J., and Sclafani, R.A. (1993). Cell cycle regulation of the yeast Cdc7 protein kinase by association with the Dbf4 protein. Molecular and Cellular Biology *13*, 2899–2908.

Kamimura, Y., Masumoto, H., Sugino, A., and Araki, H. (1998). Sld2, Which Interacts with Dpb11 in Saccharomyces cerevisiae, Is Required for Chromosomal DNA Replication. Molecular and Cellular Biology *18*, 6102–6109.

Kamimura, Y., Tak, Y.-S., Sugino, A., and Araki, H. (2001). Sld3, which interacts with Cdc45 (Sld4), functions for chromosomal DNA replication in Saccharomyces cerevisiae. The EMBO Journal *20*, 2097–2107.

Kanemaki, M., and Labib, K. (2006). Distinct roles for Sld3 and GINS during establishment and progression of eukaryotic DNA replication forks. The EMBO Journal *25*, 1753–1763.

Knott, S.R.V., Viggiani, C.J., Tavare, S., and Aparicio, O.M. (2009). Genome-wide replication profiles indicate an expansive role for Rpd3L in regulating replication initiation timing or efficiency, and reveal genomic loci of Rpd3 function in Saccharomyces cerevisiae. Genes & Development *23*, 1077–1090.

Knott, S.R.V., Peace, J.M., Ostrow, A.Z., Gan, Y., Rex, A.E., Viggiani, C.J., Tavaré, S., and Aparicio, O.M. (2012). Forkhead Transcription Factors Establish Origin Timing and Long-Range Clustering in S. cerevisiae. Cell *148*, 99–111.

Kobayashi, T. (2003). The Replication Fork Barrier Site Forms a Unique Structure with Fob1p and Inhibits the Replication Fork. Mol Cell Biol *23*, 9178–9188.

Kobayashi, T., Heck, D.J., Nomura, M., and Horiuchi, T. (1998). Expansion and contraction of ribosomal DNA repeats in Saccharomyces cerevisiae: requirement of replication fork blocking (Fob1) protein and the role of RNA polymerase I. Genes & Development *12*, 3821–3830.

Koren, A., Polak, P., Nemesh, J., Michaelson, J.J., Sebat, J., Sunyaev, S.R., and McCarroll, S.A. (2012). Differential Relationship of DNA Replication Timing to Different Forms of Human Mutation and Variation. The American Journal of Human Genetics *91*, 1033–1040.

Koren, A., Handsaker, R.E., Kamitaki, N., Karlić, R., Ghosh, S., Polak, P., Eggan, K., and McCarroll, S.A. (2014). Genetic Variation in Human DNA Replication Timing. Cell *159*, 1015–1026.

Kubota, T., Nishimura, K., Kanemaki, M., and Donaldson, A. (2013). The Elg1 replication factor C-like complex functions in PCNA unloading during DNA replication. Molecular Cell *50*, 273–280.

Kwan, E.X., Foss, E.J., Tsuchiyama, S., Alvino, G.M., Kruglyak, L., Kaeberlein, M., Raghuraman, M.K., Brewer, B.J., Kennedy, B.K., and Bedalov, A. (2013). A Natural Polymorphism in rDNA Replication Origins Links Origin Activation with Calorie Restriction and Lifespan. PLoS Genetics *9*, e1003329.

Kwan, E.X., Wang, X.S., Amemiya, H.M., Brewer, B.J., and Raghuraman, M.K. (2016). rDNA Copy Number Variants Are Frequent Passenger Mutations in *Saccharomyces cerevisiae* Deletion Collections and *de Novo* Transformants. G3: Genes|Genomes|Genetics *6*, 2829–2838.

Labib, K. (2010). How do Cdc7 and cyclin-dependent kinases trigger the initiation of chromosome replication in eukaryotic cells? Genes & Development *24*, 1208–1219.

Langley, A.R., Smith, J.C., Stemple, D.L., and Harvey, S.A. (2014). New insights into the maternal to zygotic transition. Development *141*, 3834–3841.

Lei, M., Kawasaki, Y., and Tye, B.K. (1996). Physical interactions among Mcm proteins and effects of Mcm dosage on DNA replication in Saccharomyces cerevisiae. Molecular and Cellular Biology *16*, 5081–5090.

Lima-de-Faria, A., and Jaworksa, H. (1968). Late DNA Synthesis in Heterochromatin. Nature *217*.

Lopez-Mosqueda, J., Maas, N.L., Jonsson, Z.O., DeFazio Eli, L.G., Wohlschlegel, J., and Toczyski, D.P. (2010). Damage-Induced Phosphorylation of Sld3 is Important to Block Late Origin Firing. Nature *467*, 479–483.

MacAlpine, D.M. (2004). Coordination of replication and transcription along a Drosophila chromosome. Genes & Development *18*, 3094–3105.

Mantiero, D., Mackenzie, A., Donaldson, A., and Zegerman, P. (2011). Limiting replication initiation factors execute the temporal programme of origin firing in budding yeast. EMBO J *30*, 4805–4814.

Marahrens, Y., and Stillman, B. (1992). A Yeast Chromosomal Origin of DNA Replication Defined by Multiple Functional Elements. Science *255*, 817–823.

Masumoto, H., Muramatsu, S., Kamimura, Y., and Araki, H. (2002). S-Cdk-dependent phosphorylation of Sld2 essential for chromosomal DNA replication in budding yeast. Nature *415*, 651.

Matsuno, K., Kumano, M., Kubota, Y., Hashimoto, Y., and Takisawa, H. (2006). The N-Terminal Noncatalytic Region of Xenopus RecQ4 Is Required for Chromatin Binding of DNA Polymerase in the Initiation of DNA Replication. Molecular and Cellular Biology *26*, 4843–4852.

Mattarocci, S., Shyian, M., Lemmens, L., Damay, P., Altintas, D.M., Shi, T., Bartholomew, C.R., Thomä, N.H., Hardy, C.F.J., and Shore, D. (2014). Rif1 Controls DNA Replication Timing in Yeast through the PP1 Phosphatase Glc7. Cell Reports *7*, 62–69.

McCune, H.J., Danielson, L.S., Alvino, G.M., Collingwood, D., Delrow, J.J., Fangman, W.L., Brewer, B.J., and Raghuraman, M.K. (2008). The Temporal Program of Chromosome Replication: Genomewide Replication in clb5 Saccharomyces cerevisiae. Genetics *180*, 1833–1847.

McGuffee, S.R., Smith, D.J., and Whitehouse, I. (2013). Quantitative, Genome-Wide Analysis of Eukaryotic Replication Initiation and Termination. Molecular Cell *50*, 123–135.

McKnight, S.L., and Miller, O.L. (1977). Electron microscopic analysis of chromatin replication in the cellular blastoderm drosophila melanogaster embryo. Cell *12*, 795–804.

Melters, D.P., Bradnam, K.R., Young, H.A., Telis, N., May, M.R., Ruby, J., Sebra, R., Peluso, P., Eid, J., Rank, D., et al. (2013). Comparative analysis of tandem repeats from hundreds of species reveals unique insights into centromere evolution. Genome Biology *14*, R10.

de Moura, A.P.S., Retkute, R., Hawkins, M., and Nieduszynski, C.A. (2010). Mathematical modelling of whole chromosome replication. Nucleic Acids Res *38*, 5623–5633.

Mueller, A.C., Keaton, M.A., and Dutta, A. (2011). DNA replication: Mammalian Treslin-TopBP1 interaction mirrors yeast Sld3-Dpb11. Curr Biol *21*, R638–R640.

Müller, C.A., Hawkins, M., Retkute, R., Malla, S., Wilson, R., Blythe, M.J., Nakato, R., Komata, M., Shirahige, K., de Moura, A.P.S., et al. (2014). The dynamics of genome replication using deep sequencing. Nucleic Acids Res *42*, e3.

Muramatsu, S., Hirai, K., Tak, Y.-S., Kamimura, Y., and Araki, H. (2010). CDK-dependent complex formation between replication proteins Dpb11, Sld2, Pol , and GINS in budding yeast. Genes & Development *24*, 602–612.

Muscarella, D.E., and Vogt, V.M. (1993). A mobile group I intron from Physarum polycephalum can insert itself and induce point mutations in the nuclear ribosomal DNA of saccharomyces cerevisiae. Mol Cell Biol *13*, 1023–1033.

Natsume, T., Müller, C.A., Katou, Y., Retkute, R., Gierliński, M., Araki, H., Blow, J.J., Shirahige, K., Nieduszynski, C.A., and Tanaka, T.U. (2013). Kinetochores Coordinate

Pericentromeric Cohesion and Early DNA Replication by Cdc7-Dbf4 Kinase Recruitment. Molecular Cell *50*, 661–674.

Newlon, C.S., Petes, T.D., Hereford, L.M., and Fangman, W.L. (1974). Replication of Yeast Chromosomal DNA. Nature *247*, 32–35.

Newlon, C.S., Lipchitz, L.R., Collins, I., Deshpande, A., Devenish, R.J., Green, R.P., Klein, H.L., Palzkill, T.G., Ren, R., Synn, S., et al. (1991). Analysis of a Circular Derivative of Saccharomyces Cerevisiae Chromosome III: A Physical Map and Identification and Location of Ars Elements. Genetics *129*, 343–357.

Nishimura, K., and Kanemaki, M.T. (2014). Rapid Depletion of Budding Yeast Proteins via the Fusion of an Auxin-Inducible Degron (AID): Generation and Analysis of Budding Yeast AID Mutants. In Current Protocols in Cell Biology, J.S. Bonifacino, M. Dasso, J.B. Harford, J. Lippincott-Schwartz, and K.M. Yamada, eds. (Hoboken, NJ, USA: John Wiley & Sons, Inc.), pp. 20.9.1-20.9.16.

Nishimura, K., Fukagawa, T., Takisawa, H., Kakimoto, T., and Kanemaki, M. (2009). An auxin-based degron system for the rapid depletion of proteins in nonplant cells. Nature Methods *6*, 917–922.

Nordman, J., and Orr-Weaver, T.L. (2012). Regulation of DNA replication during development. Development *139*, 455–464.

Paulovich, A.G., and Hartwell, L.H. (1995). A checkpoint regulates the rate of progression through S phase in S. cerevisiae in response to DNA damage. Cell *82*, 841–847.

Petes, T.D. (1979). Yeast ribosomal DNA genes are located on chromosome XII. Proceedings of the National Academy of Sciences *76*, 410–414.

Petes, T.D., Byers, B., and Fangman, W.L. (1973). Size and structure of yeast chromosomal DNA. Proceedings of the National Academy of Sciences *70*, 3072–3076.

Pohl, T.J. (2013). Identification and Characterization of cis-acting DNA Elements that Regulate Early Origin Activation. University of Washington.

Pohl, T.J., Brewer, B.J., and Raghuraman, M.K. (2012). Functional Centromeres Determine the Activation Time of Pericentric Origins of DNA Replication in Saccharomyces cerevisiae. PLoS Genetics *8*, e1002677.

Prioleau, M.-N., and MacAlpine, D.M. (2016). DNA replication origins—where do we begin? Genes Dev *30*, 1683–1697.

Pugh, B.F. (2010). A preoccupied position on nucleosomes. Nature Structural & Molecular Biology *17*, 923–923.

Raghuraman, M.K., Brewer, B.J., and Fangman, W.L. (1997). Cell Cycle-Dependent Establishment of a Late Replication Program. Science *276*, 806–809.

Raghuraman, M.K., Winzeler, E.A., Collingwood, D., Hunt, S., Wodicka, L., Conway, A., Lockhart, D., Davis, R.W., Brewer, B.J., and Fangman, W.L. (2001). Replication dynamics of the yeast genome. Science *294*, 115–121.

Remus, D., and Diffley, J.F. (2009). Eukaryotic DNA replication control: Lock and load, then fire. Current Opinion in Cell Biology *21*, 771–777.

Reusswig, K.-U., Zimmermann, F., Galanti, L., and Pfander, B. (2016). Robust Replication Control Is Generated by Temporal Gaps between Licensing and Firing Phases and Depends on Degradation of Firing Factor Sld2. Cell Reports *17*, 556–569.

Rhind, N. (2006). DNA replication timing: random thoughts about origin firing. Nat Cell Biol *8*, 1313–1316.

Rhind, N., and Gilbert, D.M. (2013). DNA Replication Timing. Cold Spring Harb Perspect Biol *5*, a010132.

Rose, M.D. (1990). Methods in yeast genetics: a laboratory course manual (Cold Spring Harbor, N.Y.: Cold Spring Harbor Laboratory Press).

Ryba, T., Hiratani, I., Lu, J., Itoh, M., Kulik, M., Zhang, J., Schulz, T.C., Robins, A.J., Dalton, S., and Gilbert, D.M. (2010). Evolutionarily conserved replication timing profiles predict long-range chromatin interactions and distinguish closely related cell types. Genome Research *20*, 761–770.

Sanchez, J.C., Kwan, E.X., Pohl, T.J., Amemiya, H.M., Raghuraman, M.K., and Brewer, B.J. (2017). Defective replication initiation results in locus specific chromosome breakage and a ribosomal RNA deficiency in yeast. PLOS Genetics *13*, e1007041.

Sanchez-Pulido, L., Diffley, J.F.X., and Ponting, C.P. (2010). Homology explains the functional similarities of Treslin/Ticrr and Sld3. Current Biology *20*, R509–R510.

Sangrithi, M.N., Bernal, J.A., Madine, M., Philpott, A., Lee, J., Dunphy, W.G., and Venkitaraman, A.R. (2005). Initiation of DNA Replication Requires the RECQL4 Protein Mutated in Rothmund-Thomson Syndrome. Cell *121*, 887–898.

Santocanale, C., and Diffley, J.F. (1998). A Mec1- and Rad53-dependent checkpoint controls late-firing origins of DNA replication. Nature *395*, 615–618.

Sasaki, T., Sawado, T., Yamaguchi, M., and Shinomiya, T. (1999). Specification of Regions of DNA Replication Initiation during Embryogenesis in the 65-Kilobase DNApol␣-dE2F Locus of Drosophila melanogaster. Molecular and Cellular Biology *19*, 9.

Segurado, M., and Tercero, J.A. (2009). The S-phase checkpoint: targeting the replication fork. Biology of the Cell *101*, 617–627.

Sheu, Y.-J., Kinney, J.B., Lengronne, A., Pasero, P., and Stillman, B. (2014). Domain within the helicase subunit Mcm4 integrates multiple kinase signals to control DNA replication initiation and fork progression. Proc Natl Acad Sci U S A *111*, E1899–E1908.

Shimada, K., Pasero, P., and Gasser, S.M. (2002). ORC and the intra-S-phase checkpoint: a threshold regulates Rad53p activation in S phase. Genes Dev. *16*, 3236–3252.

Siefert, J.C., Georgescu, C., Wren, J.D., Koren, A., and Sansam, C.L. (2017). DNA replication timing during development anticipates transcriptional programs and parallels enhancer activation. Genome Res. *27*, 1406–1416.

Siow, C.C., Nieduszynska, S.R., Muller, C.A., and Nieduszynski, C.A. (2012). OriDB, the DNA replication origin database updated and extended. Nucleic Acids Research *40*, D682–D686.

Smogorzewska, A., and Lange, and T. de (2004). Regulation of Telomerase by Telomeric Proteins. Annual Review of Biochemistry *73*, 177–208.

Sogo, J.M., Lopes, M., and Foiani, M. (2002). Fork reversal and ssDNA accumulation at stalled replication forks owing to checkpoint defects. Science *297*, 599–602.

Stevenson, J.B., and Gottschling, D.E. (1999). Telomeric chromatin modulates replication timing near chromosome ends. Genes & Development *13*, 146–151.

Stinchcomb, D.T., Thomas, M., Kelly, J., Selker, E., and Davis, R.W. (1980). Eukaryotic DNA segments capable of autonomous replication in yeast. Proceedings of the National Academy of Sciences *77*, 4559–4563.

Stults, D.M., Killen, M.W., Pierce, H.H., and Pierce, A.J. (2008). Genomic architecture and inheritance of human ribosomal RNA gene clusters. Genome Res. *18*, 13–18.

Sun, J., Evrin, C., Samel, S., Fernández-Cid, A., Riera, A., Kawakami, H., Stillman, B., Speck, C., and Li, H. (2013). Cryo-EM structure of a helicase loading intermediate containing ORC-Cdc6-Cdt1-MCM2-7 bound to DNA. Nat Struct Mol Biol *20*, 944–951.

Tanaka, S., and Araki, H. (2011). Multiple Regulatory Mechanisms to Inhibit Untimely Initiation of DNA Replication Are Important for Stable Genome Maintenance. PLoS Genetics *7*, e1002136.

Tanaka, S., Umemori, T., Hirai, K., Muramatsu, S., Kamimura, Y., and Araki, H. (2007). CDK-dependent phosphorylation of Sld2 and Sld3 initiates DNA replication in budding yeast. Nature *445*, 328–332.

Tanaka, S., Nakato, R., Katou, Y., Shirahige, K., and Araki, H. (2011a). Origin Association of Sld3, Sld7, and Cdc45 Proteins Is a Key Step for Determination of Origin-Firing Timing. Current Biology *21*, 2055–2063.

Tanaka, T., Umemori, T., Endo, S., Muramatsu, S., Kanemaki, M., Kamimura, Y., Obuse, C., and Araki, H. (2011b). Sld7, an Sld3-associated protein required for efficient chromosomal DNA replication in budding yeast. The EMBO Journal *30*, 2019–2030.

Taylor, J.H. (1960). Asynchronous Duplication of Chromosomes in Cultured Cells of Chinese Hamster. J Biophys Biochem Cytol *7*, 455–463.

Tercero, J.A., Longhese, M.P., and Diffley, J.F. (2003). A central role for DNA replication forks in checkpoint activation and response. Molecular Cell *11*, 1323–1336.

Ticau, S., Friedman, L.J., Ivica, N.A., Gelles, J., and Bell, S.P. (2015). Single-Molecule Studies of Origin Licensing Reveal Mechanisms Ensuring Bidirectional Helicase Loading. Cell *161*, 513–525.

Venema, J., and Tollervey, D. (1999). Ribosome Synthesis in Saccharomyces cerevisiae. Annual Review of Genetics *33*, 261–311.

Vogelauer, M., Rubbi, L., Lucas, I., Brewer, B.J., and Grunstein, M. (2002). Histone Acetylation Regulates the Time of Replication Origin Firing. Molecular Cell *10*, 1223–1233.

Willard, H.F. (1990). Centromeres of mammalian chromosomes. Trends in Genetics *6*, 410–416.

Willer, M., Rainey, M., Pullen, T., and Stirling, C.J. (1999). The yeast CDC9 gene encodes both a nuclear and a mitochondrial form of DNA ligase I. Current Biology *9*, 1085-S1.

Woolford, J.L., and Baserga, S.J. (2013). Ribosome Biogenesis in the Yeast *Saccharomyces cerevisiae*. Genetics *195*, 643–681.

Yamashita, M., Hori, Y., Shinomiya, T., Obuse, C., Tsurimoto, T., Yoshikawa, H., and Shirahige, K. (1997). The efficiency and timing of initiation of replication of multiple replicons of Saccharomyces cerevisiae chromosome VI. Genes to Cells *2*, 655–665.

Yang, S.C.-H., Rhind, N., and Bechhoefer, J. (2010). Modeling genome-wide replication kinetics reveals a mechanism for regulation of replication timing. Molecular Systems Biology *6*.

Yoshida, K., Bacal, J., Desmarais, D., Padioleau, I., Tsaponina, O., Chabes, A., Pantesco, V., Dubois, E., Parrinello, H., Skrzypczak, M., et al. (2014). The Histone Deacetylases Sir2 and Rpd3 Act on Ribosomal DNA to Control the Replication Program in Budding Yeast. Molecular Cell *54*, 691–697.

Zegerman, P., and Diffley, J.F.X. (2007). Phosphorylation of Sld2 and Sld3 by cyclin-dependent kinases promotes DNA replication in budding yeast. Nature *445*, 281–285.

Zegerman, P., and Diffley, J.F.X. (2010). Checkpoint-dependent inhibition of DNA replication initiation by Sld3 and Dbf4 phosphorylation. Nature *467*, 474–478.

Zentner, G.E., and Henikoff, S. (2014). High-resolution digital profiling of the epigenome. Nature Reviews Genetics *15*, 814–827.

Zhang, Y., and Hunter, T. (2014). Roles of Chk1 in Cell Biology and Cancer Therapy. Int J Cancer *134*.

Zhong, Y., Nellimoottil, T., Peace, J.M., Knott, S.R.V., Villwock, S.K., Yee, J.M., Jancuska, J.M., Rege, S., Tecklenburg, M., Sclafani, R.A., et al. (2013). The level of origin firing inversely affects the rate of replication fork progression. The Journal of Cell Biology *201*, 373–383.

Zhu, J., Newlon, C.S., and Huberman, J.A. (1992). Localization of a DNA replication origin and termination zone on chromosome III of Saccharomyces cerevisiae. Mol. Cell. Biol. *12*, 4733–4741.

APPENDIX A: AID STRAIN INDUCTION TESTING

Based on inconsistent degron strain behavior observed by flow cytometry in some of my preliminary experiments, I suspected that the time of galactose induction was not long enough to allow full expression of the plant-derived E3 ubiquitin ligase. Previously, to test how tunable the AID system is, I added different concentrations of auxin to the degron strains but did not observe much variation in cell cycle progression by flow cytometry. The lack of variation in response to auxin concentration suggested that the auxin concentration was not to blame for my inconsistent results. Another time, I inadvertently used 1% instead of 2% galactose to induce ligase expression and had noticed that the S phase phenotype after auxin induction was not as striking (data not shown). Therefore, I suspected that the inconsistent cell cycle effects in the degron strains were due to a problem with the galactose component of the system, not the auxin.

To test the appropriate time of galactose induction, I varied the time of 2% galactose induction for two tester strains before inducing depletion of a target protein by 2 hours of auxin treatment, then assayed the outcome by flow cytometry (see outline of experiment in Figure A.1). I used the *SLD2*-AID strain as well as a *CDC9*-AID strain from M.K. Raghuraman. Depleting Cdc9 should cause G2 arrest (Willer et al., 1999). I did not add galactose (YC + 1% raffinose) to one portion of each culture, but still treated the cells with auxin to verify that cell cycle defects are dependent upon gal-driven expression of the ubiquitin ligase [Figure A.1]. The shorter times of galactose induction (0, 1, and 2 hours) displayed striking differences in terms of the severity of S phase progression phenotype in the *SLD2*-AID strain—the shorter the galactose induction, the fewer cells in S phase. The 3- and 4-hour galactose induction times resulted in very similar cell cycle profiles for the *SLD2*-AID strain. The *CDC9*-AID strain seemed not to require as long of a

galactose-induction window. Regardless, based on these results, I decided to use a minimum of 3-hour galactose induction for all subsequent degron experiments.

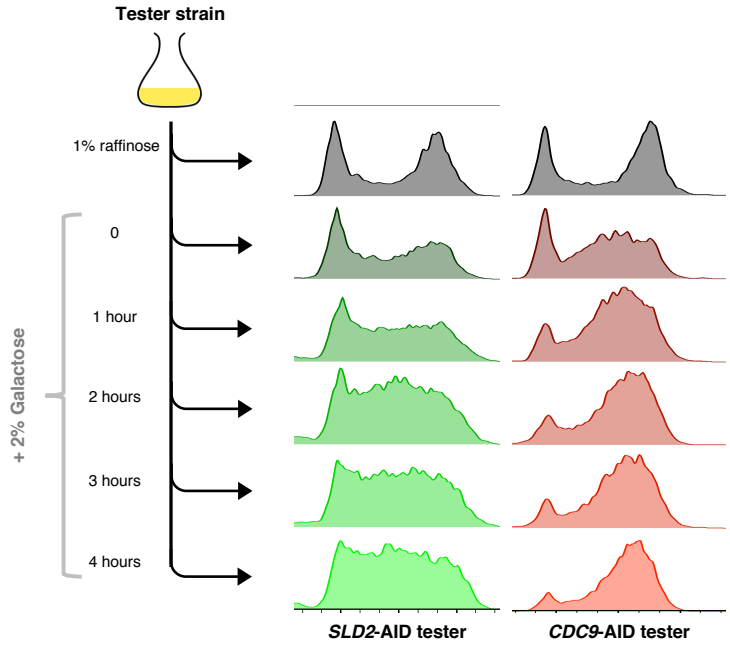

Figure A.1. Determining time of galactose induction for AID strains.[3]

Since many of the experiments performed on the AID strains, such as the ssDNA mapping assay, required an α-factor arrest and release, I also wanted to determine whether adding auxin at different times relative to release from arrest impacted progression through S phase. Additionally, if the time of auxin did have an impact, it could be a useful technique for manipulating the abundance of AID-tagged protein relative to the onset of S phase. Therefore, I set up an arrest-and-release experiment in which I added auxin 60 minutes before release, 30 minutes before release, at the time of release, 15 minutes after release into S phase, and did not add auxin to one

[3] I determined the ideal time of galactose-driven expression of the *Os*TIR1 ligase component of the AID system by adding galactose for varying amounts of time to a tester strain, then adding auxin for 2 hours after galactose induction. The severity of protein-depletion induced cell cycle progression phenotype depends on how long galactose induction lasts.

culture. I tested both the *SLD2*-AID and *SLD3*-AID strains. Surprisingly, S phase progression did not change in either strain despite the differences in when auxin was added [Figure A.2]. This means that the effects of auxin are extremely rapid and that adding auxin in advance of release does not cause exhaustion of auxin in the media. Based on this test, I added 0.5 mM auxin to arrested cells 60 minutes in advance of release from α-factor arrest for all experiments.

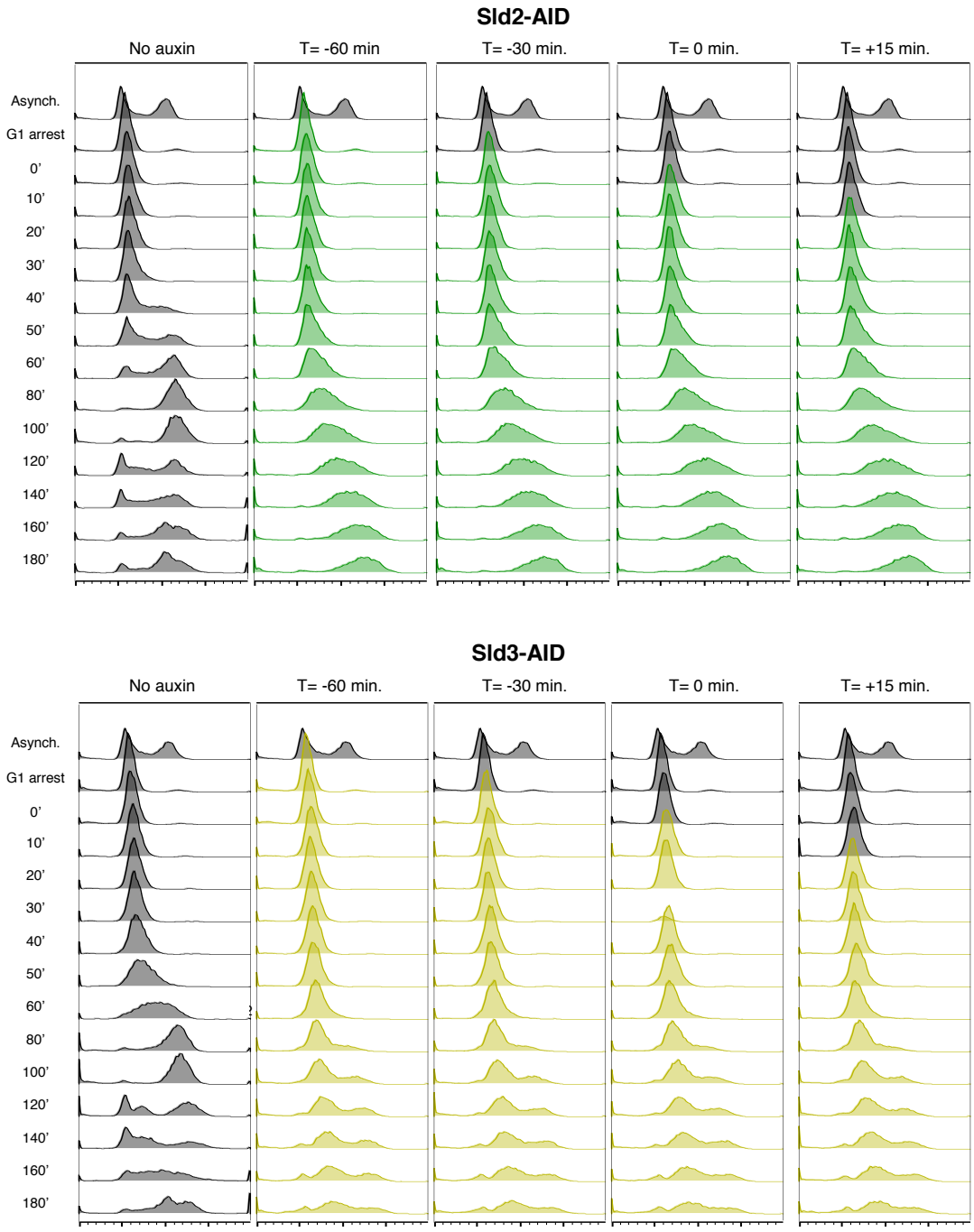

Figure A.1. Differences in synchronized S phase progression in *SLD2*-AID and *SLD3*-AID strains were assessed by adding auxin at different times relative to release from α-factor arrest.

APPENDIX B: ORIGINS AND TY ELEMENTS

The list of origins used in the peak area and peak width analyses from the ssDNA mapping assay data is shown in Table B.1. The Ty elements indicated on the ssDNA replication profiles are listed in Table B.2.

Table B.1. List of origins based on WT (W303) ssDNA assay.

Name	Other name(s)	Status (ARS)	Genomic location	Chromosome	Start	End	Middle
ARS107	proARS107	Confirmed	I-124	1	124350	124599	124500
ARS108	proARS108	Confirmed	I-147	1	146703	147690	147000
ARS110	ADE1	Confirmed	I-176	1	176154	176402	176500
ARS202	proARS202	Confirmed	II-63	2	63186	63421	63500
ARS207.5	ARS231	Confirmed	II-198	2	198193	198434	198500
ARS208	proARS208	Confirmed	II-238	2	237644	237879	238000
ARS209	ARSH4, proARS209	Confirmed	II-255	2	254890	255136	255000
ARS214	proARS214	Confirmed	II-408	2	407831	408064	408000
ARS216	proARS216	Confirmed	II-487	2	486661	486909	487000
ARS220	proARS220	Confirmed	II-623	2	622625	622894	623000
ARS305	ARS A6C, proARS305	Confirmed	III-39	3	39158	39706	39500
ARS306		Confirmed	III-75	3	74457	74677	74500
ARS307	ARS C2G1, proARS307	Confirmed	III-109	3	109000	109000	109000
ARS309	ARS J11D1, proARS309	Confirmed	III-132	3	132000	132000	132000
ARS310	proARS310	Confirmed	III-167	3	166000	167000	167000
ARS315		Confirmed	III-225	3	225000	225000	225000
ARS406	proARS406	Confirmed	IV-124	4	124000	124000	124000
ARS413	proARS413	Confirmed	IV-330	4	330000	330000	330000
ARS414	proARS414	Confirmed	IV-408	4	408000	408000	408000
ARS415	proARS415	Confirmed	IV-435	4	435000	435000	435000
ARS416	ARS1, proARS416	Confirmed	IV-463	4	462000	463000	463000
ARS417	proARS417	Confirmed	IV-484	4	484000	484000	484000
ARS417.5	ARS450	Confirmed	IV-505	4	505000	506000	506000
ARS418	proARS418	Confirmed	IV-555	4	555000	555000	556000
ARS419	proARS419	Confirmed	IV-568	4	567490	567737	567500
ARS428	proARS428	Confirmed	IV-914	4	914000	914000	914000
ARS430	proARS430	Confirmed	IV-1017	4	1020000	1020000	1020000
ARS431	proARS431	Confirmed	IV-1058	4	1060000	1060000	1060000
ARS432	proARS432	Confirmed	IV-1159	4	1160000	1160000	1160000
ARS432.5	ARS453	Confirmed	IV-1166	4	1170000	1170000	1170000
ARS442	proARS443	Confirmed	IV-1462	4	1460000	1460000	1460000
ARS507	proARS507	Confirmed	V-59	5	59282	59516	59500
ARS508	proARS508	Confirmed	V-94	5	93977	94218	94000
ARS510	proARS510	Confirmed	V-146	5	145539	145782	145500
ARS511	proARS511	Confirmed	V-174	5	173636	173874	174000
ARS514	proARS514	Confirmed	V-288	5	287504	287750	287500
		Likely	V-317	5	316043	317307	316500
ARS516	tRNAgluARS, proARS516	Confirmed	V-354	5	353504	353751	353500
ARS517	proARS517	Confirmed	V-407	5	406747	406949	407000
ARS518	proARS518	Confirmed	V-439	5	438929	439178	439000
ARS520	proARS520	Confirmed	V-499	5	498417	499343	499000
ARS603.5	proARS603.5	Confirmed	VI-119	6	118630	118950	119000
ARS605	proARS605	Confirmed	VI-136	6	135980	136080	136000
ARS606	proARS606	Confirmed	VI-168	6	167610	168040	168000
ARS607	proARS607	Confirmed	VI-199	6	199380	199490	199500
ARS608		Confirmed	VI-217	6	216344	216692	216500
ARS707	proARS707	Confirmed	VII-163	7	163180	163447	163500
ARS710	proARS710	Confirmed	VII-204	7	203917	204159	204000
ARS714	proARS714	Confirmed	VII-286	7	285951	286246	286000
ARS717	proARS717	Confirmed	VII-389	7	388658	388892	389000
ARS718	proARS718	Confirmed	VII-421	7	421093	421342	421000
ARS719	proARS719	Confirmed	VII-485	7	484932	485160	485000
ARS720	proARS720	Confirmed	VII-509	7	508729	508978	509000
ARS722	proARS722	Confirmed	VII-575	7	574622	574916	575000
ARS727	proARS727	Confirmed	VII-660	7	659809	660054	660000
ARS728	proARS728	Confirmed	VII-715	7	715273	715556	715500
ARS729	proARS729	Confirmed	VII-778	7	777967	778216	778000
ARS731	proARS731	Confirmed	VII-835	7	834492	834736	834500
ARS731.5	ARS737	Confirmed	VII-888	7	888350	888599	888500
ARS805	SPO11, proARS805	Confirmed	VIII-64	8	64255	64489	64500
ARS805.7		Confirmed	VIII-112	8	111293	111766	111500
ARS807		Confirmed	VIII-133	8	133347	133591	133500
ARS815	proARS815	Confirmed	VIII-297	8	296882	297475	297000
ARS818	proARS818, proARS819	Confirmed	VIII-392	8	392148	392391	392500
ARS820	proARS820	Confirmed	VIII-448	8	447619	447853	447500
ARS907	proARS907	Confirmed	IX-74	9	73803	74220	74000
ARS909	proARS909	Confirmed	IX-106	9	105821	106048	106000
ARS913	ARS901, proARS913	Confirmed	IX-215	9	214675	214826	215000
ARS914	proARS914	Confirmed	IX-248	9	247579	247800	247500
ARS919	proARS919	Confirmed	IX-342	9	341853	342096	342000

ARS920	proARS920	Confirmed	IX-357	9	357156	357393	357500
ARS922	proARS922	Confirmed	IX-412	9	411817	412053	412000
ARS1005	proARS1005	Confirmed	X-68	10	67467	67949	67500
ARS1006	proARS1006	Confirmed	X-100	10	99359	99796	99500
ARS1008	proARS1008	Confirmed	X-204	10	203730	204610	204000
ARS1009	proARS1009	Confirmed	X-228	10	228250	228740	228500
ARS1012	proARS1012	Confirmed	X-375	10	374570	374820	374500
ARS1014	proARS1014	Confirmed	X-417	10	416890	417130	417000
ARS1015	proARS1015	Confirmed	X-442	10	442250	442660	442500
ARS1018	proARS1018	Confirmed	X-540	10	540240	540470	540500
ARS1019	proARS1019	Confirmed	X-613	10	612540	612970	613000
ARS1021	ARS121, proARS1021	Confirmed	X-684	10	683330	683820	683500
ARS1103	proARS1103	Confirmed	XI-56	11	55670	55917	56000
ARS1106	proARS1106	Confirmed	XI-153	11	152934	153173	153000
ARS1106.7	ARS1127	Confirmed	XI-213	11	213080	213385	213000
ARS1107	proARS1107	Confirmed	XI-258	11	257390	257839	257500
ARS1107.5		Confirmed	XI-302	11	302152	302524	302500
ARS1109	proARS1109	Confirmed	XI-329	11	329322	329571	329500
ARS1113	proARS1113	Confirmed	XI-417	11	416822	417055	417000
ARS1114	proARS1114	Confirmed	XI-448	11	447657	447892	448000
ARS1114.5		Confirmed	XI-457	11	454453	459197	457000
ARS1116	proARS1116	Confirmed	XI-517	11	516653	516902	517000
ARS1205	proARS1205	Confirmed	XII-77	12	76711	77163	77000
ARS1206	proARS1206	Confirmed	XII-92	12	91417	91659	91500
	proARS1207	Dubious	XII-140	12	139293	140447	140000
ARS1209	proARS1209	Confirmed	XII-157	12	156646	156883	157000
ARS1211	proARS1211	Confirmed	XII-231	12	231179	231422	231500
ARS1213	proARS1213	Confirmed	XII-373	12	373156	373400	373500
ARS1215	proARS1215	Confirmed	XII-413	12	412668	412897	413000
ARS1217	proARS1217	Confirmed	XII-513	12	512868	513117	513000
		Dubious	XII-599	12	595804	602804	599500
ARS1218	proARS1218	Confirmed	XII-603	12	602938	603155	603000
ARS1220	proARS1220	Confirmed	XII-660	12	659823	660072	660000
ARS1222	proARS1222	Confirmed	XII-731	12	730275	730832	730500
	proARS1224	Dubious	XII-749	12	748375	749534	749000
ARS1226	proARS1226	Confirmed	XII-794	12	794020	794269	794000
ARS1232	proARS1232	Confirmed	XII-1007	12	1007180	1007470	1007500
ARS1303	proARS1303	Confirmed	XIII-32	13	31687	31935	32000
ARS1305	proARS1305	Confirmed	XIII-94	13	94216	94463	94500
ARS1307	proARS1307	Confirmed	XIII-137	13	137299	137548	137500
ARS1308	proARS1308	Confirmed	XIII-184	13	183793	184037	184000
ARS1309	proARS1309	Confirmed	XIII-263	13	263062	263296	263000
ARS1310	proARS1310	Confirmed	XIII-287	13	286782	287067	287000
ARS1312	proARS1312	Confirmed	XIII-371	13	370976	371221	371000
ARS1319	proARS1319	Confirmed	XIII-504	13	503346	504087	503500
ARS1320	proARS1320	Confirmed	XIII-536	13	535595	535843	535500
ARS1323	proARS1323	Confirmed	XIII-611	13	611273	611488	611500
ARS1325	proARS1325	Confirmed	XIII-649	13	649307	649551	649500
ARS1330	proARS1330	Confirmed	XIII-815	13	815341	815567	815500
ARS1332	proARS1332	Confirmed	XIII-898	13	897804	898040	898000
ARS1407	proARS1407	Confirmed	XIV-90	14	89528	89802	89500
ARS1415	proARS1415	Confirmed	XIV-322	14	321920	322210	322000
ARS1421	proARS1421	Confirmed	XIV-546	14	545966	546201	546000
		Likely	XIV-556	14	550890	560890	556000
ARS1424	proARS1424	Confirmed	XIV-610	14	609460	609710	609500
ARS1426	proARS1426	Confirmed	XIV-636	14	635660	635900	636000
ARS1506.5	ARS1531	Confirmed	XV-36	15	35667	35903	36000
ARS1508	proARS1508	Confirmed	XV-85	15	85195	85444	85500
ARS1509	proARS1509	Confirmed	XV-114	15	113840	114080	114000
ARS1510	proARS1510	Confirmed	XV-167	15	166970	167220	167000
ARS1510.5		Confirmed	XV-228	15	227480	228120	228000
ARS1511	proARS1511	Confirmed	XV-278	15	277530	277780	277500
ARS1512	proARS1512	Confirmed	XV-309	15	308970	309460	309000
ARS1513	proARS1513	Confirmed	XV-337	15	337280	337530	337500
		Likely	XV-348	15	347633	348862	348000
ARS1513.5	ARS1501	Confirmed	XV-437	15	436730	436970	437000
		Likely	XV-464	15	463698	464877	464500
ARS1514		Confirmed	XV-490	15	489640	490130	490000
ARS1523	proARS1522, proARS1523	Confirmed	XV-767	15	766620	766860	766500
ARS1526	proARS1526	Confirmed	XV-874	15	874190	874430	874500
ARS1528	proARS1528	Confirmed	XV-908	15	908290	908540	908500
ARS1529	proARS1529	Confirmed	XV-982	15	981450	981690	981500
ARS1529.5		Confirmed	XV-1054	15	1053500	1053900	1053500
ARS1605	proARS1605	Confirmed	XVI-73	16	73038	73283	73000
ARS1614	proARS1614	Confirmed	XVI-290	16	289483	289704	289500
ARS1618	proARS1618	Confirmed	XVI-385	16	384536	384784	384500
ARS1619	proARS1619	Confirmed	XVI-418	16	418132	418359	418000
ARS1621	proARS1621	Confirmed	XVI-512	16	511619	511940	512000
		Likely	XVI-553	16	552403	554287	553500
ARS1622	proARS1622	Confirmed	XVI-564	16	563822	564061	564000
ARS1623	proARS1623	Confirmed	XVI-634	16	633868	634117	634000
ARS1624	proARS1624	Confirmed	XVI-685	16	684383	684632	684500
ARS1626.5	ARS1635	Confirmed	XVI-777	16	776921	777152	777000
ARS1627	proARS1627	Confirmed	XVI-819	16	819153	819393	819500
ARS1628	proARS1628	Confirmed	XVI-843	16	842646	842894	843000

Table B.2 Ty elements noted on ssDNA replication profiles.

Chromosome	Coord (kb)	Ty element name
2	32.5	YBLWTy2-1
2	268.5	YBRWTy1-2
3	88	YCLWTy2-1
4	516.5	YDRCTy2-1
4	648.5	YDRCTy1-1
4	875	YDRWTy2-2
7	538.5	YGRWTy1-1
7	814.5	YGRWTy2-2
8	88.5	YHLWTy4-1
10	475.5	YJRWTy1-1
12	217	YLR035C-A
12	944	YLRWTy2-1
12	979	YLRCTy2-2
13	200	YMLWTy1-2
13	360	YMRCTy1-3
13	375.5	YMRCTy1-4
14	99.5	YNLCTy1-1
15	707	YORCTy2-1
15	973.5	YORWTy2-2
16	59.5	YPLWTy1-1
16	440	YPLCTy4-1
16	807.5	YPRCTy1-2

APPENDIX C: SSDNA MAPPING ASSAY REPLICATION PROFILES

Additional ssDNA replication assay profiles for WT and AID strains are shown below. Orange triangles indicate origins called from the WT data. Green circles denote increased S/G1 ratio near Ty elements. Yellow circles indicate the centromere. Chromosome coordinates are on the X axis and the S/G1 ssDNA ratio is mapped on the Y axis.

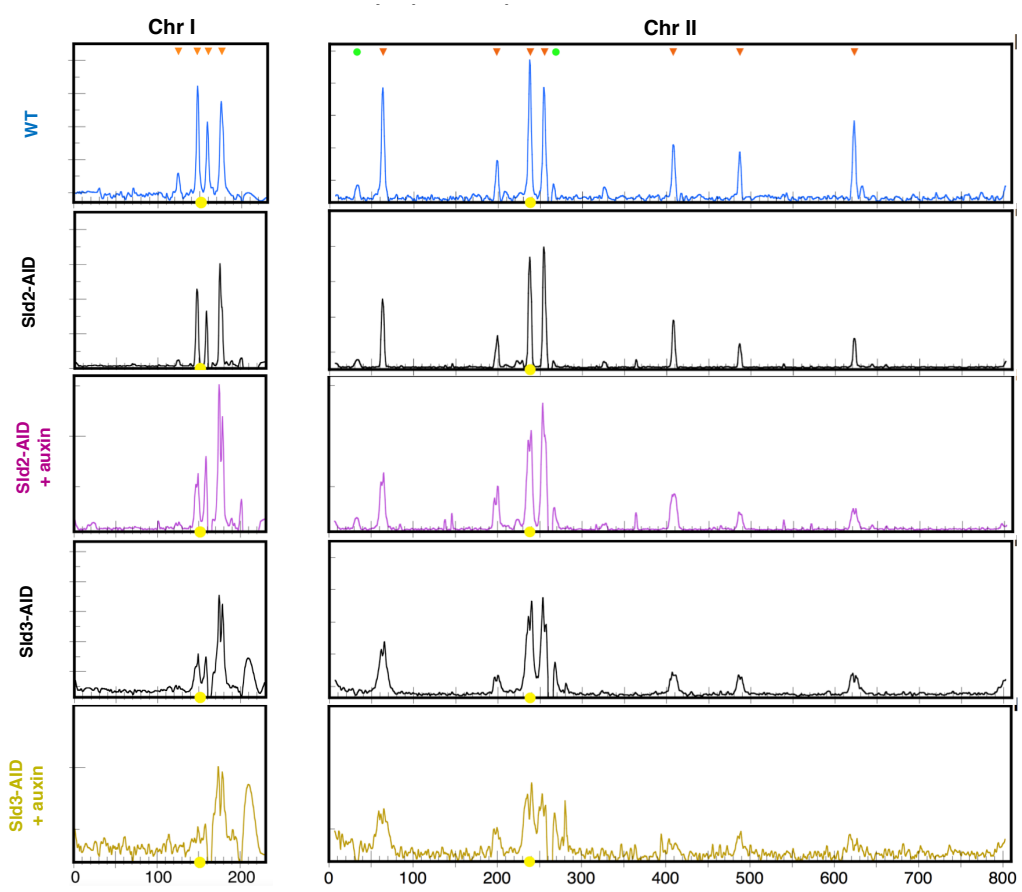

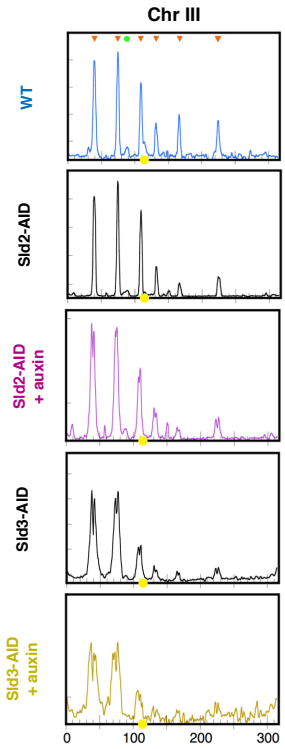
Chr III
WT
Sld2-AID
Sld2-AID + auxin
Sld3-AID
Sld3-AID + auxin
0
100
200
300

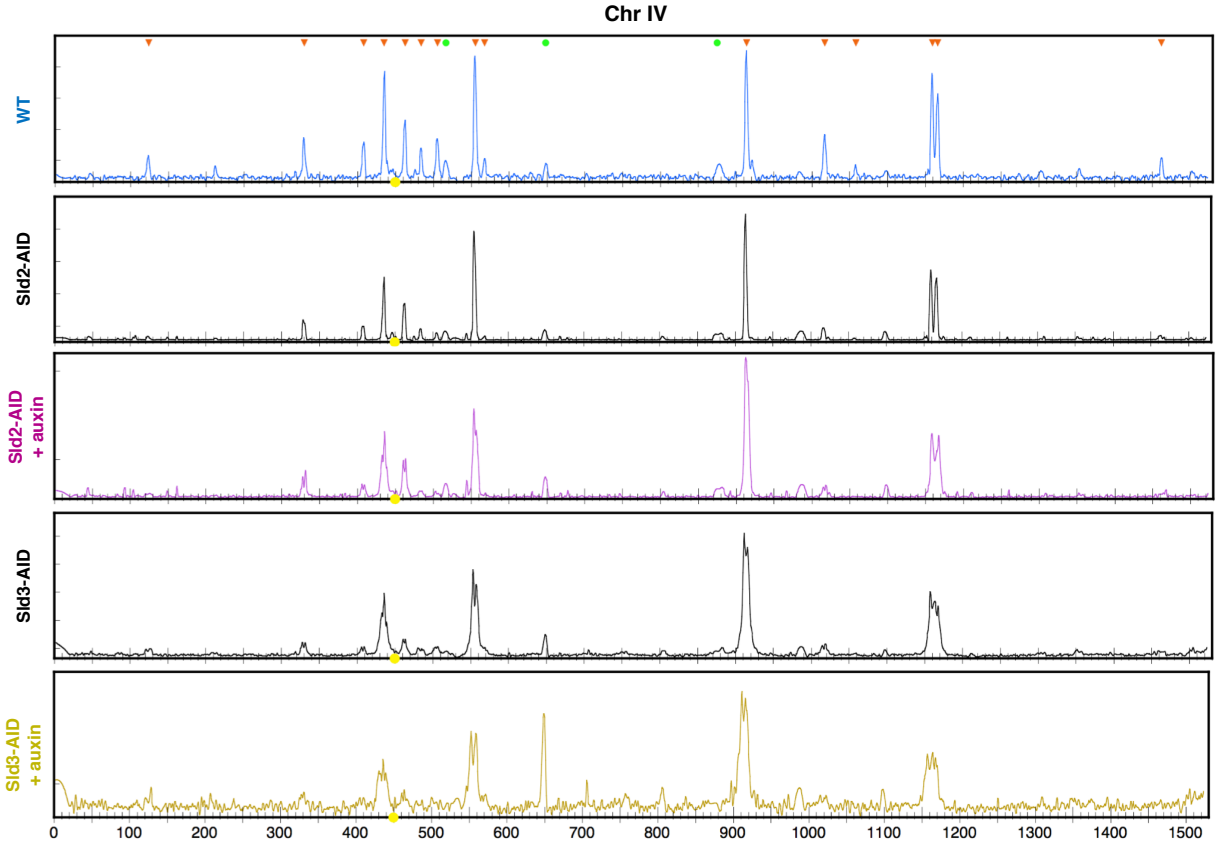
Chr IV
WT
Sld2-AID
Sld2-AID + auxin
Sld3-AID
Sld3-AID + auxin
0
100
200
300
400
500
600
700
800
900
1000
1100
1200
1300
1400
1500

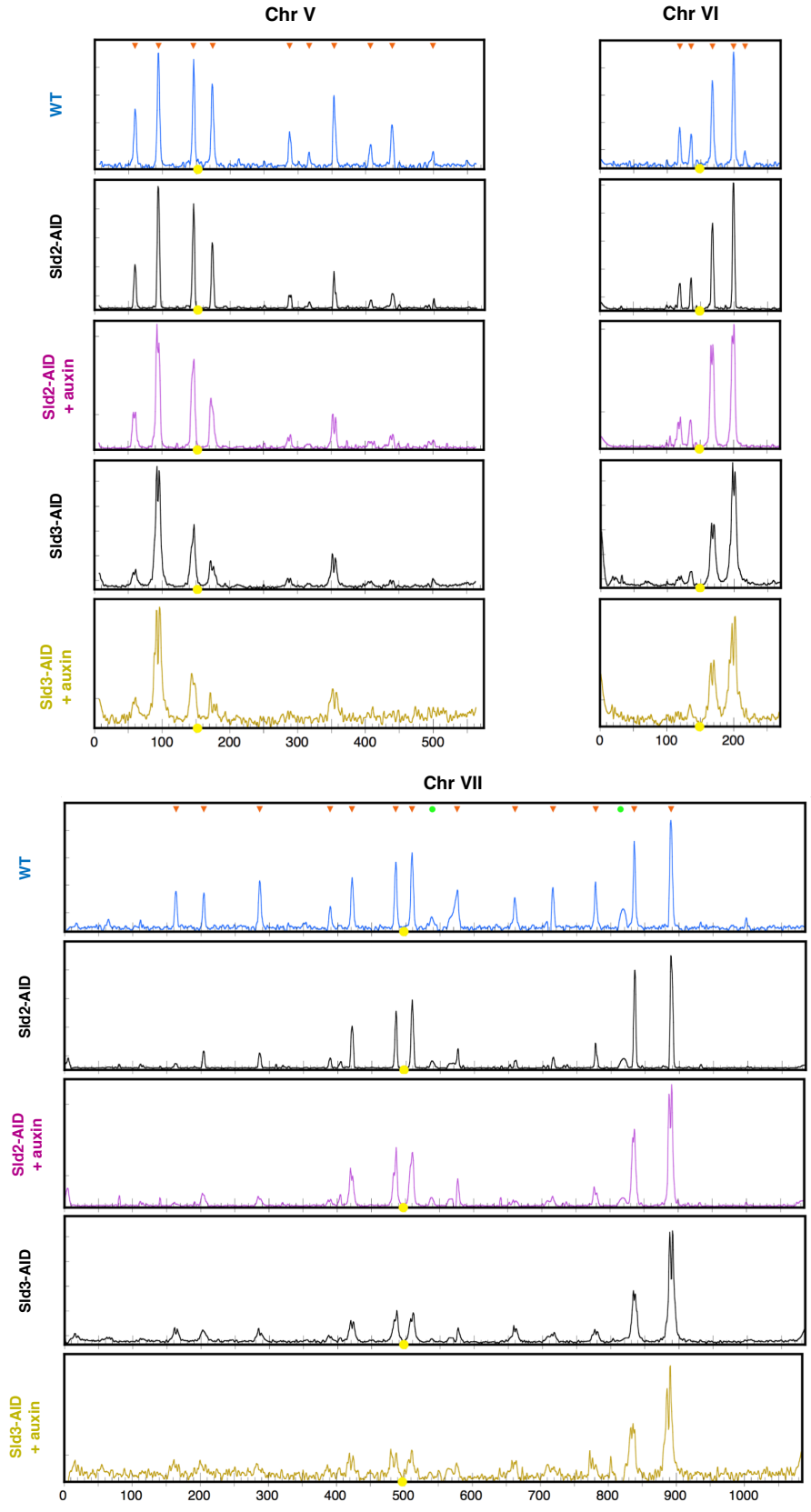
Chr V
Chr VI
WT
Sld2-AID
Sld2-AID + auxin
Sld3-AID
Sld3-AID + auxin
0
100
200
300
400
500
0
100
200
Chr VII
WT
Sld2-AID
Sld2-AID + auxin
Sld3-AID
Sld3-AID + auxin
0
100
200
300
400
500
600
700
800
900
1000

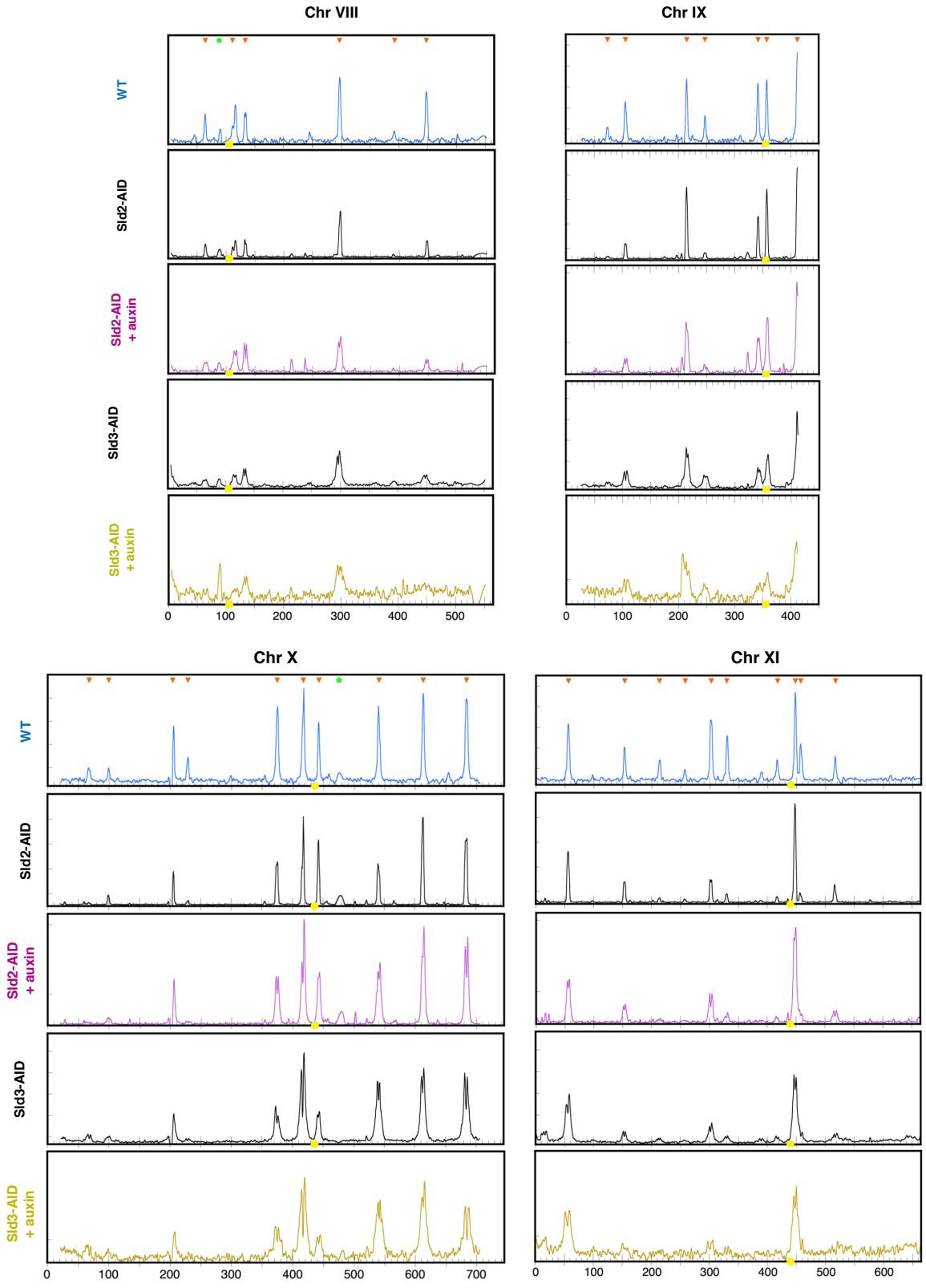
Chr VIII
Chr IX
Chr X
Chr XI
WT
Sld2-AID
Sld2-AID + auxin
Sld3-AID
Sld3-AID + auxin
0
100
200
300
400
500
600
700

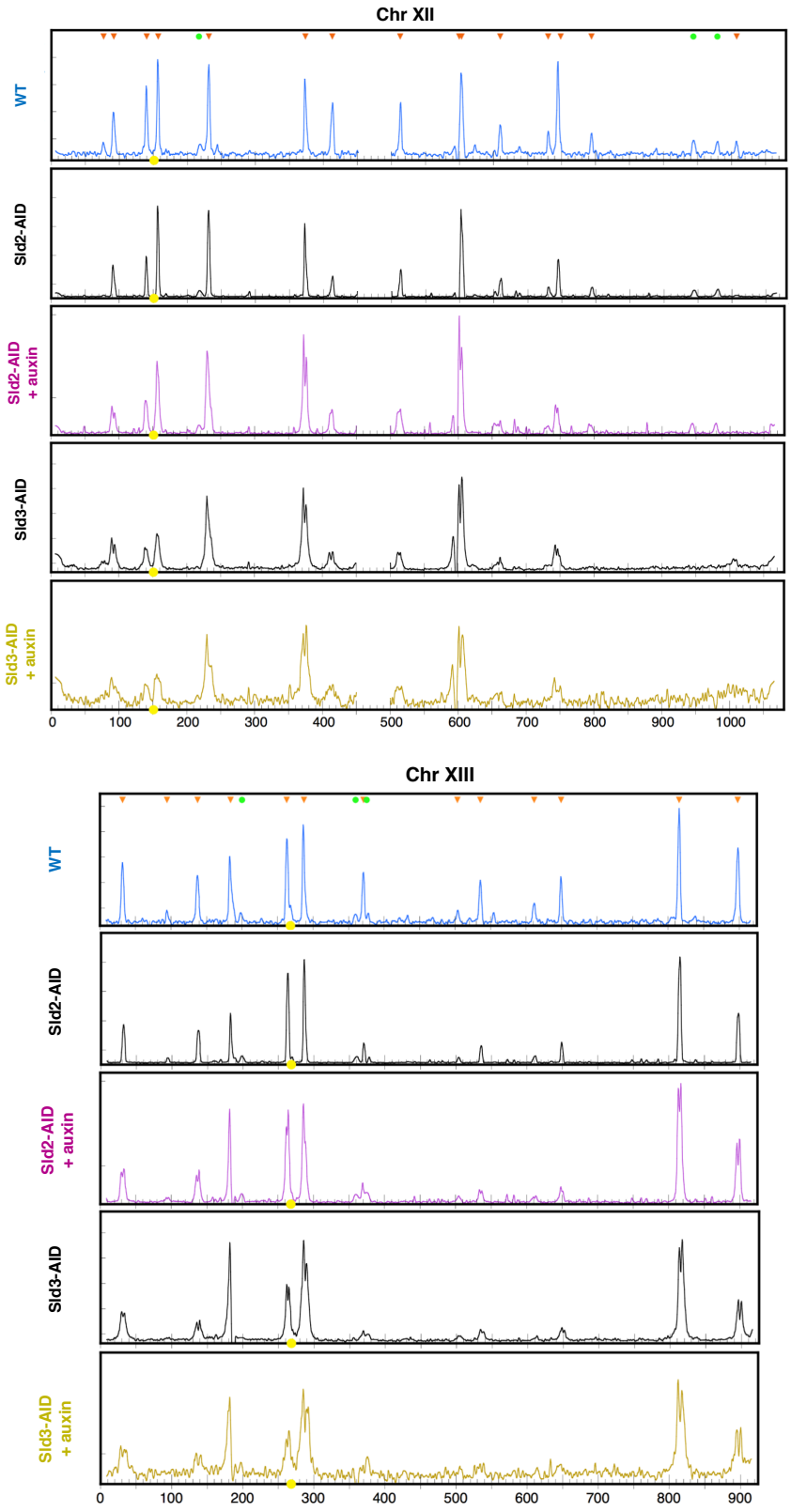
Chr XII
WT
Sld2-AID
Sld2-AID + auxin
Sld3-AID
Sld3-AID + auxin
0
100
200
300
400
500
600
700
800
900
1000
Chr XIII
WT
Sld2-AID
Sld2-AID + auxin
Sld3-AID
Sld3-AID + auxin
0
100
200
300
400
500
600
700
800
900

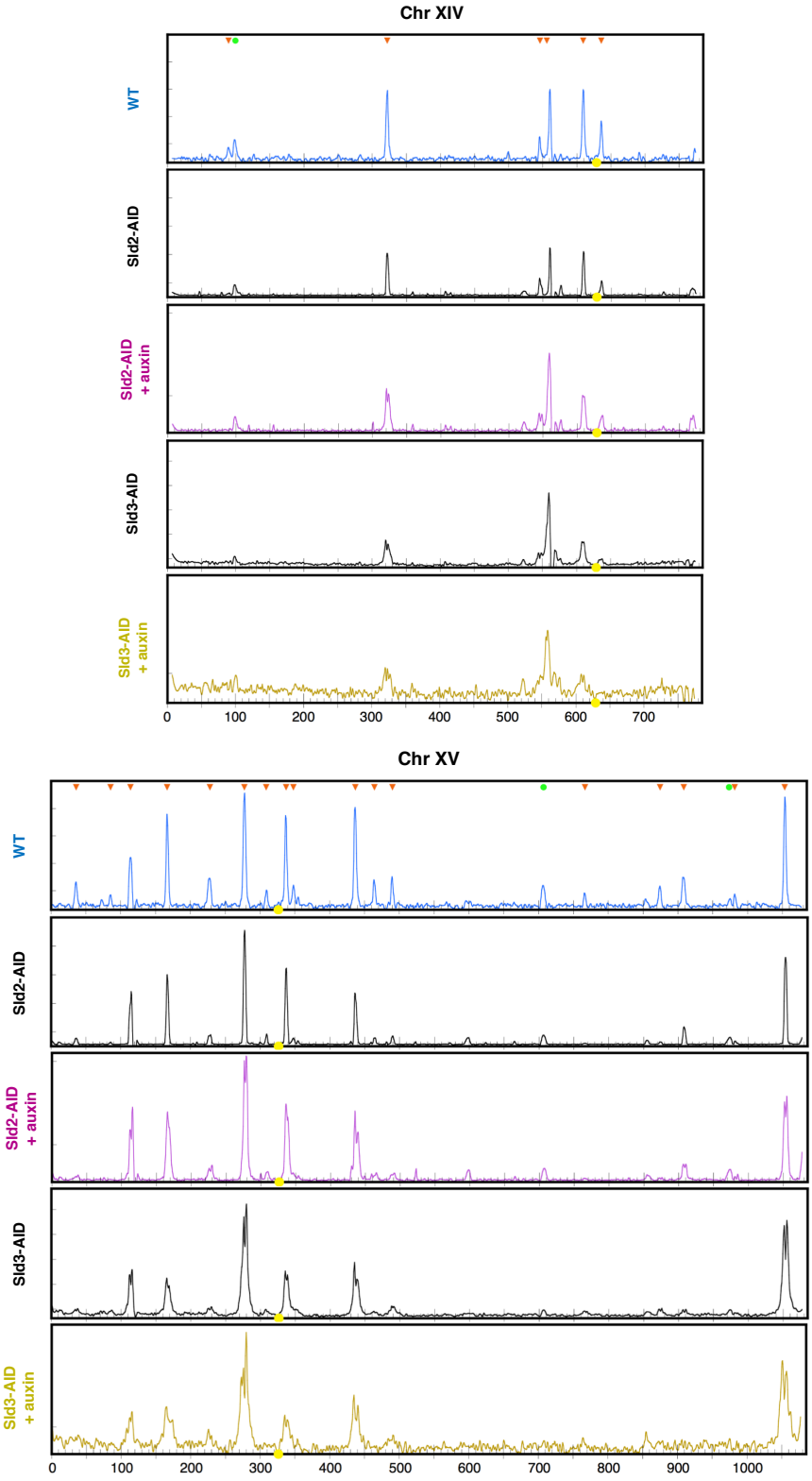
Chr XIV
WT
Sld2-AID
Sld2-AID + auxin
Sld3-AID
Sld3-AID + auxin
0
100
200
300
400
500
600
700
Chr XV
WT
Sld2-AID
Sld2-AID + auxin
Sld3-AID
Sld3-AID + auxin
0
100
200
300
400
500
600
700
800
900
1000

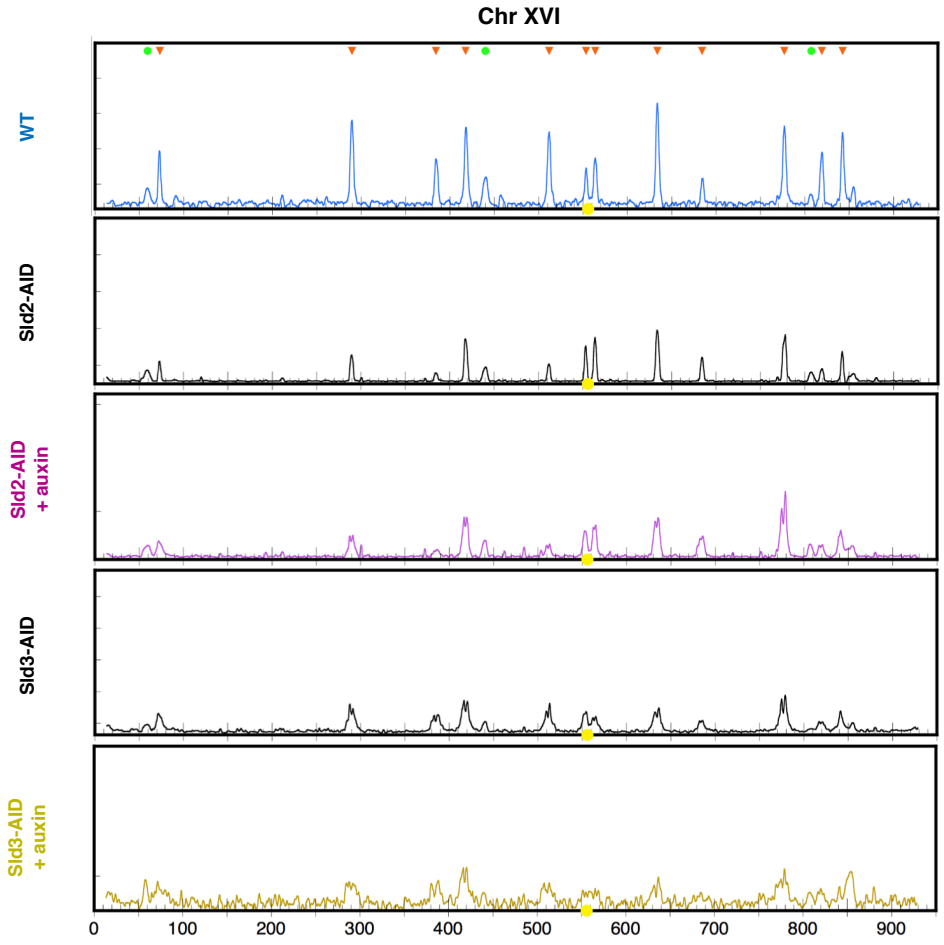
Chr XVI
WT
Sld2-AID
Sld2-AID
+ auxin
Sld3-AID
Sld3-AID
+ auxin
0
100
200
300
400
500
600
700
800
900

APPENDIX D: ZYMOLYASE CELL LYSIS CONDITIONS

To obtain clear results from 2D gel electrophoresis of single origins of replication, the delicate replication intermediate structures must be preserved by minimally handling the DNA samples to prevent breakage. Most DNA extraction protocols for yeast use a glass bead-beating/vortexing step to mechanically disrupt the cell wall. I noticed that my first batches of 2D gels had a lot of broken DNA that migrated at smaller sizes than the 1N spot. I suspected that the bead-beating steps over-sheared the DNA. Others in the lab had recently begun using zymolyase, a mixture of lytic enzymes that act on cell wall polysaccharides, to disrupt the cell wall structure. I wanted to systematically determine a procedure that combined cell wall lysis using zymolyase with our existing nuclear isolation buffer (NIB)-based DNA extraction protocol.

I began by determining whether lysing yeast cells in 1 mg/ml zymolyase in nuclear isolation buffer (NIB) resulted in comparable DNA yield as the bead beating used in our standard "NIB & Grab" protocol (Brewer). I compared the quantity of DNA and the amount of shearing resulting from the standard bead beating NIB protocol. I varied the number of rounds of bead-beating/vortexing and compared the quality of purified DNA to DNA derived from incubating the cells for 2 hours in zymolyase + NIB at 30°C. I ran the same same volume of each DNA sample on a low percentage agarose gel to examine the yield and quality of DNA. I recovered more DNA from the zymolyase-treated sample and observed less shearing compared to bead-beaten cells [see Figure D.1].

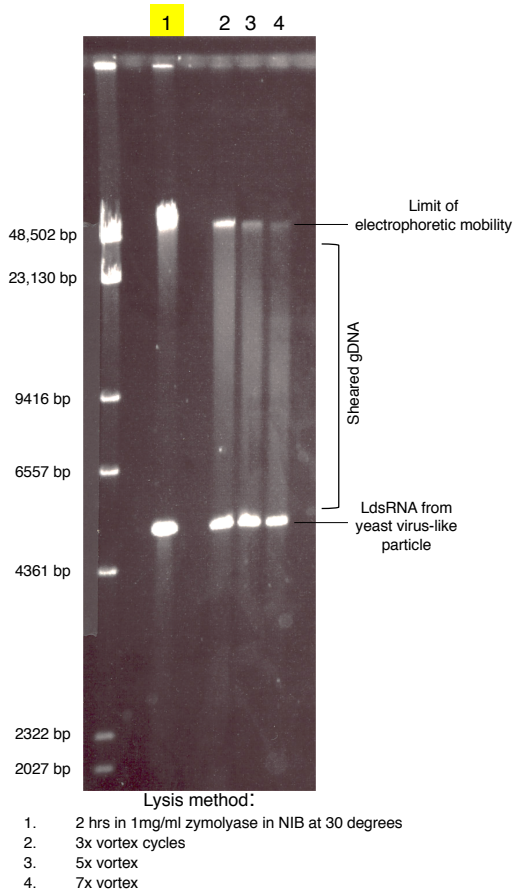

Figure D.1. DNA yield and quality from bead-beating vs. zymolyase cell lysis.[4]

Next, I determined parameters to reduce the incubation time for zymolyase treatment and maximize DNA yield without compromising the integrity of the replication intermediates. I harvested mid log-phase cells, then purified DNA using the conditions shown in Figure D.2. In the interest of shortening the length of the zymolyase incubation step, I tested whether using a combination of zymolyase + NIB with a single 30s cycle of bead beating would result in better DNA yield without as much shearing of DNA. I compared DNA yield and shearing by

[4] Cell lysis in NIB + zymolyase can recovery high yield of large DNA molecules. EtBr stained 0.4% agarose gel with 1 µl of each DNA sample loaded per lane. The smear of DNA fragments that migrate at a smaller size than the band at the very top of each lane are results from shearing. The average sheared fragment size becomes smaller with additional vortexing. I detected very little shearing in the sample in which I used zymolyase to disrupt the cell wall—sample indicated by yellow highlight.

electrophoresis on a low percentage agarose gel, which is shown in Figure D.2. EtBr-staining of the gel revealed that each zymolyase treatment resulted in large, intact DNA molecules with minimal shearing. The shortest incubation period produced the least amount of DNA.

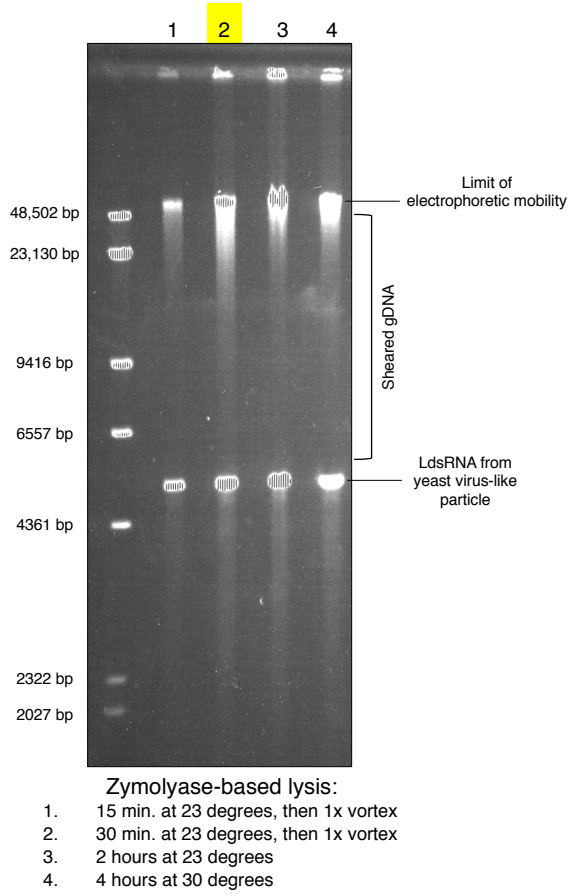

Figure C.2. Comparison of DNA yield across zymolyase-based lysis conditions.[5]

Satisfied that the shorter zymolyase treatments with a single vortexing step provided adequate amounts of DNA, I tested how well replication intermediates survived each treatment by running 2D gels of the rDNA origin of replication from the same DNA samples shown in Figure D.2. I found that the longer, higher temperature incubation periods reduced the prevalence of replication intermediates. The shorter incubations followed by 30s of vortexing resulted in high

[5] Highlighted lane indictes the lysis condition I've used for all subsequent experiments.

DNA yield and preserved the replication intermediates. For all subsequent 2D gel experiments, I used a 30-minute incubation in NIB + zymolyase at room temperature followed by 30s vortexing with glass beads to disrupt the cell wall before continuing with the nuclear isolation and DNA purification.

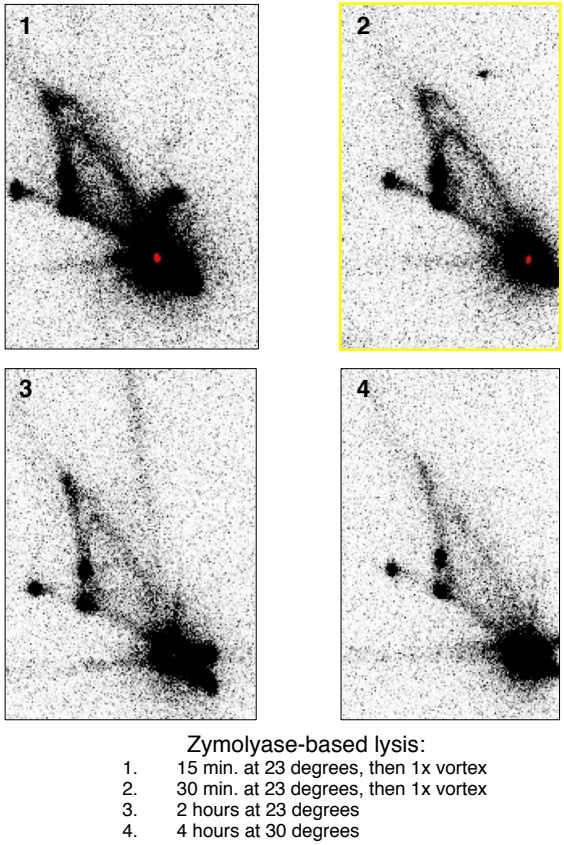

Figure D.3. 2-D gel analysis of the rDNA origin using different zymolyase cell lysis conditions.[6]

[6] Highlighted box shows the treatment condition that I've used for all subsequent DNA purifications. Blots are probed with *NTS2* fragment. Note the reduced intensity of both the bubble and Y arcs in the samples incubated for longer times.

APPENDIX E: WHOLE GENOME SEQUENCING REPLICATION PROFILES

Additional WGS-based replication profiles for the degron strains are shown. Centromeres are shown as yellow circles. Origins classified as "confirmed" in OriDB are indicated by orange diamonds (Siow et al., 2012). Chromosome coordinates are on the X axis and read depth relative to G1-arrested cells is mapped on the Y axis. Tables indicate the 1 kb bins excluded from the ends of chromosomes and excluded outliers stemming from mappability problems at Ty elements, paralogs, segmental duplications, etc.

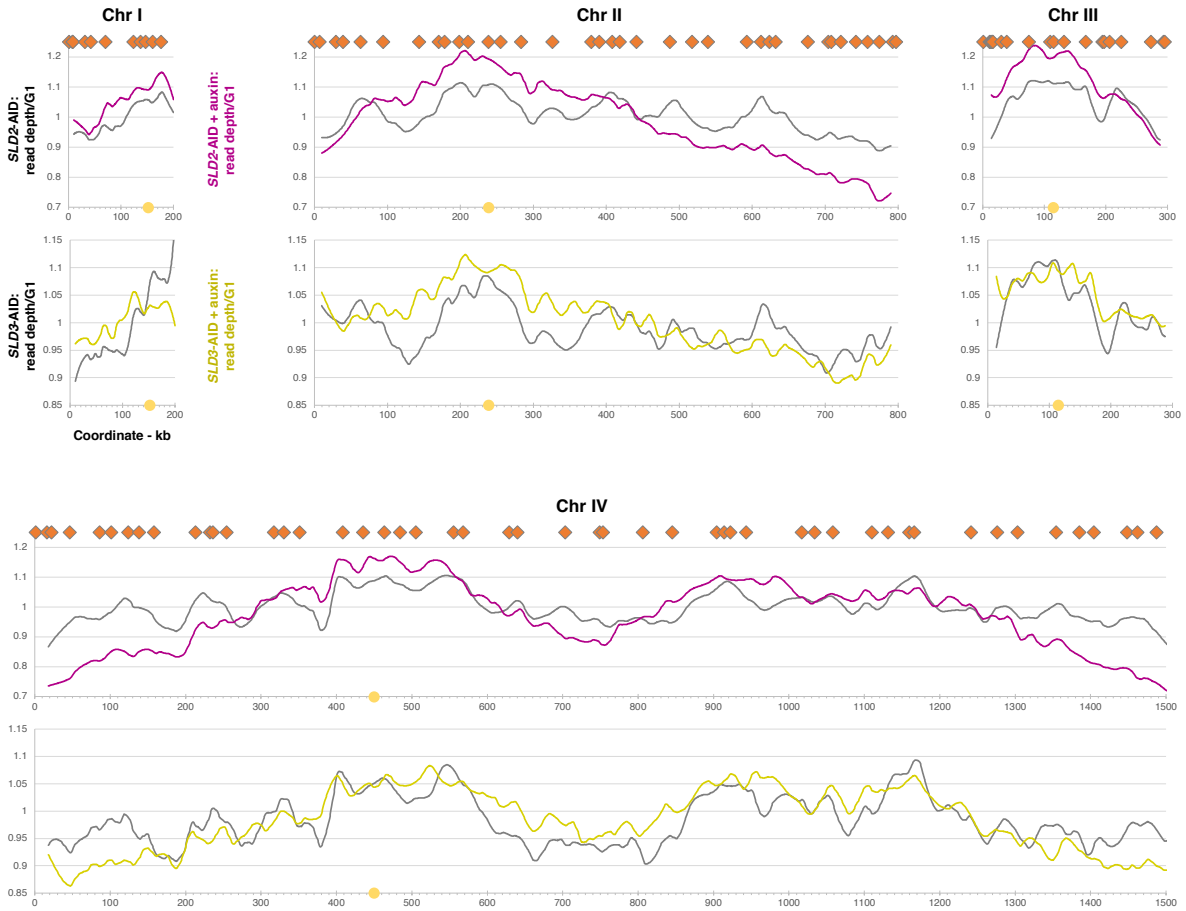

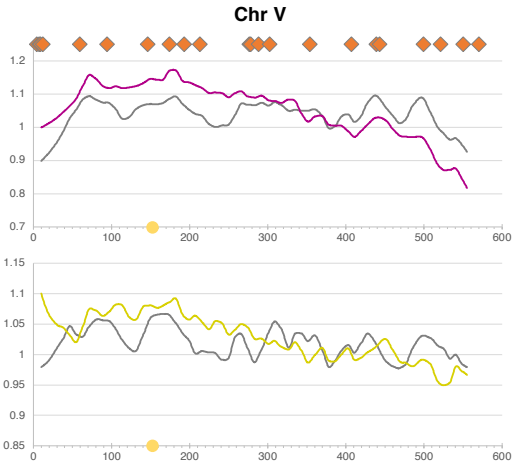
Chr V

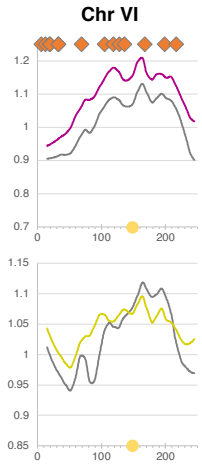
Chr VI

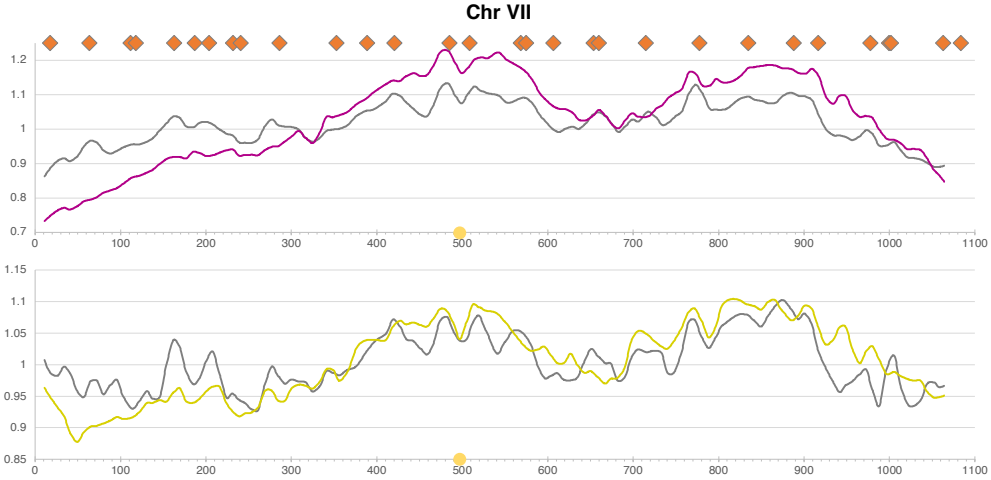
Chr VII

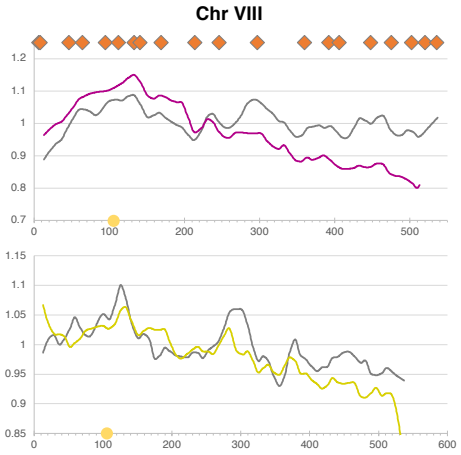
Chr VIII

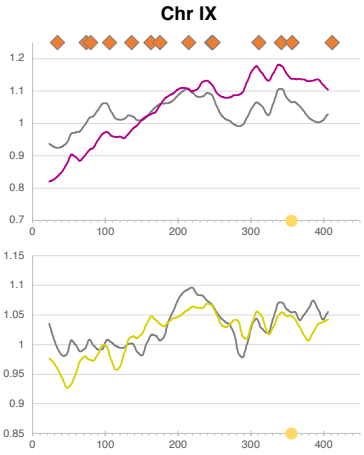
Chr IX

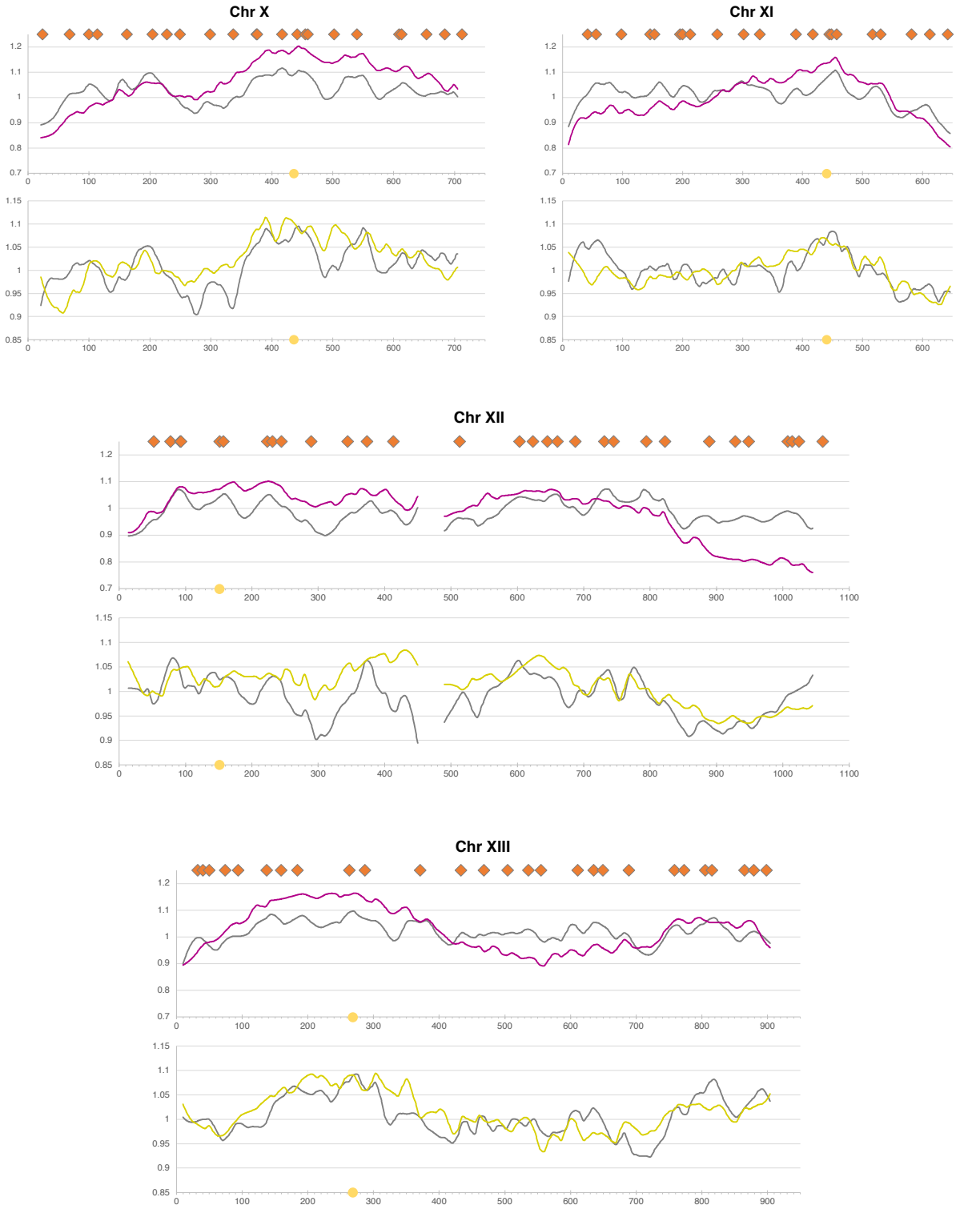
Chr X
Chr XI
Chr XII
Chr XIII

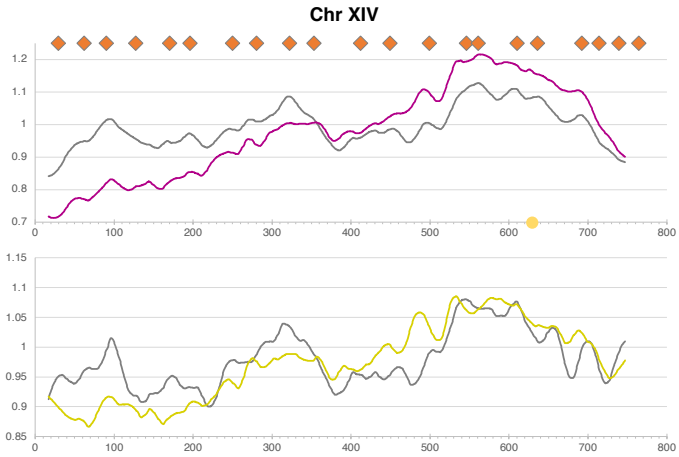
Chr XIV
1.2
1.1
1
0.9
0.8
0.7
0
100
200
300
400
500
600
700
800
1.15
1.1
1.05
1
0.95
0.9
0.85

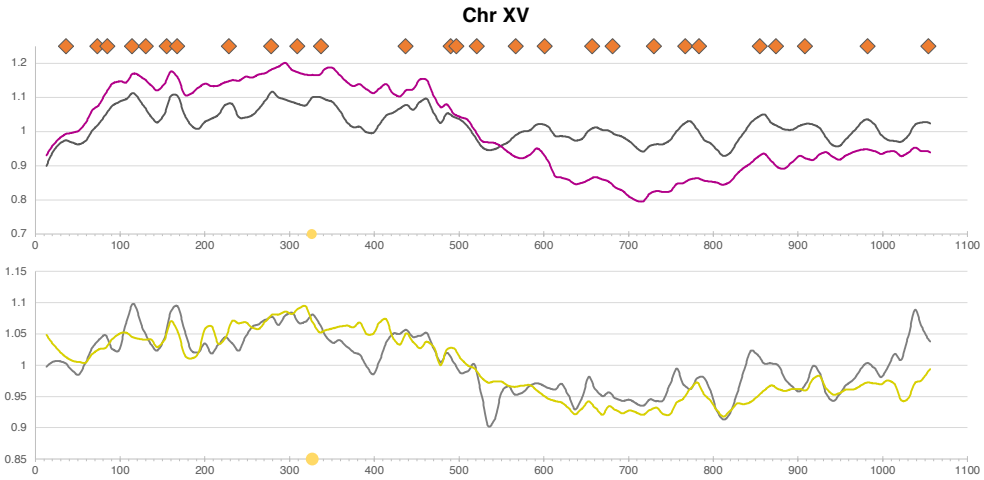
Chr XV
1.2
1.1
1
0.9
0.8
0.7
0
100
200
300
400
500
600
700
800
900
1000
1100
1.15
1.1
1.05
1
0.95
0.9
0.85

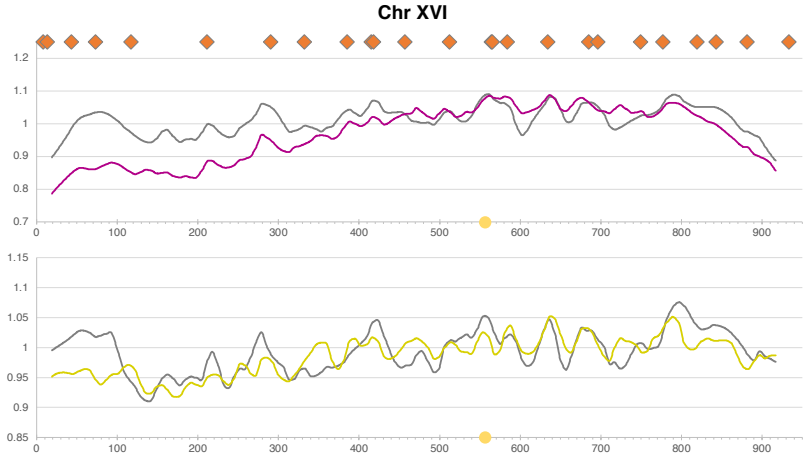
Chr XVI
1.2
1.1
1
0.9
0.8
0.7
0
100
200
300
400
500
600
700
800
900
1.15
1.1
1.05
1
0.95
0.9
0.85

Table E.1. 1 kb bins excluded from the ends of each chromosome.

Chromosome	Start - kb	End - kb
1	0	9
1	801	813
2	0	9
2	801	813
3	0	9
3	303	315
4	0	17
4	1520	1525
5	1	9
5	566	571
6	0	14
6	261	270
7	7	10
7	1076	1084
8	0	12
8	551	562
9	0	22
9	430	439
10	0	20
10	736	745
11	0	9
11	657	666
12	0	13
12	1060	1071
13	0	9
13	915	924
14	0	16
14	765	784
15	0	12
15	1070	1091
16	0	18
16	937	946

Table E.2. 1 kb bins excluded at Ty elements, paralogs, and duplicated sequences.

Type	Name	Chr	Start - kb	End - kb
ncRNA	XUT_1F-4	chr01	14	22
Ty1 LTR	YALWdelta1	chr01	22	25
Ty1 LTR	YALCdelta2	chr01	139	140
LTR_retrotransposon	YARCTy1-1	chr01	160	166
Ty1 LTR	YARCdelta3	chr01	160	160
Ty3 LTR	YARWsigma1	chr01	182	183
Ty1 LTR	YARWdelta6	chr01	182	183
Ty2 LTR	YARWdelta7	chr01	187	190
Ohnolog	FLO1	chr01	202	202
Ohnolog	FLO1	chr01	204	209
Ty1 LTR	YARCdelta8	chr01	209	210
Pseudogene with paralog	YAR061W	chr01	219	219
Ty2 element, LTR retrotransposon	YBLWTy2-1	chr02	30	36
Ty1 LTR	YBLWdelta6	chr02	36	36
Ty1 LTR	YBLCdelta7	chr02	197	197
Ty1 LTR	YBLWdelta8	chr02	221	221
Ty1 element, LTR retrotransposon	YBLWTy1-1	chr02	221	227
Ty1 LTR	YBRCdelta11	chr02	259	259

Ty1 element, LTR retrotransposon	YBRWTy1-2	chr02	260	265
Ty1 LTR	YBRCdelta14	chr02	266	266
Ohnolog	RPL4A	chr02	300	301
Ty1 LTR	YBRWdelta15	chr02	327	327
Ohnolog	RPS11B	chr02	333	334
Ohnolog	RFS1	chr02	339	339
Ohnolog	RPL19A	chr02	414	415
Ohnolog	TEF2	chr02	477	479
Ty4 LTR	YBRCtau2	chr02	643	644
Ohnolog	PYC2	chr02	659	662
Paralog	HML	chr03	10	13
Ty2 element, LTR retrotransposon	YCLWTy2-1	chr03	85	91
Ty1 LTR	YCRWdelta11	chr03	168	169
Repeat	MATALPHA	Chr03	198	201
Ty5 LTR	YCRWomega3	chr03	292	293
Ohnolog	SSB1	chr04	44	46
Ohnolog	RPL35A	chr04	118	119
Ohnolog	PPH22	chr04	124	125
Ohnolog	LYS20	chr04	133	135
Ohnolog	RGT2	chr04	213	216
Ohnolog	ARF2	chr04	217	217
Ohnolog	RPL35B	chr04	218	218
Ohnolog	LYS21	chr04	227	229
Ohnolog	RPL4A	chr04	300	301
Ohnolog	RPS16B	chr04	307	308
Ohnolog	RPL13A	chr04	308	309
Ohnolog	RPL31A	chr04	322	323
Ty1 LTR	YDLCdelta1	chr04	434	435
Ty4 LTR	YDLWtau1	chr04	437	438
Ohnolog	RPL4B	chr04	472	473
Ty1 LTR	YDRCdelta2	chr04	513	513
Ty1 LTR	YDRCdelta3	chr04	513	514
Ty2 element, LTR retrotransposon	YDRCTy2-1	chr04	514	520
Ty1 LTR	YDRCdelta6a	chr04	520	520
Ty1 LTR	YDRWdelta7	chr04	520	521
Ty1 LTR	YDRCdelta6b	chr04	521	521
?	ENA1	chr04	527	527
?	ENA1	chr04	528	528
?	ENA1	chr04	535	535
?	ENA1	chr04	536	536
Ohnolog	GRX3	chr04	644	645
Ty1 element, LTR retrotransposon	YDRCTy1-1	chr04	646	651
?	NUM1	chr04	758	758
Ty1 LTR	YDRWdelta11	chr04	803	803
Retrotransposon TYA Gag gene	YDR170W-A	chr04	803	805
Ty2 element, LTR retrotransposon	YDRWTy2-2	chr04	872	878
Ty1 element, LTR retrotransposon	YDRCTy1-2	chr04	878	884
Histone	HTB1	chr04	914	915
Ty1 LTR	YDRWdelta12	chr04	945	946
Ty3 LTR	YDRCsigma3	chr04	946	946
Ty2 element, LTR retrotransposon	YDRWTy2-3	chr04	981	987
Ty1 element, LTR retrotransposon	YDRCTy1-3	chr04	987	993
Ty3 LTR	YDRWsigma5	chr04	1023	1023
Ohnolog	SSF2	chr04	1088	1089
Ohnolog		chr04	1152	1154
Ohnolog	HXT7	chr04	1154	1156
Ohnolog	HXT6	chr04	1160	1161
Ohnolog	HXT3	chr04	1163	1165
Ty3 LTR	YDRCsigma6	chr04	1175	1176
Ohnolog	EFT2	chr04	1243	1246
Ohnolog	RPL12B	chr04	1302	1302
Ty1 LTR	YDRWdelta29	chr04	1353	1353
Ty1 LTR	YDRWdelta30	chr04	1353	1353
Ohnolog	RPL27B	chr04	1402	1403
Paralog	DSF1	chr05	19	21
Paralog	HXT13	chr05	21	23
Ohnolog	HYP2	chr05	86	86
Ohnolog	GEA2	chr05	111	116
Ty1 LTR	YELCdelta4	chr05	135	136
Ty1 LTR	YELWdelta5	chr05	137	138
Ohnolog	YPT31	chr05	214	215
Ty1 LTR	YERCdelta8	chr05	249	249
Ohnolog	RGI1	chr05	292	293
Ohnolog	SER3	chr05	323	324
Ty1 LTR	YERWdelta13	chr05	354	355
Ohnolog	RPS8B	chr05	363	364
Ohnolog	RPL23B	chr05	397	398
Ty3 LTR	YERCsigma3	chr05	435	435
Ty1 LTR	YERCdelta15	chr05	435	435
Ty1 LTR	YERWdelta17	chr05	442	443
Ty1 element, LTR retrotransposon	YERCTy1-2	chr05	493	498
Ohnolog	DNF1	chr05	513	517

Ty1 LTR	YFLWdelta2	chr06	138	138
Ty2 element, LTR retrotransposon	YFLWTy2-1	chr06	138	144
Ty4 LTR	YGLWtau1	chr07	111	111
Ty1 LTR	YGLCdelta1	chr07	111	112
Ty1 LTR	YGLWdelta2	chr07	112	112
Ty1 LTR	YGLWdelta3	chr07	115	115
Ohnolog	RMD9	chr07	304	306
Ty1 LTR	YGLWdelta4	chr07	319	319
Ty1 LTR	YGLCdelta5	chr07	319	319
Ty3 LTR	YGLCsigma1	chr07	319	320
Ohnolog	RPL7A	chr07	364	366
?	HSF1	chr07	368	371
Ohnolog	PYC1	chr07	385	389
Ohnolog	SDS23	chr07	396	398
Ohnolog	ERV14	chr07	401	401
Ty3 LTR	YGLWsigma2	chr07	402	402
Ty1 LTR	YGLWdelta7	chr07	402	402
Ty1 LTR	YGLWdelta8	chr07	405	405
Ty1 LTR	YGLWdelta9	chr07	405	405
Ty3 LTR	YGLCsigma3	chr07	405	405
Ohnolog	RPL24A	chr07	437	438
Ty1 element, LTR retrotransposon	YGRWTy1-1	chr07	536	542
Ohnolog	RPL26B	chr07	556	557
Ohnolog	ORM1	chr07	561	561
Ty1 element, LTR retrotransposon	YGRCTy1-2	chr07	562	568
Ty2 element, LTR retrotransposon	YGRCTy2-1	chr07	569	575
Ohnolog	RPL11B	chr07	648	649
Ty3 element, LTR retrotransposon	YGRWTy3-1	chr07	707	713
Ohnolog	ASN2	chr07	740	742
Ohnolog	TPO2	chr07	764	766
Ohnolog	RPL24B	chr07	787	788
Ty1 element, LTR retrotransposon	YGRCTy1-3	chr07	817	823
Ohnolog	TIF4631	chr07	824	827
Ty3 LTR	YGRWsigma7	chr07	845	846
Ty1 LTR	YGRWdelta31	chr07	876	876
Ohnolog	TDH3	chr07	883	884
Ohnolog	RPS0A	chr07	921	922
Ty4 LTR	YGRCtau3	chr07	931	932
Ohnolog	ENO1	chr07	1001	1002
?	IMA1	chr07	1068	1068
Ohnolog	RPL8A	chr08	35	36
Ty3 LTR	YHLCsigma1	chr08	85	86
Ty4 element, LTR retrotransposon	YHLWTy4-1	chr08	86	92
Ty1 LTR	YHLCdelta1	chr08	92	92
Ty1 LTR	YHLWdelta2	chr08	92	92
Ohnolog	RPL14B	chr08	104	105
Ty1 LTR	YHRCdelta3	chr08	116	117
Ohnolog	STP1	chr08	117	118
Ty3 LTR	YHRCsigma2	chr08	146	147
Ty4 LTR	YHRWtau3	chr08	147	147
Ohnolog	RPS27B	chr08	148	149
Seg dup	YHR054C	chr09	214	214
Ohnolog	HXT4	chr08	287	289
Ohnolog	HXT1	chr08	291	293
Ohnolog	HXT5	chr08	295	296
Ty2 LTR	YHRCdelta10	chr08	389	390
Ty1 LTR	YHRCdelta11	chr08	390	390
Ohnolog	ENO2	chr08	451	453
Ohnolog	GND1	chr08	471	472
Ohnolog	RPS4B	chr08	504	506
Ohnolog	FLO5	chr08	527	528
Ty1 LTR	YHRCdelta14	chr08	529	530
Ty1 element, LTR retrotransposon	YHRCTy1-1	chr08	544	550
Ohnolog	RPL40A	chr09	69	70
Ohnolog	RPL16A	chr09	98	99
Ohnolog	SDP1	chr09	150	150
Ty4 LTR	YILCtau1	chr09	196	197
Ty1 LTR	YILCdelta1	chr09	197	197
Ty3 element, LTR retrotransposon	YILWTy3-1	chr09	205	211
Ohnolog	SER33	chr09	221	222
Ohnolog	RPS24B	chr09	231	232
Ty2 LTR	YILWdelta2	chr09	246	247
Ty1 LTR	YILCdelta3	chr09	300	301
Ohnolog	RPL2B	chr09	317	318
Ty3 LTR	YILWsigma3	chr09	324	325
ncRNA	ICR1	chr09	390	392
Ty4 element, LTR retrotransposon	YJLWTy4-1	chr10	198	204
Ty1 element, LTR retrotransposon	YJRWTy1-1	chr10	472	478
Ohnolog	GEA1	chr10	487	491
Ty1 LTR	YJRCdelta16	chr10	537	538
Ty1 LTR	YJRWdelta17	chr10	538	538
Ty1 LTR	YJRWdelta18	chr10	540	541

?	DAN1	chr10	714	714
?	AAD10	chr10	727	730
Ohnolog	RPL17A	chr11	109	110
?	STE3	chr11	114	114
Ohnolog	MYO3	chr11	196	200
Ohnolog	YPK1	chr11	206	208
ncRNA		chr11	230	230
Ty1 LTR	YKLCdelta5	chr11	302	303
Ty1 LTR	YKLCdelta6	chr11	313	314
Ty1 LTR	YKLCdelta6	chr11	314	314
Ty1 LTR	YKLWdelta7	chr11	314	315
Ty1 LTR	YKRCdelta8	chr11	458	458
Ohnolog	TIF1	chr11	555	556
?	TRZ1	chr11	589	589
Ty1 LTR	YLLCdelta1	chr12	92	92
Ohnolog	SSA2	chr12	96	96
Pseudogene with paralog	SDC25	chr12	122	122
?	AAT2	chr12	197	197
Ohnolog	RPL15A	chr12	202	203
Retrotransposon TYA Gag and TYB Pol genes	YLR035C-A	chr12	215	220
Ohnolog	TRX1	chr12	232	233
Ohnolog	RPS0B	chr12	242	243
Ty3 LTR	YLRWsigma2	chr12	374	374
Ohnolog	SAM1	chr12	515	516
Ty1 LTR	YLRCdelta9	chr12	592	593
Ty1 element, LTR retrotransposon	YLRWTy1-2	chr12	593	599
Ty1 LTR	YLRWdelta12	chr12	599	600
?	THI7	chr12	613	613
Ty1 element, LTR retrotransposon	YLRWTy1-3	chr12	651	657
Ty2 LTR	YLRCdelta18	chr12	731	732
?	VRP1	chr12	804	804
Ty2 element, LTR retrotransposon	YLRWTy2-1	chr12	941	947
Ty2 element, LTR retrotransposon	YLRCTy2-2	chr12	976	982
Ohnolog	IMD3	chr12	1002	1003
Ohnolog	RPS1A	chr12	1018	1019
Ohnolog	TUB1	chr13	98	99
Ohnolog	YML082W	chr13	102	104
Ohnolog	CMP2	chr13	160	162
Ty2 LTR	YMLCdelta2	chr13	168	169
Ty1 element, LTR retrotransposon	YMLWTy1-1	chr13	184	190
Ty1 element, LTR retrotransposon	YMLWTy1-2	chr13	196	202
Ohnolog	RPS18B	chr13	223	224
Ohnolog	RPS17A	chr13	226	227
?	PSP2	chr13	237	237
Ohnolog	SOK2	chr13	304	304
Ty1 element, LTR retrotransposon	YMRCTy1-3	chr13	357	363
Ty1 LTR	YMRCdelta13	chr13	463	463
Ty4 LTR	YMRWtau2	chr13	504	504
Ohnolog	RPL13B	chr13	550	551
Ohnolog	RPS16A	chr13	552	553
Ohnolog	HSC82	chr13	632	634
Ohnolog	RPL36A	chr13	651	652
?	RNT1	chr13	748	748
Ohnolog	URA10	chr13	807	808
Ohnolog	BUL1	chr13	816	819
?	YMR317W	chr13	908	909
Ohnolog	RPS19B	chr14	62	63
?	MON2	chr13	74	74
Ty1 element, LTR retrotransposon	YNLCTy1-1	chr14	97	103
Ty3 LTR	YNLCsigma1	chr14	103	103
Ohnolog	SSB2	chr14	252	254
Ohnolog	LEU4	chr14	425	427
Ohnolog	RPS7B	chr14	443	444
Ty1 element, LTR retrotransposon	YNLWTy1-2	chr14	519	525
Ohnolog	MSG5	chr14	530	530
Ohnolog	COX5A	chr14	532	532
Ty4 LTR	YNLWtau2	chr14	562	562
Ty2 LTR	YNLCdelta5	chr14	562	562
Ty2 element, LTR retrotransposon	YNLCTy2-1	chr14	562	568
Ohnolog	YNL034W	chr14	570	572
Seg dup	YNL019C	chr14	598	601
Ty4 LTR	YNRCtau3	chr14	632	632
Ty3 LTR	YNRWsigma4	chr14	726	727
?	YNR063W	chr14	746	746
?	YNR065C	chr14	751	752
?	DSE4	chr14	755	755
Paralog	HXT11	chr15	23	29
Ty1 element, LTR retrotransposon	YOLWTy1-1	chr15	118	124
Ohnolog	LEU9	chr15	523	525
Ohnolog	EFT1	chr15	575	578
Ty1 LTR	YORCdelta18	chr15	703	704

Ty1 LTR	YORWdelta19	chr15	704	704
Ty4 LTR	YORWtau2	chr15	704	704
Ty2 element, LTR retrotransposon	YORCTy2-1	chr15	704	710
Ty4 LTR	YORWtau3	chr15	710	710
Ohnolog	RPS10A	chr15	867	868
Ohnolog	RPL20B	chr15	900	901
Ty3 LTR	YORWsigma4	chr15	969	969
Ty1 LTR	YORWdelta22	chr15	969	969
Ty2 element, LTR retrotransposon	YORWTy2-2	chr15	970	976
Ty1 LTR	YORCdelta25	chr15	980	981
Ty1 LTR	YPLCdelta1	chr16	56	56
Ty3 LTR	YPLWsigma1	chr16	56	56
Ty1 LTR	YPLWdelta2	chr16	56	56
Ty1 element, LTR retrotransposon	YPLWTy1-1	chr16	56	62
Ohnolog	HSP82	chr16	96	99
Ohnolog	RPL7B	chr16	172	175
Ohnolog	RPS6A	chr16	377	378
Ohnolog	RPS9A	chr16	405	406
Ohnolog	RPL21B	chr16	407	408
Ty4 element, LTR retrotransposon	YPLCTy4-1	chr16	436	443
Paralog	PMA2	chr17	484	484
Ty1 LTR	YPRWdelta12	chr16	560	561
tRNA	tF(GAA)P2	chr16	622	622
Ohnolog	TEF1	chr16	701	702
Ty3 LTR	YPRWsigma2	chr16	769	769
Ohnolog	CLB5	chr16	775	775
Ty1 LTR	YPRCdelta15	chr16	777	777
Ty1 LTR	YPRWdelta16	chr16	778	778
Ty1 LTR	YPRWdelta17	chr16	805	805
Ty1 element, LTR retrotransposon	YPRCTy1-2	chr16	805	811
Ohnolog	ASN1	chr16	823	824
Ohnolog	TPO3	chr16	838	840
Ty1 LTR	YPRCdelta22	chr16	850	851
Ty1 element, LTR retrotransposon	YPRCTy1-4	chr16	851	857
Ty3 LTR	YPRWsigma3	chr16	857	858
Ty3 LTR	YPRWsigma4	chr16	880	881

APPENDIX F: ADDITIONAL SOUTHERN BLOTS AND QUANTIFICATION OF CHEF GELS

To determine whether the effects of Sld2 or Sld3 depletion were unique to ChrXII, I stripped and re-probed membranes from the synchronous pulsed field gel experiment with a succession of single copy sequences from a selection of different chromosomes. After ChrXII, I probed the blots with a sequence located at coordinate 810 kb on chromosome XV. ChrXV is also large (~1.1 Mb in length), like ChrIV and ChXII, and harbors a large, late-replicating region approximately from coordinates 550 kb – 850 kb. I wanted to determine whether the late-replicating region and longer chromosome length impacted the stability of ChrXV over time. The auxin-treated *SLD2*-AID and *SLD3*-AID samples show that ChrXV is partially replicated for a longer period than the control condition [Figure F.1]. Unlike ChrXII, ChrXV finishes replicating, and the full-length chromosome is evident in the lane at the later time points [Figure F.1].

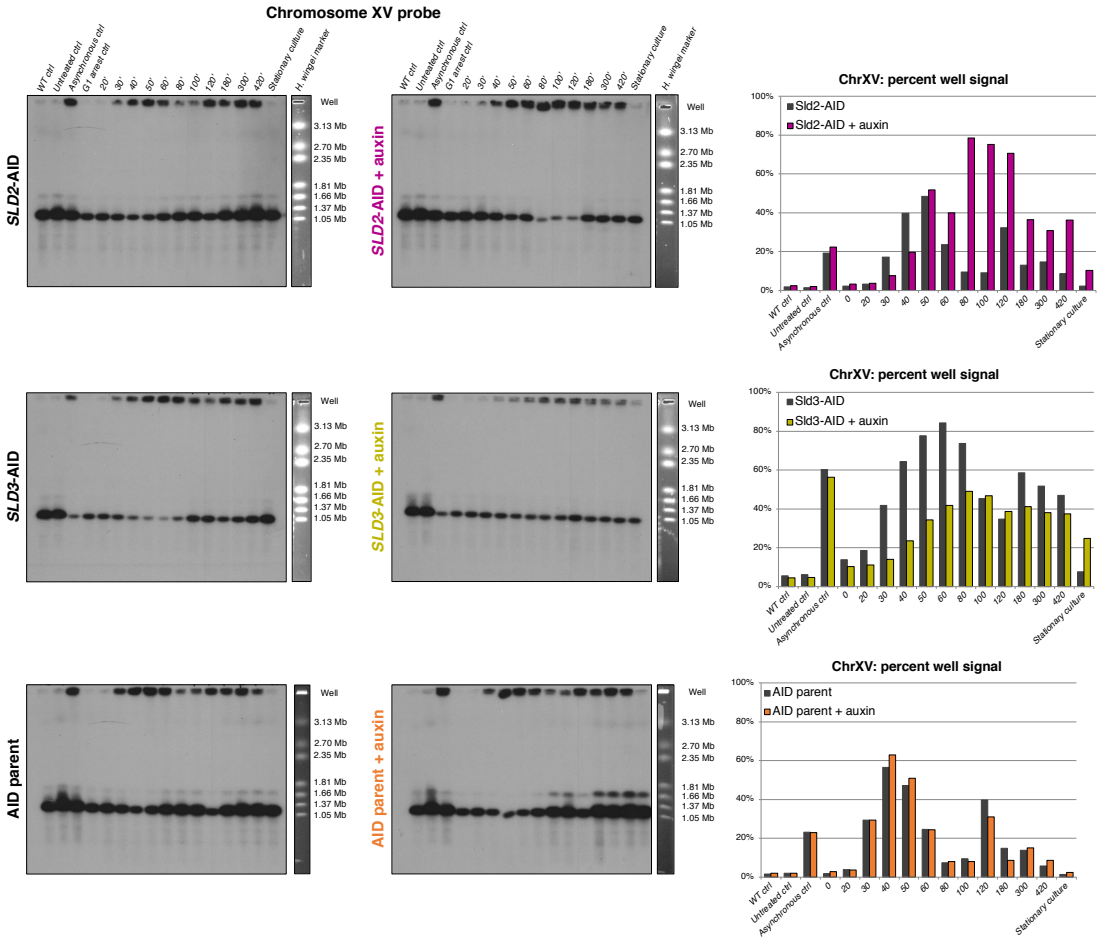

Figure F.1. Chromosome XV-probed CHEF gel blots and quantification of well signal.

Next, I probed for chromosome X with the *ARS1011* sequence. I chose ChrX as a representative intermediate-sized yeast chromosome (~750 kb). Again, partially-replicated chromosome structures persist for a longer time when origin efficiency is reduced, but no significant breakage is observed for ChrX [Figure F.2].

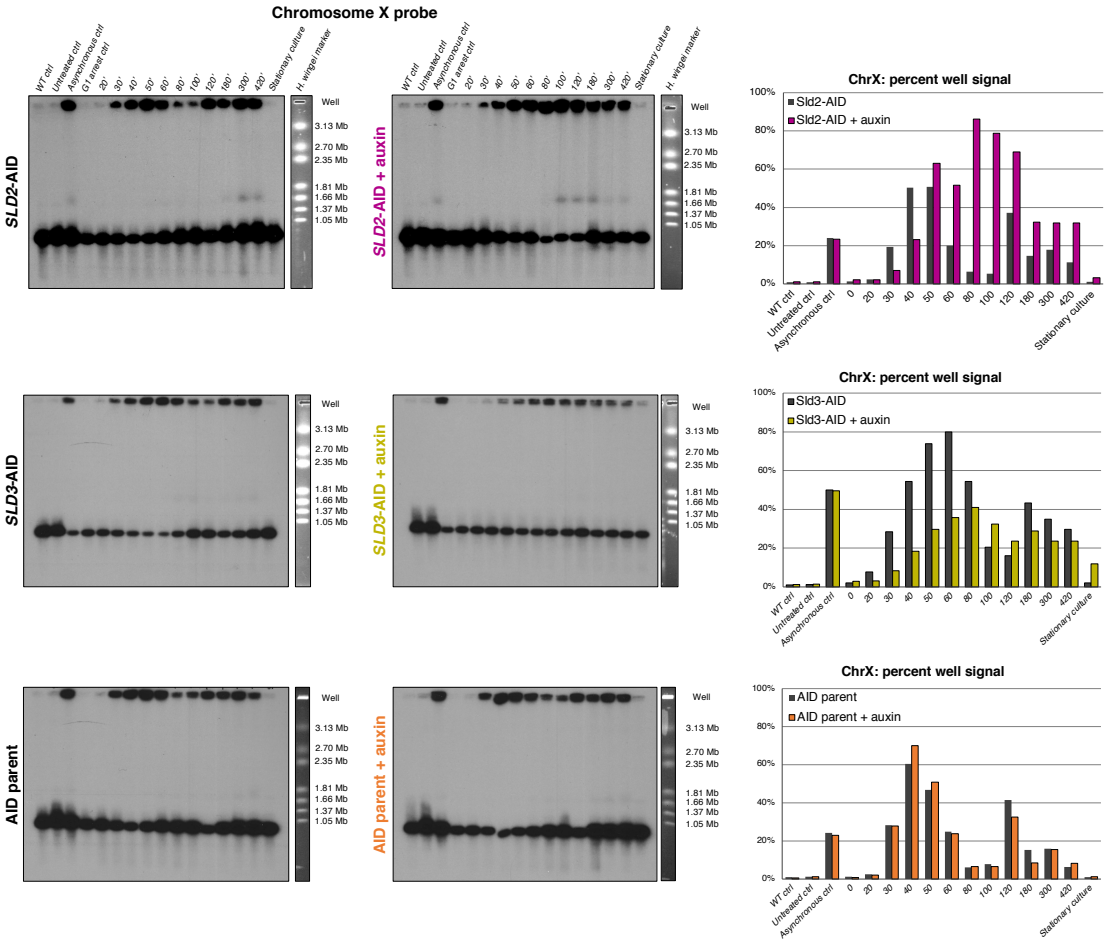

Figure F.2. Chromosome X-probed CHEF gel blots and quantification of well signal.

After stripping the ChrX probe fragment, I next probed the CHEF gel blots with a chromosome III sequence (*ARS306* fragment). I used ChrIII as an example of a small chromosome (~300 kb). The changes to chromosome migration upon depletion of Sld2 or Sld3 are similar to the other chromosomes, with the exception of ChrXII [Figure F.3]. The maximum well-retained signal is lower for ChrIII than the other chromosomes tested, likely due to its much smaller size. Again, ChrIII is stable over the entire time course.

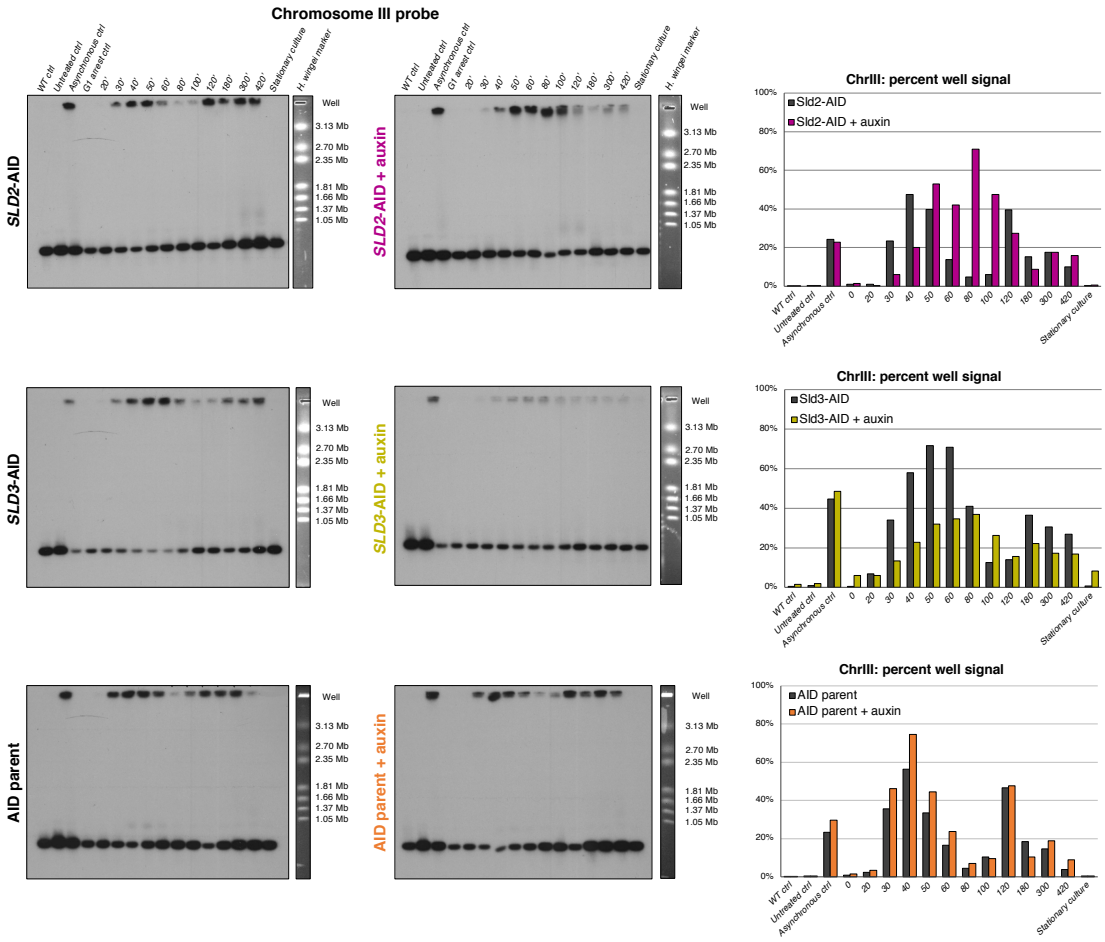

Figure F.3. Chromosome III-probed CHEF gel blots and quantification of well signal.

Finally, I probed these blots for a single copy mitochondrial DNA sequence--the gene *COX1*. Replication of mtDNA should proceed continuously, regardless of impediments to nuclear DNA replication or the different phases of the cell cycle. I probed for a mitochondrial sequence to ascertain that the changes in nuclear DNA migration were, indeed, specific to the nucleus. The retention of mtDNA in the well did not fluctuate in response to α-factor arrest and release. The well signal in the G1-arrested cells is not much different than the well signal in the synchronized, timed samples [Figure F.4]. Although the percent well signal was, on average, lower in the *SLD2*-AID and *SLD3*-AID strains, the overall trends in mtDNA migration were the same among the three

strains, signifying that the changes in ChrXII stability and the persistence of partial replication observed for other chromosomes is unique to the nuclear genome.

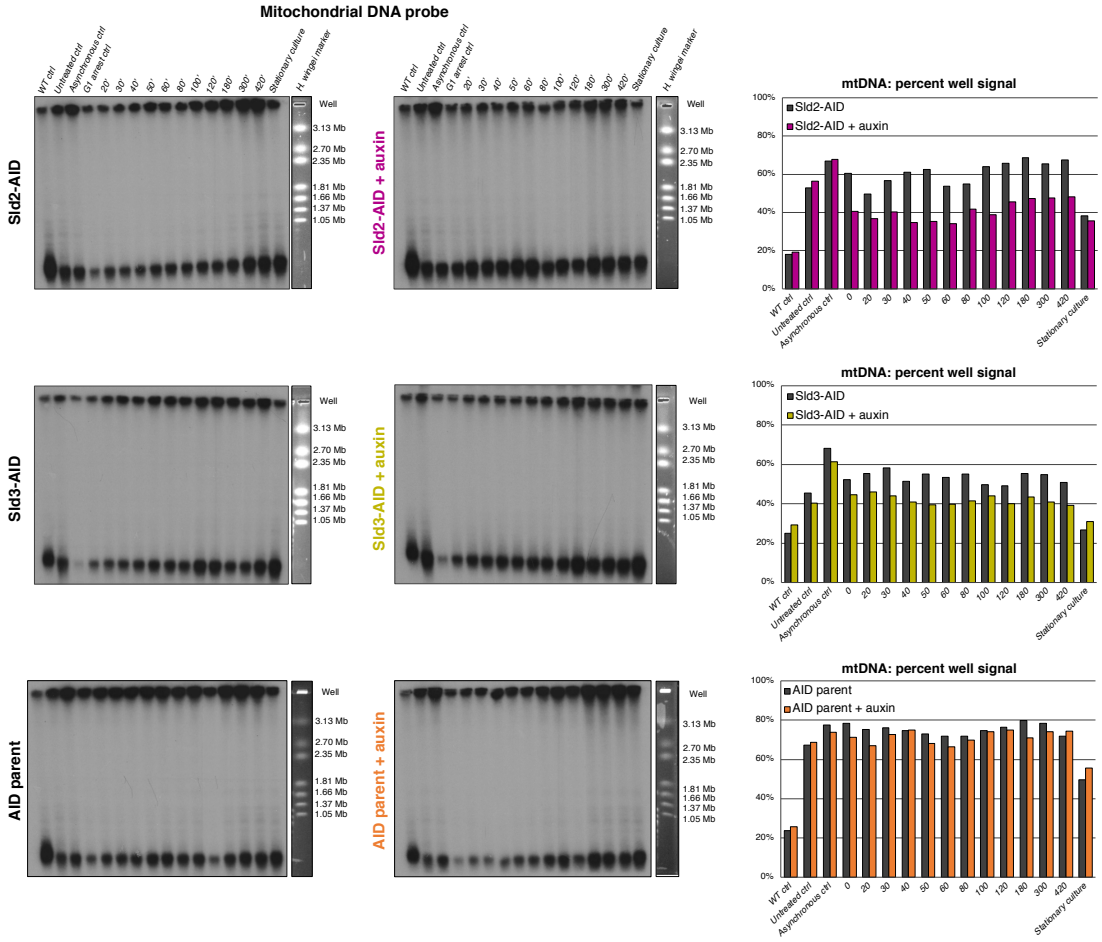

Figure F.4. mtDNA-probed CHEF gel blots and quantification of well signal.

APPENDIX G: I-PPO1 CHEF GEL DIGEST CONDITIONS

To test whether incomplete replication of the rDNA locus causes instability of chromosome XII, I used the intron-encoded endonuclease (I-Ppo1) from *Physarum polycephalum*, which cuts within the *S. cerevisiae* rDNA locus, but not elsewhere in the yeast genome. The enzyme recognizes the 15-bp sequence CTCTCTTAAGGTAGC (Muscarella and Vogt, 1993). An initial experiment, however, revealed undesirable off-target activity if the enzyme is allowed to act for too long on agarose-embedded DNA. I wanted to test different enzyme reaction conditions to determine whether I could use I-Ppo1 on the small pieces of agarose in which yeast chromosomes are embedded for the pulsed field gel running conditions. I used W303 plugs prepared for a previous experiment to test the different enzyme conditions. Rather than apply the enzyme directly to the agarose plugs containing the yeast DNA, I decided to pipette a small volume (75μL) of I-Ppo1 buffer around the plug, then add variable amounts of enzyme (between 0.2 – 2.0 μL) to the plug/buffer and incubate at 37°C for varying amounts of time (15 minutes – 3 hours). To confirm that the DNA was not over-digested, I ran the digested samples on a pulsed field gel [see Figure G.1]. I probed the transferred gels with a non-rDNA ChrXII sequence to confirm that the rest of ChrXII was intact after I-Ppo1 treatment. Next, I probed with a ChrIV sequence to confirm that I-Ppo1 did not cut outside of ChrXII. And, finally, I probed with an rDNA sequence (*NTS2-2*) to confirm that the small DNA fragments that appeared at the bottom of the gel in the I-Ppo1 treated samples were from single rDNA repeats. Ultimately, I found that only the longest incubation period (3 hours) and the greatest volume of enzyme (2 μL) resulted in overdigestion of the DNA. For subsequent experiments, I used 0.5 μL of enzyme and incubated the plugs for 1 hour at 37°C.

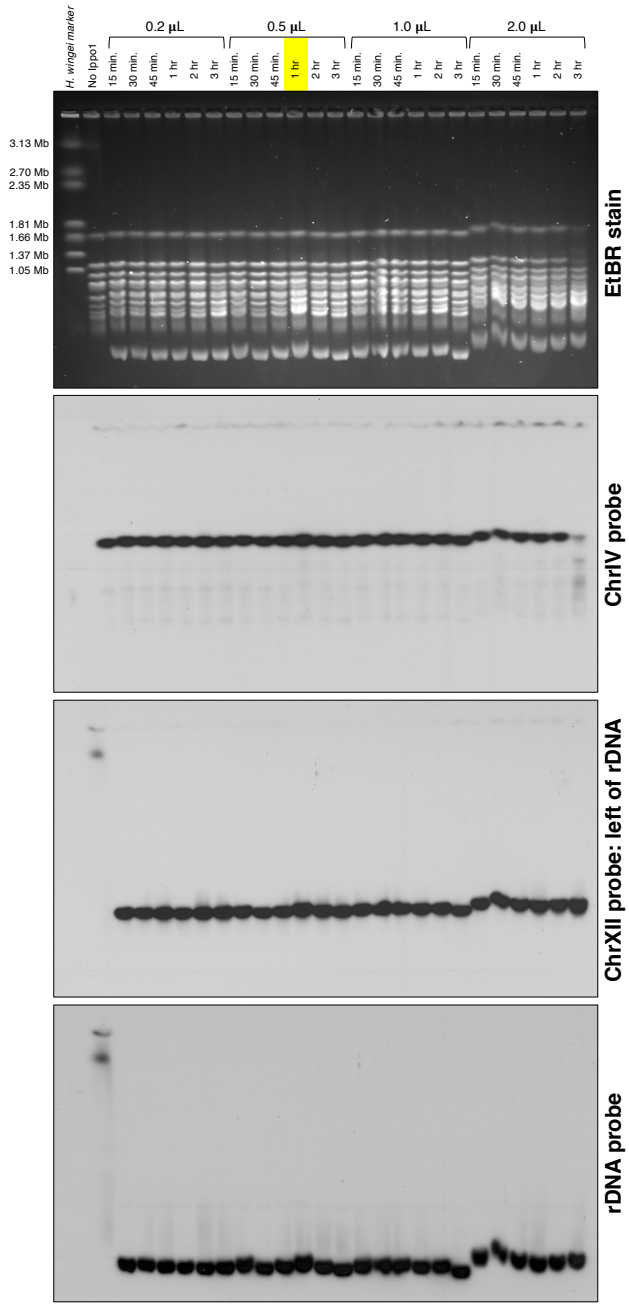

Figure G.1. I-Ppo1 test CHEF gel and Southern blot results.[7]

[7] The presence of multiple bands in the rightmost sample that are smaller ChrIV indicate over-digest of the DNA. The highlighted condition indicates the digest conditions used for all subsequent experiments.

VITA

Kelsey L. Lynch was born and raised in Bloomington, Indiana. She graduated magna cum laude from Bryn Mawr College in 2011 with an A.B. in Biology and Italian Literature. As an undergraduate student, she received an HHMI Science Horizons Fellowship for summer research at the University of Oregon. In 2012, after working as a research technician at the University of Georgia, she moved to Seattle, Washington, where she joined the MCB Ph.D. program at the University of Washington. She completed her thesis work in the Brewer/Raghuraman Lab in the UW Department of Genome Sciences in April 2018.